



**AFRL-RQ-ED-TR-2013-0054**

# **Transition Delay in Hypervelocity Boundary Layers by Means of Vibrational Relaxation and Acoustic Instability Interactions**

---

Ivett Leyva

Air Force Research Laboratory (AFMC)  
AFRL/RQRE  
4 Draco Drive  
Edwards AFB CA 93524-7160

January 2014

In-House Final Report

---

**Distribution A: To be approved for Public Release; distribution unlimited. PA No.14137**

---

**AIR FORCE RESEARCH LABORATORY  
AEROSPACE SYSTEMS DIRECTORATE**

■ Air Force Materiel Command    ■ United States Air Force    ■ Edwards Air Force Base, CA 93524

**- STINFO COPY -  
NOTICE AND SIGNATURE PAGE**

Using Government drawings, specifications, or other data included in this document for any purpose other than Government procurement does not in any way obligate the U.S. Government. The fact that the Government formulated or supplied the drawings, specifications, or other data does not license the holder or any other person or corporation; or convey any rights or permission to manufacture, use, or sell any patented invention that may relate to them.

Qualified requestors may obtain copies of this report from the Defense Technical Information Center (DTIC) (<http://www.dtic.mil>).

AFRL-RQ-ED-TR-2013-0054 HAS BEEN REVIEWED AND IS APPROVED FOR PUBLICATION IN ACCORDANCE WITH ASSIGNED DISTRIBUTION STATEMENT.

FOR THE DIRECTOR:

//signature//

---

IVETT A. LEYVA, Ph.D.  
Program Manager

//signature//

---

JEREMY J. SELSTROM, CAPT, USAF  
Chief, Engines Branch

//signature//

---

Technical Advisor  
Rocket Propulsion Division

This report is published in the interest of scientific and technical information exchange, and its publication does not constitute the Government's approval or disapproval of its ideas or findings.

# REPORT DOCUMENTATION PAGE

Form Approved  
OMB No. 0704-0188

Public reporting burden for this collection of information is estimated to average 1 hour per response, including the time for reviewing instructions, searching existing data sources, gathering and maintaining the data needed, and completing and reviewing this collection of information. Send comments regarding this burden estimate or any other aspect of this collection of information, including suggestions for reducing this burden to Department of Defense, Washington Headquarters Services, Directorate for Information Operations and Reports (0704-0188), 1215 Jefferson Davis Highway, Suite 1204, Arlington, VA 22202-4302. Respondents should be aware that notwithstanding any other provision of law, no person shall be subject to any penalty for failing to comply with a collection of information if it does not display a currently valid OMB control number. **PLEASE DO NOT RETURN YOUR FORM TO THE ABOVE ADDRESS.**

<b>1. REPORT DATE (DD-MM-YYYY)</b> 4 January 2014		<b>2. REPORT TYPE</b> In-House Final Technical Report		<b>3. DATES COVERED (From - To)</b> 5 Jan 2007 - 7 Oct 2013	
<b>4. TITLE AND SUBTITLE</b> Transition Delay in Hypervelocity Boundary Layers by Means of Vibrational Relaxation and Acoustic Instability Interactions				<b>5a. CONTRACT NUMBER</b>	
				<b>5b. GRANT NUMBER</b> 13RQ14COR	
				<b>5c. PROGRAM ELEMENT NUMBER</b>	
<b>6. AUTHOR(S)</b> Ivett Leyva				<b>5d. PROJECT NUMBER</b>	
				<b>5e. TASK NUMBER</b>	
				<b>5f. WORK UNIT NUMBER</b> Q0AF	
<b>7. PERFORMING ORGANIZATION NAME(S) AND ADDRESS(ES)</b> Air Force Research Laboratory (AFMC) AFRL/RQRE 4 Draco Drive Edwards AFB CA 93524-7160				<b>8. PERFORMING ORGANIZATION REPORT NO.</b>	
<b>9. SPONSORING / MONITORING AGENCY NAME(S) AND ADDRESS(ES)</b> Air Force Research Laboratory (AFMC) AFRL/RQR 5 Pollux Drive Edwards AFB CA 93524-7048				<b>10. SPONSOR/MONITOR'S ACRONYM(S)</b>	
				<b>11. SPONSOR/MONITOR'S REPORT NUMBER(S)</b> AFRL-RQ-ED-TR-2013-0054	
<b>12. DISTRIBUTION / AVAILABILITY STATEMENT</b> Approved for public release; distribution unlimited. PA No. 14137					
<b>13. SUPPLEMENTARY NOTES</b>					
<b>14. ABSTRACT</b> A novel method to delay transition in hypervelocity flows by using non-equilibrium effects has been studied under Grant 13RQ14COR. The first molecule studied was carbon dioxide (CO <sub>2</sub> ). The motivation arises from experimental and numerical data showing that when pure CO <sub>2</sub> is in vibrational and chemical non-equilibrium, these relaxation processes absorb energy from acoustic disturbances whose growth in the boundary layer is responsible for transition through the 2nd or Mack mode in certain hypervelocity configurations. By absorbing energy at the same frequencies of the acoustic disturbances, non-equilibrium CO <sub>2</sub> delays transition in hypervelocity flows. Before this program, no effort had been made to extend these results to CO <sub>2</sub> injection into base air boundary layers.					
<b>15. SUBJECT TERMS</b> Carbon dioxide; argon; hypervelocity flows; hypersonic vehicles; boundary layer transition; shock tunnels; enthalpy; mach number; damping					
<b>16. SECURITY CLASSIFICATION OF:</b>			<b>17. LIMITATION OF ABSTRACT</b>  SAR	<b>18. NUMBER OF PAGES</b>  97	<b>19a. NAME OF RESPONSIBLE PERSON</b> Dr. Ivett Leyva
<b>a. REPORT</b> Unclassified	<b>b. ABSTRACT</b> Unclassified	<b>c. THIS PAGE</b> Unclassified			<b>19b. TELEPHONE NO (include area code)</b> N/A

This Page Intentionally Left Blank

## TABLE OF CONTENTS

Executive Summary .....	1
Motivation .....	2
Overall Objectives .....	2
Summary of Accomplishments .....	3
Summary of Accomplishments in FY13 .....	7
List of Symbols, Abbreviations, and Acronyms .....	11
References .....	12
Appendix .....	13

## LIST OF FIGURES

Figure 1. Image Showing the Three Different Sections of the Test Model and the Injector in Detail (right) ..	3
Figure 2. Transition Reynolds Numbers for No-injection Cases as well as CO <sub>2</sub> and Argon Injection at Nominal Conditions of P <sub>res</sub> = 55MPa and h <sub>res</sub> = 10MJ/kg .....	4
Figure 3. Transition Onset Location Non-dimensionalized by $\delta_{.99tr}$ at the Transition Location Versus (left) the Edge Mach Number and (right) the Most Amplified Second Mode Frequency at the Transition Location .....	5
Figure 4. Transition Onset Location Versus Reservoir Enthalpy for Air, CO <sub>2</sub> , and Mixture Test Gases .....	6
Figure 5. Transition N-factor for Selected Air and 50/50 Air/CO <sub>2</sub> Running Conditions .....	7
Figure 6. Normalized Transition Onset Location as a Function of the Damping per Wavelength of the 2 <sup>nd</sup> Mode Most Amplified Frequency Evaluated at the Transition Onset Location .....	8
Figure 7. Transition Reynolds Number Evaluated at Dorrance Reference Conditions, Re* <sub>tr</sub> Versus the Damping per Wavelength at the 2 <sup>nd</sup> Mode Most Amplified Frequency Evaluated at the Transition Onset Location .....	8
Figure 8. N Factor Growth for a Baseline Configuration with no Injection and Several other Geometries with Injection .....	9
Figure 9. Model used to Test Injection Process in Ludwig Tube .....	10

This Page Intentionally Left Blank

## Executive Summary

A novel method to delay transition in hypervelocity flows by using non-equilibrium effects has been studied under Grant 13RQ14COR. The first molecule studied was carbon dioxide ( $\text{CO}_2$ ). The motivation arises from experimental and numerical data showing that when pure  $\text{CO}_2$  is in vibrational and chemical non-equilibrium, these relaxation processes absorb energy from acoustic disturbances whose growth in the boundary layer is responsible for transition through the 2<sup>nd</sup> or Mack mode in certain hypervelocity configurations [1-4]. By absorbing energy at the same frequencies of the acoustic disturbances, non-equilibrium  $\text{CO}_2$  delays transition in hypervelocity flows. Before this program, no effort had been made to extend these results to  $\text{CO}_2$  injection into base air boundary layers.

The first part of this program was aimed at injecting  $\text{CO}_2$  to a base air boundary layer flow and to measure its impact on transition delay. The experiments were conducted at Caltech's high-enthalpy reflected shock tunnel, T5. The injector was integrated to a sharp 5° half-angle cone. This canonical shape was chosen because of the wealth of experimental and numerical data available, with which to compare the results from this program. The model was heavily instrumented with thermocouples and shadow-graphs were taken as well. From the heat transfer measurements, the transition locations and effectiveness of  $\text{CO}_2$  can be measured. A set of promising results were obtained by injecting  $\text{CO}_2$  in a narrow band of free-stream conditions [5]. Argon was also injected for comparison and it promoted transition in all cases tested. The fact that injection only seemed to work for a limited set of free-stream conditions led the team to focus on free-stream mixtures versus injection. A thorough investigation of how non-equilibrium effects can be used to delay transition ensued without the added complications of injection and the disturbances that this process causes to the base flow. It was confirmed, through the use of a mixing tank, to ensure thorough mixing of air/ $\text{CO}_2$  test gas mixtures that transition delays occur even for 50/50 air/ $\text{CO}_2$  mixtures as compared with pure air for different conditions studied.

A surprising result consistently found in the course of this grant is that the N-factors measured for typical T5 running conditions with air,  $\text{CO}_2$  and mixtures can be much higher than traditionally accepted empirical correlations predicted for noisy tunnels such as T5. This result deserves further investigation.

As a way to more directly connect local boundary layer conditions to transition, new parameters were explored to non-dimensionalize the transition onset distances instead of only focusing on Reynolds number (Re). A promising new way to collapse transition onset data from different running conditions and gases was found. The traditional correlation of  $Re_{tr}^*$  with both  $P_{res}$  and  $h_{res}$  was also re-examined.

Through a European Office of Aerospace Research & Development (EOARD) grant, analysis was performed to assess the effect of injection on the boundary layer instability growth for potential new injection configurations. Finally, injection visualizations are being carried out at Caltech's Ludwig tube to better understand the impact of injection on the cone flow field.

This project has advanced the state of the art in understanding how to exploit non-equilibrium processes such as vibrational relaxation and chemical dissociation to delay transition caused by 2<sup>nd</sup> mode instabilities. A follow on project could be focused on learning how to determine a-priori what molecules are needed to damp the most unstable modes for a given operating envelope. After the molecule(s) have been specified, experiments could be run in high-enthalpy or other hypersonic facilities to validate the analysis.

## **Motivation**

The main justification for this work is the pressing need to reduce aerodynamic heating rates on hypersonic vehicles. In a simple approximation, hypersonic aerodynamic heating grows as the cube of the free-stream velocity and linearly with free-stream density [6]. This is in addition to the fact that turbulent heat transfer rates can be 5-8 times larger than laminar rates for hypersonic Mach numbers [7]. Hence, for high velocities, the heating loads become dominant in the design of a hypersonic vehicle [6]. A reduction in heating loads means less thermal protection needed and hence less weight to carry, or conversely more payload to deliver for a given thrust. While one might not have control over the free-stream velocity, heating rates can be reduced by keeping the boundary layer laminar for longer lengths with schemes like the one proposed here.

As a 6.2-6.3 continuation to this program, two studies could be completed: 1) optimization of injector schemes to a particular application and 2) feasibility study on using the exhaust from an airbreathing engine as the source of CO<sub>2</sub>.

## **Overall Objectives**

The overall objectives of this task are to understand the effects of vibrational relaxation processes and dissociation on the absorption of acoustic instabilities in the boundary layer of slender cones at zero angle of attack at hypersonic Mach numbers. This knowledge can then lead to the creation of control techniques to delay boundary layer transition. A slender cone at zero angle of attack at hypersonic M is a canonical configuration to study the second or Mack mode transition, which is due to the growth of acoustic waves trapped in the boundary layer, and its interactions with non-equilibrium processes. The experiments are carried out at Caltech's T5 reflected shock tunnel. Based on previous studies [1-4], it is shown that the

relaxation process of non-equilibrium CO<sub>2</sub>, at conditions achieved in T5, can damp the second mode, and therefore transition. This is why CO<sub>2</sub> has been chosen as the first molecule to test for any transition control schemes.

### Summary of Accomplishments

The first part of this program was focused on injection experiments involving CO<sub>2</sub> injection into an air boundary layer in a 5° half angle cone (1 m in length) at zero angle of attack. The results are summarized in [5], which is included in the appendix. A total of 16 shots were analyzed in that study. The conditions were set to be nominally: air at 10 MJ/kg and 55 MPa in the reflected shock region. The cone is made of three sections (Figure 1): a molybdenum sharp tip needed to withstand the high stagnation heat fluxes, followed by an interchangeable piece which can be either the porous injector used in this study or a smooth section, and the main body with 80 thermocouples evenly spaced at 20 lengthwise locations. The porous injector is made of sintered 316L stainless steel with an average pore size of 10 microns and it is 4.13 cm in length. Both CO<sub>2</sub> and argon were injected into the boundary layer for comparison. Argon is a good comparison gas since it does not have any vibrational modes or dissociation and it has about the same molecular weight as CO<sub>2</sub>.

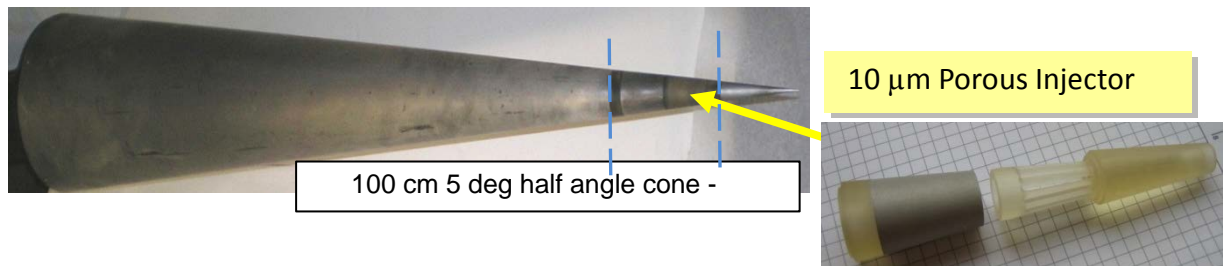


**Figure 1. Image Showing the Three Different Sections of the Test Model and the Injector in Detail (right)**

The onset transition distance was calculated with two methods, an intermittency method applied to the heat flux [5] and the traditional method used in the past in T5 whereby the transition onset is set to where the average normalized heat flux departs the predicted laminar values. The results are shown in Figure 2. *Transition delays were realized for some CO<sub>2</sub> injection cases, compared to both shots with a porous injector but no injection, and control shots with a smooth injector section.* This was the first team transition delay that was measured by using the concept studied in this grant. Initially, delay increased with injection rate, but there is a sharp dropoff at the highest injection rate, due possibly to boundary layer detachment. All three Argon injection conditions transitioned far earlier than any CO<sub>2</sub>. For future injection cases, the injection mass flow rates need to be more accurately determined.

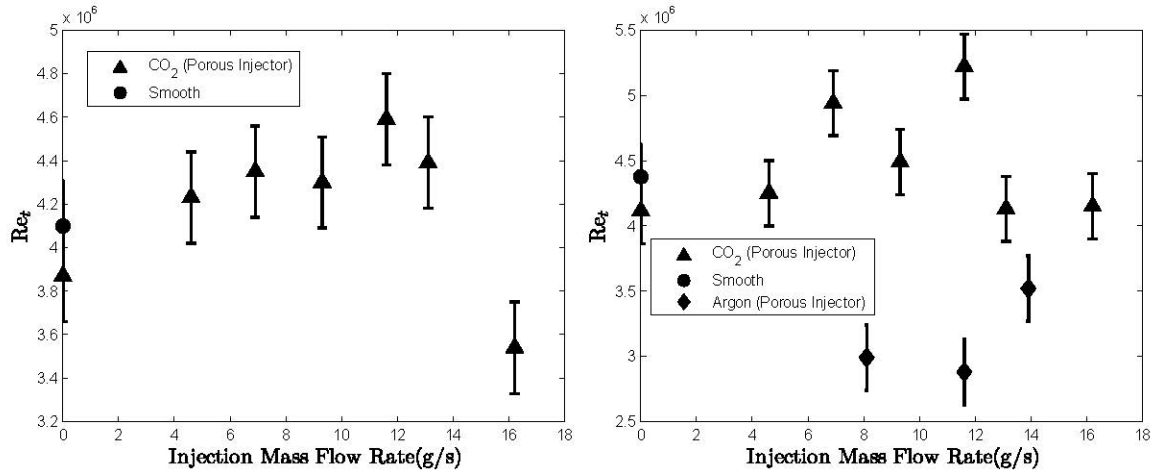


**Figure 2. Transition Reynolds Numbers for No-injection Cases as well as  $CO_2$  and Argon Injection at Nominal Conditions of  $P_{res} = 55MPa$  and  $h_{res} = 10MJ/kg$**

Left: transition  $Re$  obtained by the intermittency method. Right: transition  $Re$  obtained by the average normalized heat flux trends.

The above results looked very promising and many more cases were run at different tunnel conditions. Because transition delays were achieved only for the condition explored before, it was decided to switch the emphasis of the program away from injection to more controllable gas-mixtures in the test section with no injection. By studying gas-mixtures as the test gas, the effects of non-equilibrium processes on transition can be isolated from those of injection. Injection introduces an extra layer of complexity to the problem since the injection process should not disturb the boundary layer and cause it to transition earlier.

The team also devoted a lot of attention to re-examining the dependencies of transition onset on the operating parameters of T5 and in terms of local boundary layer properties. The results of this work are detailed in Jewell et al [8] and only highlights will be presented here. The motivation was twofold: to understand if a new set of variables could better collapse transition onset data and to re-examine the effects of both reservoir pressure ( $P_{res}$ ) and reservoir enthalpy ( $h_{res}$ ) on transition Reynolds numbers. Traditionally  $Re$  and  $Re^*$  (using Dorrance reference conditions) evaluated at the transition onset location  $x_{tr}$ , are used to express the transition onset in a non-dimensional form. However, because the transition mode we are studying is an inviscid mode, we explored if the instability mechanism could be more directly related to the boundary layer properties, such as thickness and edge velocity (which dictate the most amplified 2<sup>nd</sup> mode frequency) or thermodynamic variable profiles. To this end, the onset transition was non-dimensionalized by the boundary layer thickness ( $x_{tr}/\delta_{99tr}$ ) at the transition location, and plotted against the edge Mach number,  $M_{edge}$ , (left plot on Figure 3) and the most amplified 2<sup>nd</sup> mode frequency at the transition location  $\sim 0.6u_e/2\delta_{99tr}$  (right plot in Figure 3).

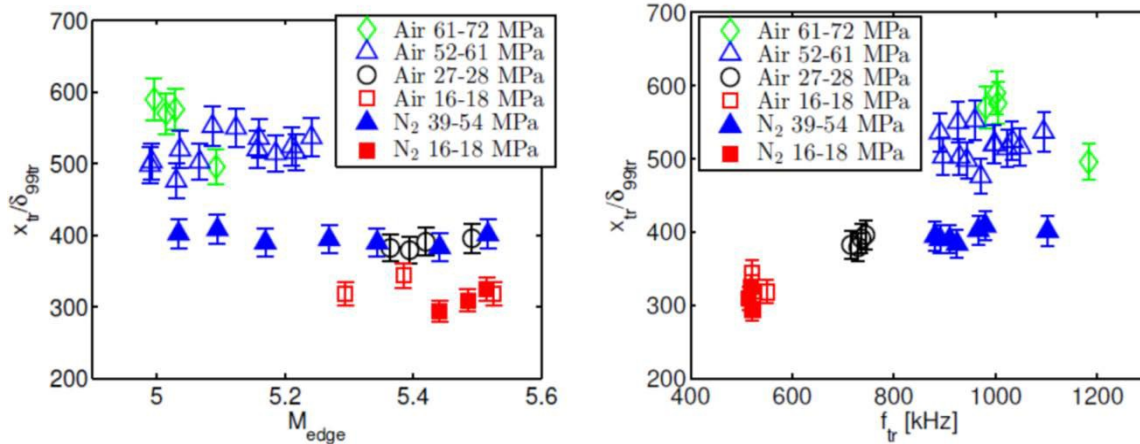


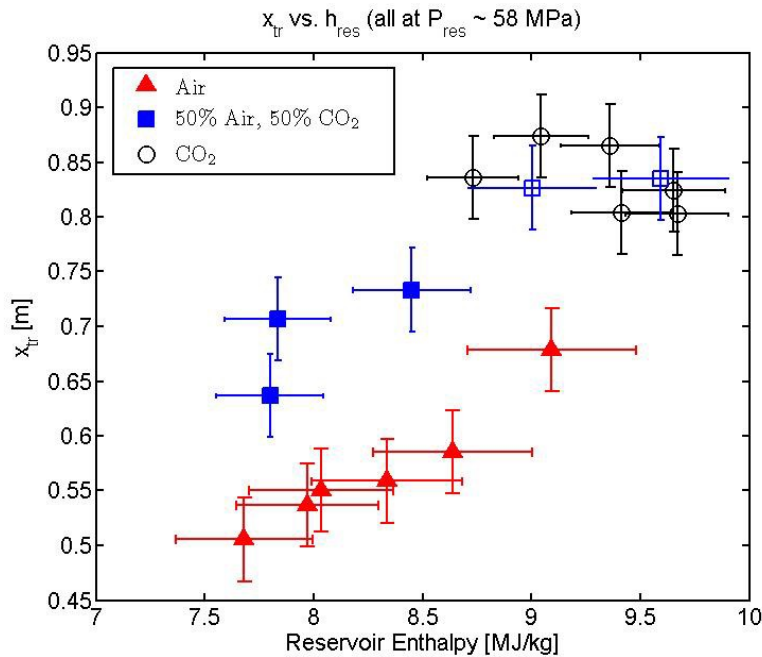
**Figure 3. Transition Onset Location Non-dimensionalized by  $\delta_{99tr}$  at the Transition Location Versus (left) the Edge Mach Number and (right) the Most Amplified Second Mode Frequency at the Transition Location**

The data shows a dependence on  $M_{edge}$  for a given gas type and reservoir pressure, but within a given pressure range there does not seem to be a strong dependence on  $M_{edge}$ . On the other hand,  $x_{tr}/\delta_{99tr}$  seems to increase with  $f_{tr}$ . Two observations might explain this trend. First, lower reservoir pressure results in thicker boundary layers with lower most amplified frequencies. Second, Parziale et al [9] found that there is a frequency-dependency on the amplitude of noise present in T5's free stream with the highest amplitudes being for less than 500 kHz. Therefore, one would expect that systems with dominant unstable frequencies in that range would transition faster.

In terms of the effects of  $P_{res}$  and  $h_{res}$  on transition Reynolds number, another key finding from Jewell et al [8] is that  $Re^*_{tr}$ , commonly used to express the transition location, has a positive correlation with  $P_{res}$ , but no statistically significant dependence on  $h_{res}$  for the wide range of air and N<sub>2</sub> data analyzed. On the other hand,  $x_{tr}$  has a positive correlation with  $h_{res}$  in both air and N<sub>2</sub> but a negative correlation with  $P_{res}$ .

A series of experiments with pure CO<sub>2</sub> and air as the test gas as well as mixtures of CO<sub>2</sub> and air (50/50 by mass) was then completed and are presented in Figure 4. The main objective was to measure the effect of different concentrations of CO<sub>2</sub> on transition. The reservoir pressure was held about constant for all cases so that effects of reservoir enthalpy could be isolated. The hollow symbols signify cases where no transition onset was measured by the end of the cone. What is remarkable about this data is that even for 50/50 air/CO<sub>2</sub> mixtures there is a measurable delay in transition compared to pure air cases for a given  $h_{res}$ . *These results are encouraging as the foundation to design new injection cases, assuming the injection process does not trip the boundary layer.* However, for these mixture cases, CO<sub>2</sub> and air were mixed in the shock tube

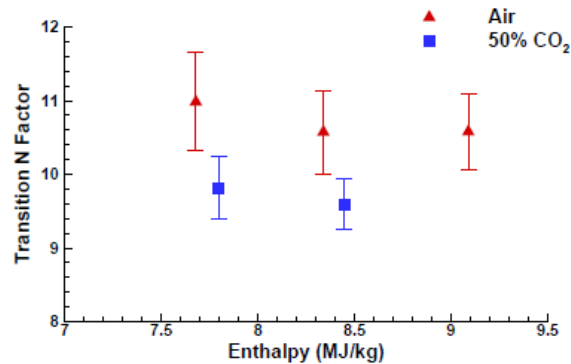
and thorough mixing was not guaranteed since no active mixing occurred. Furthermore, to be able to quantify transition delays in CO<sub>2</sub>, cases are needed where transition occurs in the cone and therefore can be measured. All these reasons led the team to design and build a mixing tank where CO<sub>2</sub>/air mixtures are actively mixed before they are introduced into the shock tube. Also, a new set of conditions with pure CO<sub>2</sub> that would transition before the end of the cone was designed based on the findings from this test campaign and computations of N-factors. These tasks were successfully completed in FY 13.



**Figure 4. Transition Onset Location Versus Reservoir Enthalpy for Air, CO<sub>2</sub>, and Mixture Test Gases**

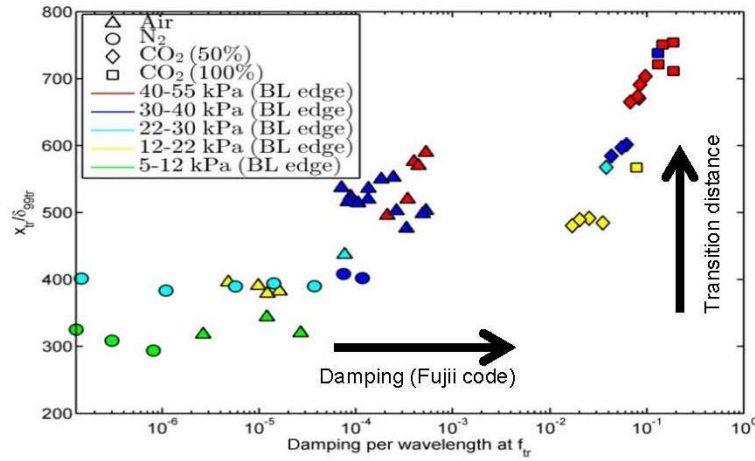
### Summary of Accomplishments in FY13

The N-factors corresponding to the measured transition locations from some of the data points included in Figure 4 are presented in Figure 5. The N-factors were calculated using the STABL code developed by the University of Minnesota and with the help of Dr. Ross Wagnild, now at Sandia National Labs. The details of these calculations are found in Jewell et al [10]. Empirical correlations predict a transition N-factor of about 5-6 for noisy tunnels like T5. What is striking from the data is that the measured N-factors are much bigger than 5-6 for both air and air/CO<sub>2</sub> mixtures. In fact, this empirical rule of thumb was used to design some of the conditions shown in Figure 4 which did not transition before the end of the cone. To the author's knowledge, the analysis performed on the experiments executed under this grant is one of the first to show much larger transition N-factors for a noisy tunnel.



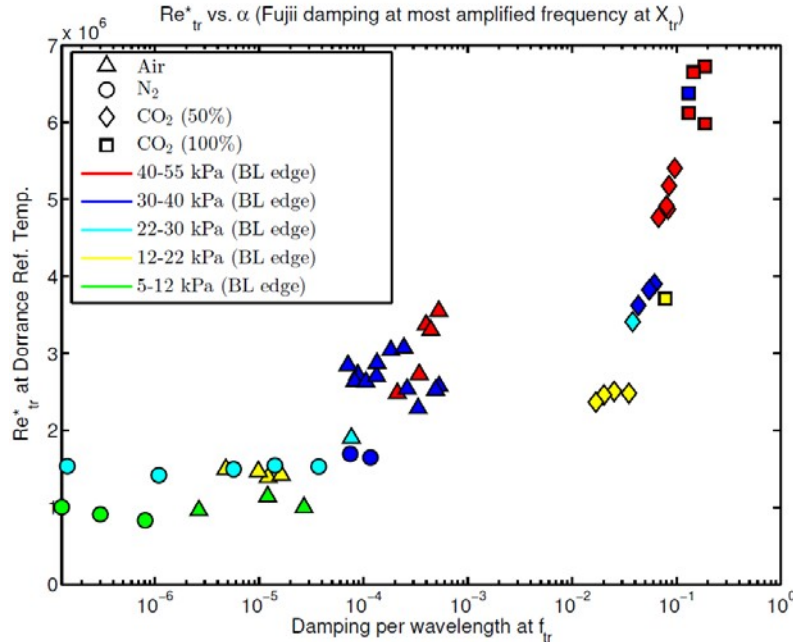
**Figure 5. Transition N-factor for Selected Air and 50/50 Air/CO<sub>2</sub> Running Conditions**

The results from the new test campaign completed in FY 13 are presented in Figure 6. In this case, the normalized transition onset distances are plotted against damping per wavelength at the 2<sup>nd</sup> mode most amplified transition computed at the transition onset location (see [1] for details on calculating damping rates). Note that the earliest transitions happen where there is the least amount of damping at the most unstable frequencies by non-equilibrium relaxation processes. Among the many possible reasons for low damping are: a large mismatch between the gas temperature and the characteristic relaxation temperatures of the gas; dissociation rates at relevant frequencies are too low; or the characteristic vibration relaxation frequencies of the gas might be far from the most amplified frequencies. As the damping per wavelength at the most amplified frequencies increases, so does the transition onset distance. That is, the more damping per wavelength that happens close to the most unstable frequencies, the more transition delay is achieved. *This new way to analyze the data is a great step toward collapsing transition on-set data from different running conditions and gases onto a single trend.* Also note that the new CO<sub>2</sub> conditions run were successfully designed to transition before the end of the cone. The next step is incorporating the frequency-dependent amplification of the noise present in T5 free-stream in the analysis. That question could be the subject of a future research project.



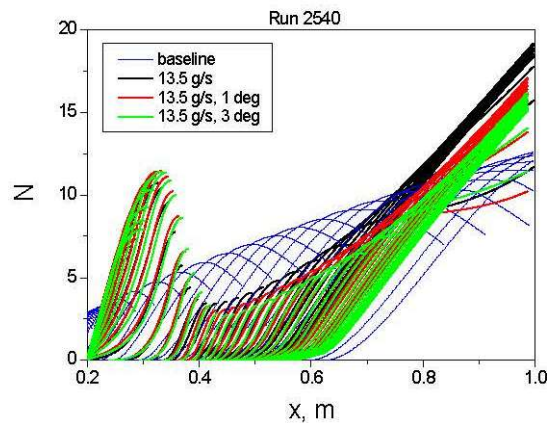
**Figure 6. Normalized Transition Onset Location as a Function of the Damping per Wavelength of the 2<sup>nd</sup> Mode Most Amplified Frequency Evaluated at the Transition Onset Location**

Figure 7 offers another method to analyze the same data presented in Figure 6. In this case, the transition onset location is normalized through the use of  $Re^*$ . The trends and conclusions are similar to those drawn from Figure 6 except that the data collapse appears to be somewhat better. The results of this research will be published in detail in an upcoming Ph.D. thesis from Joe Jewell from Caltech, expected to be available in the spring of 2014.



**Figure 7. Transition Reynolds Number Evaluated at Dorrance Reference Conditions,  $Re^*_{tr}$  Versus the Damping per Wavelength at the 2<sup>nd</sup> Mode Most Amplified Frequency Evaluated at the Transition Onset Location**

Through an EOARD grant with Prof. Alexander Fedorov, from the Moscow Institute of Physics and Technology, he was able to study the growth of the instabilities in a cone boundary layer when CO<sub>2</sub> is injected. He was able to run different injection geometries which try to compensate for the CO<sub>2</sub> blowing effect on the displacement thickness and minimize the disturbance to the boundary layer. Although these computations are made with perfect gases, they provide insight into the disturbance created by injection. The results are shown in Figure 8. His results show a big disturbance to the boundary layer in the injection region. In fact, the N-factor grows to around 12, which is most likely enough to trip the boundary layer. If the flow can tolerate the effects from injection, the results show that the disturbances decrease and eventually grow again at a faster rate than they would with no injection. The results are encouraging in that they show that the analysis captures the process of injection and its effects on the boundary layer instability growth. Alternative injection schemes to reduce the impact to the boundary layer in the injection region and the incorporation of real gas effects could be the subject of a renewal contract through EOARD.



**Figure 8. N Factor Growth for a Baseline Configuration with no Injection and Several other Geometries with Injection**

The last topic covered in FY 13 was injection visualization through experiments performed in Caltech's Mach 4 Ludwig tube to visualize CO<sub>2</sub> injection in supersonic flow. A schematic representation of the test model is shown in Figure 9. The model has a 127 mm long sharp tip, followed by a 38 mm porous injector made by Mott (10 μm). Preliminary test results done with different injection mass flow rates show qualitatively the effect of the injection on the boundary layer and the formation of a shock wave off the cone tip for some conditions. The injection process can create a shear-layer like instability which can be seen to grow on the visualizations completed. Future studies are focused on how to minimize the velocity difference between the injected gases and the base boundary layer gases so that the shear-layer instability growth is reduced.



***Figure 9. Model used to Test Injection Process in Ludwig Tube***

## List of Symbols, Abbreviations, and Acronyms

CO <sub>2</sub>	carbon dioxide
EOARD	European Office of Aerospace Research & Development
Re	Reynolds number

## References

1. Fujii, K. and Hornung, H. G., "A Procedure to Estimate Absorption Rate of Sound Propagating Through High Temperature Gas," California Institute of Technology, Pasadena, CA, Aug. 2001, GALCIT Report FM2001.004.
2. Fujii, K., Hornung, H.G., "Experimental investigation of high-enthalpy effects on attachment-line boundary layer transition," AIAA Journal, Vol. 41, No. 7, July 2003.
3. Hornung, H.G., Adam, P.H., Germain, P., Fujii, K., Rasheed, A., "On transition and transition control in hypervelocity flows," Proceedings of the Ninth Asian Congress of Fluid Mechanics
4. Johnson, H.B., Seipp, T.G., Candler, G.V., "Numerical study of hypersonic reacting boundary layer transition on cones," Physics of Fluids, 10 (10): 2676-2685 Oct. 1998.
5. Jewell, J.S., Leyva, I.A., Parziale, N.J. and Shepherd, J.E., "Effect of gas injection on transition in hypervelocity boundary layers," Proceedings of the 28th International Symposium on Shock Waves, Vol. 1, pp. 735–740, 2011.
6. Anderson Jr., J.D., Hypersonic and High Temperature Gas Dynamics, McGraw-Hill 1989.
7. Heisner, W.H., Pratt, D.T., "Hypersonic Airbreathing Propulsion," AIAA Education Series, 1994.
8. Jewell, J.S., Shepherd, J.E., Leyva, I.A., "Shock tunnel operation and correlation of boundary layer transition on a cone in hypervelocity flow," to appear in the proceedings of the 29th International Symposium on Shock Waves.
9. Parziale, N.J., Shepherd, J.E. and Hornung, H.G., "Reflected shock tunnel noise measurement by focused differential interferometry," AIAA 2012-3261 (2012).
10. Jewell, J.S., Wagnild, R.M., Leyva, I.A., Candler, G.V. and Shepherd, J.E., "Transition within a hypervelocity boundary layer on a 5-degree half-angle cone in air/CO<sub>2</sub> mixtures," AIAA 2013-0523.

## Appendix

### Collection of papers published under Grant LRIR 13RQ14COR --- ordered by date

1. Leyva, I. A., Laurence, S., Beierholm, A. W., Hornung, H. G., Wagnild, R., Candler, G., "Transition delay in hypervelocity boundary layers by means of CO<sub>2</sub>/acoustic instability interactions," AIAA 2009-1287
2. Leyva, I. A., Jewell, J. S., Laurence, S., Hornung, H. G., Shepherd, J. E., "On the Impact of Injection Schemes on Transition in Hypersonic Boundary Layers," AIAA-2009-7204.
3. Wagnild, R. M., Candler, G. V., Leyva, I. A., Jewell, J. S., Hornung, H. G., "Carbon Di- oxide Injection for Hypervelocity Boundary Layer Stability," AIAA 2010-1244.
4. Jewell, J.S., Leyva, I.A., Parziale, N.J., Shepherd, J.E., "Effect of gas injection on transition in hypervelocity boundary layers," Proceedings of the 28th International Symposium on Shock Waves, Vol. 1, pp. 735–740, 2011.
5. Jewell, J.S., Parziale, N.J., Leyva I.A., Shepherd, J.E., "Turbulent Spot Observations within a Hypervelocity Boundary Layer on a 5-degree Half-Angle Cone", AIAA 2012-3062
6. Jewell, J.S., Wagnild, R.M., Leyva, I.A., Candler, G.V., and Shepherd, J.E., "Transition with- in a hypervelocity boundary layer on a 5-degree half-angle cone in air/CO<sub>2</sub> mixtures," AIAA 2013-0523.
7. Jewell, J.S., Shepherd, J.E., Leyva, I.A., "Shock tunnel operation and correlation of boundary layer transition on a cone in hypervelocity flow," to appear in the proceedings of the 29th International Symposium on Shock Waves, 2013

# Transition delay in hypervelocity boundary layers by means of CO<sub>2</sub>/acoustic instability interactions

Ivett A Leyva<sup>1</sup>,

*Air Force Research Laboratory, Edwards AFB, Ca, 93536*

Stuart Laurence<sup>2</sup>, Amy War-Kei Beierholm<sup>3</sup>, Hans G. Hornung<sup>4</sup>  
*Caltech, Pasadena, Ca, 91125*

and

Ross Wagnild<sup>5</sup>, Graham Candler<sup>6</sup>

*University of Minnesota, Minneapolis, Mn, 55455*

A novel method to delay transition in hypervelocity flows over slender bodies by injecting CO<sub>2</sub> into the boundary layer of interest is investigated. The results presented here consist of both experimental and computational data. The experimental data was obtained at Caltech's T5 reflected shock tunnel, while the computational data was obtained at the University of Minnesota. The experimental model was a 5 degree sharp cone, chosen because of its relevance to axisymmetric hypersonic vehicle designs and the wealth of experimental and numerical data available for this geometry. The model was instrumented with thermocouples, providing heat transfer measurements from which transition locations were determined and the efficacy of adding CO<sub>2</sub> in delaying transition was gauged. For CO<sub>2</sub>/N<sub>2</sub> freestream blends without injection, the transition Reynolds number more than doubled for mixtures with 40% CO<sub>2</sub> mole fraction compared to the case of 100% N<sub>2</sub>. For the cases with injection, shadowgraph visualizations were obtained, allowing verification of the injection timing. The computations provide encouraging results that for the injection schemes proposed CO<sub>2</sub> is reaching high enough temperatures to excite vibrational modes and thus delay transition.

## Nomenclature

$a$	=	speed of sound
$\tau$	=	characteristic time of relaxation process
$\omega$	=	angular acoustic frequency
Subscripts		
$e$	=	equilibrium or boundary layer edge conditions
$f$	=	frozen

<sup>1</sup> Lead, Combustion Devices Group, AFRL/RZSA, Edwards AFB, CA, AIAA Senior Member.

<sup>2</sup> Postdoctoral Researcher, Caltech, Pasadena, CA.

<sup>3</sup> Former Graduate Student, Caltech, Pasadena, CA now in London, UK.

<sup>4</sup> Professor Emeritus, Caltech, Pasadena, CA, AIAA Fellow.

<sup>5</sup> Graduate Student, University of Minnesota, Minneapolis, MN, AIAA Student Member.

<sup>6</sup> Professor, University of Minnesota, Minneapolis, MN, AIAA Fellow.

## I. Introduction

The main justification for this work is the pressing need to reduce aerodynamic heating rates and drag on hypersonic vehicles, for example, the vehicle configurations being studied for a Rocket Based Combined Cycle (RBCC). In a simple approximation, hypersonic aerodynamic heating grows as the cube of the free-stream velocity and linearly with the free-stream density [1]. This, combined with the fact that turbulent heat transfer rates can be an order of magnitude higher than laminar rates for hypersonic Mach numbers [2], result in heating loads becoming a dominant factor in the design of hypersonic vehicles [1]. A reduction in the heating loads allows less thermal protection and hence less weight to carry, or conversely more payload to deliver for a given thrust. While the free-stream velocity may be set for a given application, heating rates and frictional drag can be reduced by keeping the boundary layer laminar for over greater portions of the vehicle body with schemes such as the one proposed here.

A novel method for delaying transition in hypervelocity flows of air by injecting CO<sub>2</sub> into the boundary layer of interest is explained and investigated here. The motivation for this new technique lies in the combination of three relevant findings. The first finding is that, at high Mach numbers, transition occurs through the second (Mack) mode, i.e., amplification of acoustic waves traveling within the boundary layer. The second fact is that molecular vibration and dissociation damp acoustic waves as will be discussed in more detail later in the paper. The third fact is that at relevant conditions for hypersonic flight, CO<sub>2</sub> absorbs energy most strongly at the frequencies most amplified by the Mack mode. Experimental and numerical data show that for a range of about 4-10 MJ/kg, pure CO<sub>2</sub> flows exhibit a significant delay in transition Reynolds number as compared to air and nitrogen flows. Combining these three facts, the idea proposed and investigated here is to inject CO<sub>2</sub> into a boundary layer of interest such that transition can be delayed. Since this is the first time this idea has been put forward, a theoretical, experimental and numerical background is first laid out, then experimental results are presented using CO<sub>2</sub> mixtures in the free stream, without injection, to show the plausibility of the concept. Finally, numerical simulations are presented for proposed injection schemes into the boundary layer.

## II. Background

For hypervelocity (both high enthalpy and high Mach number) flows, and especially for highly cooled wall situations, such as those encountered in a reflected-shock tunnel, the dominant transition mechanism is the second or Mack mode [3]. This is an inviscid instability mode associated with wave-like disturbances that become trapped within the boundary layer. This is in contrast to low-speed flows in which the first mode, a viscous mode associated with Tollmien-Schlichting waves [4], is dominant. A decade of research has been carried out in the T5 reflected shock tunnel at Caltech on the effects of vibrational non-equilibrium and dissociation on transition in hypervelocity flows, and is summarized in Hornung et al. [5]. Initial studies focused on transition on a 5-degree sharp cone. The cone was instrumented with thermocouples from which heat flux profiles were obtained and transition locations were determined. A rapid rise in the heat flux denotes transition. The model was tested in air, N<sub>2</sub>, and CO<sub>2</sub>, with flow total enthalpies ranging from 3 to 15 MJ/kg. A dramatic transition delay was measured in pure CO<sub>2</sub> flows, as may be observed in Figure 1 (taken from [5]). In this figure,  $Re_{tr}^*$  is the transition Reynolds number based on the distance from the cone tip to the transition location. The flow properties are evaluated using the Eckert's reference temperature [6] which has found to be appropriate for discerning trends between different gases at different stagnation enthalpies. Figure 1 shows that the  $Re_{tr}^*$  for CO<sub>2</sub> flows is typically about four to five times that of air or N<sub>2</sub> flows of the same flow total enthalpy,  $h_o$ . This phenomenon is not observed in low speed flows. These results also point to transition occurring through the second mode, and are thus indicative of nonequilibrium effects playing a role in attenuating the acoustic waves responsible for transition in this mode.

In an effort to understand these findings, Johnson et al. [7] at the University of Minnesota teamed up with the T5 group and performed numerical studies on several of the experimental conditions ran in T5 by Adam and Hornung [8]. Linear stability analyses were carried out in which the transition  $Re^*$  in CO<sub>2</sub>, air, and N<sub>2</sub> flows were computed under the assumption that the boundary layer transition is caused by the amplification of wave-like disturbances originating in the mean flow (i.e., the second mode). The results of these computations, shown in Figure 2, confirm the experimental observations of Hornung et al. [5]. For the case of air (shot 1162,  $h_o=9.3$  MJ/kg), whether the flow disturbances are reacting or not (this includes both dissociation and vibrational processes) has no impact on the stability of the flow, since, for  $x>0.106$ m, disturbances in the boundary layer grow in either case (note that the mean flow is assumed to be reacting irrespective of the assumption made of the disturbances). The experimental data for

this condition showed transition occurring at  $Re_{tr}^* \sim 1e6$ . However, in the analysis performed in the case of  $CO_2$  (shot 1150,  $h_0=4MJ/kg$ ), a crucial difference is observed depending on whether the disturbances are assumed to be reacting or nonreacting. In the reacting case, the flow is shown to be stable at all  $x$  locations examined and thus no transition is expected over the length of the cone. In contrast, the flow is seen to be unstable if the disturbances are nonreacting. The experimental data for this shot shows almost fully laminar flow, with weak signs of transition towards the end of the cone. Johnson et al. [7] conclude that it is the low dissociation energy of the  $CO_2$  molecule, together with its large number of vibrational modes, that absorb energy from acoustic disturbances in the boundary layer and thus delay transition. It is further noted that, even though transition is a non-linear phenomenon, the frequency of the most amplified disturbance found by a linear analysis is the same as in the non-linear regime. Also, the linear amplification step is the slowest of the steps leading to transition [7]. Therefore, linear analysis can be used to give an order of magnitude prediction on the growth rate and dominant frequencies of the acoustic disturbances in the boundary layer.

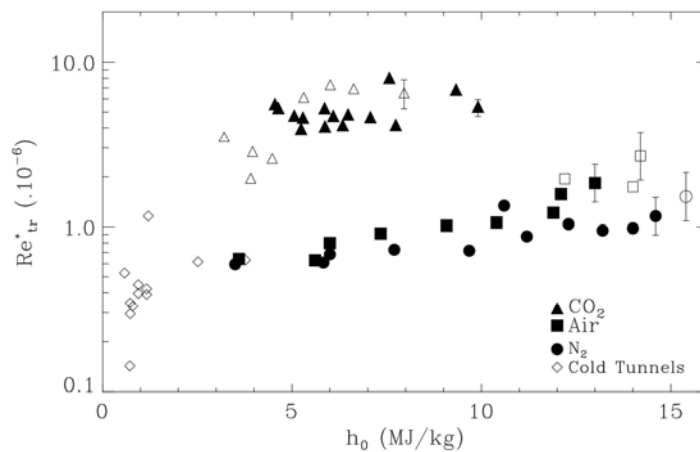


**Figure 1. Transition reference Reynolds number for  $CO_2$ , Air, and  $N_2$  flows as a function of the flow total enthalpy. The open symbols (non-diamond) are for cases where the flow was laminar to the end of the cone, and thus represent lower bounds. The “Cold Tunnels” data was obtained from independent researchers. Taken from [5].**

A few years later, Fujii et al. [9-10] performed a numerical and experimental analysis of the effects of relaxing processes on transition on swept cylinders with sweep angles of 45 and 60 degrees. In this work, the sound absorption rates per wavelength resulting from finite rate relaxation processes are computed for  $N_2$ ,  $CO_2$ , and air at different temperatures. Further details of these computations can be found in Fujii [11]. These computed absorption rates are then compared with the growth rates of wave disturbances in the boundary layer, calculated using an inviscid linear stability analysis based on the work of Reshotko and Beckwith [12], and Mack [3]. The gas is assumed to be perfect in both the mean flow and the disturbances. The results from this analysis are shown in Figure 3 (taken from [10]). In the right plot, showing the case of  $CO_2$ , the sound absorption rates (open symbols) are of the same order as the amplification rates for the acoustic disturbances (filled symbols) in the range of frequencies (1-10 MHz) where the acoustic disturbances are most amplified. From this, a significant effect of the relaxation processes on acoustic damping would be expected. It is also worth noting the breadth of the absorption curves, indicating that this damping is effective over a large range of frequencies. In contrast, for the case of air, the sound absorption rates peak at much lower frequencies than those at which the acoustic amplification rates become significant. Thus, no delay in transition due to non-equilibrium processes would be expected in this case. Experimental results were also obtained as part of this study that agree with the predictions of the numerical analysis.

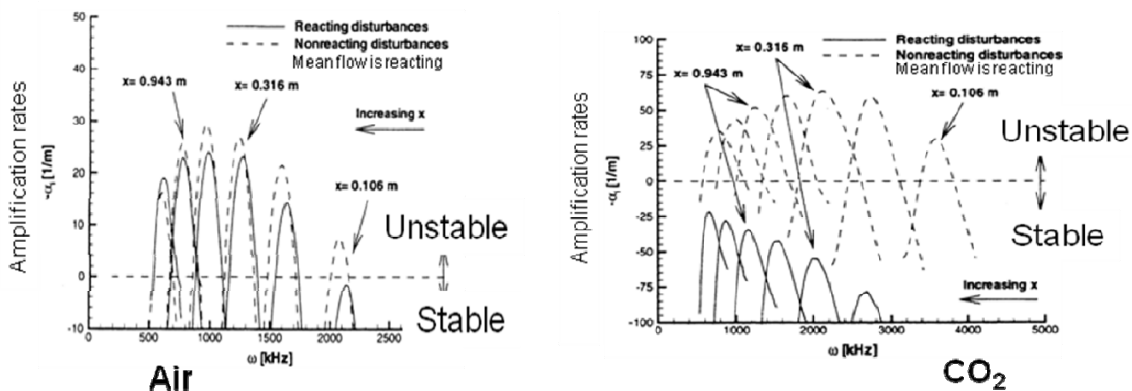


Figure 2. Numerical simulations showing the impact of reacting and nonreacting disturbances on the boundary layer flow stability. Taken from [7]

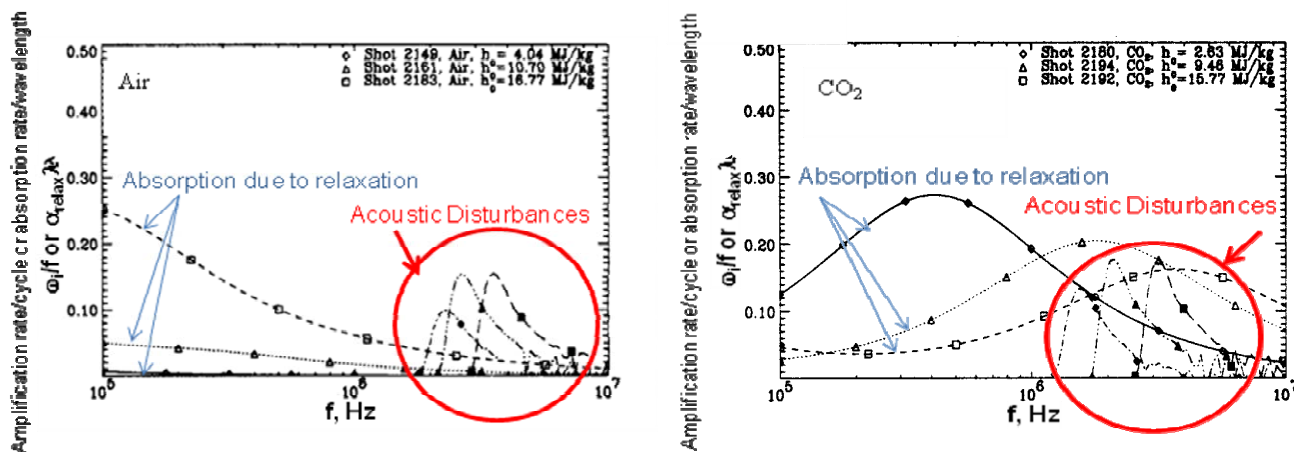


Figure 3. Comparison of absorption rate per wavelength due to relaxation (open symbols) and the amplification rate per cycle (filled symbols) for air and  $\text{CO}_2$ . The shots refer to particular conditions tested in the T5 facility for a 45-degree swept cylinder. Taken from [10].

The theory of how relaxation processes absorb energy from acoustic disturbances has been known for decades. Lighthill published an extensive article on the subject in 1956 [13], followed by other detailed treatments by Herzfeld and Litovitz [14] in 1959, Clarke and McChesney [15] in 1964 and Vincenti and Kruger [16] in 1965. An intuitive way of understanding this absorption phenomenon is presented in Figure 4. It is assumed here that the gas conditions (temperature and pressure) are close to the characteristic conditions of the given vibration or dissociation process, that the ratio of the frozen to equilibrium speeds of sound is greater than one (i.e., an endothermic reaction), and that the amplitude of the pressure disturbance is small. Examining first the case of a frozen gas, for which the product of the characteristic acoustic disturbance frequency ( $\omega$ ) and the relaxation time ( $\tau$ ) tends to infinity,  $\tau\omega \rightarrow \infty$ , if an acoustic field ( $p'$ ) is imposed, the variations in density ( $\rho'$ ) will occur along an isentrope (shown as the blue line) characterized by the frozen speed of sound,  $a_f$ . Similarly if the gas is in equilibrium ( $\tau\omega \rightarrow 0$ ), the variations in  $\rho'$  will happen along a different isentrope (shown as the red line) characterized by the equilibrium speed of sound,  $a_e$ . Given the two slopes of the isentropes, one can see that in this case  $a_f > a_e$ . For these two cases, the variations in  $p'$  and  $\rho'$  are in phase since they both cross zero at the same time. If the gas is now in nonequilibrium, however, with the acoustic characteristic time of the same order as the relaxation time,  $\tau\omega \sim 1$ , a different behavior results. For this case, changes in density imposed by changes in pressure don't happen instantly, but rather a number of

collisions are required for the gas to achieve a new value of density. This is represented in the  $p$ - $\rho$  diagram as a close curved rather than as a line, indicating the assumption of a limit cycle. As may be seen, the zeros of  $p'$  and  $\rho'$  now no longer coincide, and a lag is present between the pressure and density changes. The area encompassed by this curve is related to the energy absorbed by the relaxation process in the nonequilibrium gas, which damps the growth of the acoustic waves and thus delays transition. In the situation of interest in the present work, the  $\text{CO}_2$  gas injected into the boundary layer is quickly heated to the point where dissociation and/or vibrational nonequilibrium is excited. Then, by the mechanism shown in figure 4, these processes absorb energy from the acoustic waves trapped in the boundary layer. As the  $\text{CO}_2$  gas moves along the surface of the cone, it convects this energy away and transfers it to its environment as heat. As heat, this energy does not contribute to transition anymore.

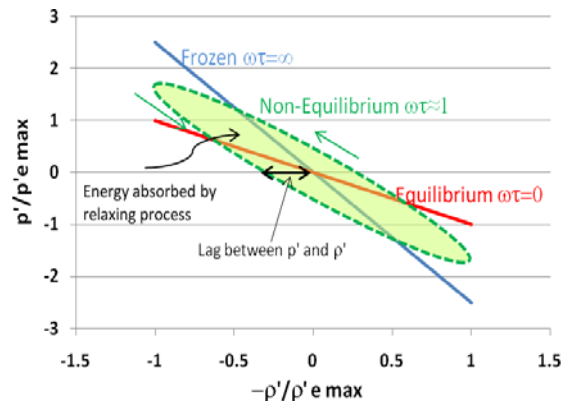


Figure 4. Schematic showing the response of frozen, equilibrium and nonequilibrium gases to small disturbances.

### III. Experimental Setup

The facility used in all experiments in the current study was the T5 hypervelocity shock tunnel at the California Institute of Technology. It is the fifth in a series of free-piston driven, reflected shock tunnels built by R.J. Stalker, H.G. Hornung and colleagues [17-18]. The T5 facility consists of four major components: the secondary air reservoir (2R), the compression tube (CT), the shock tube (ST), and the test section/dump tank. The first three of these components are illustrated in Figure 5.

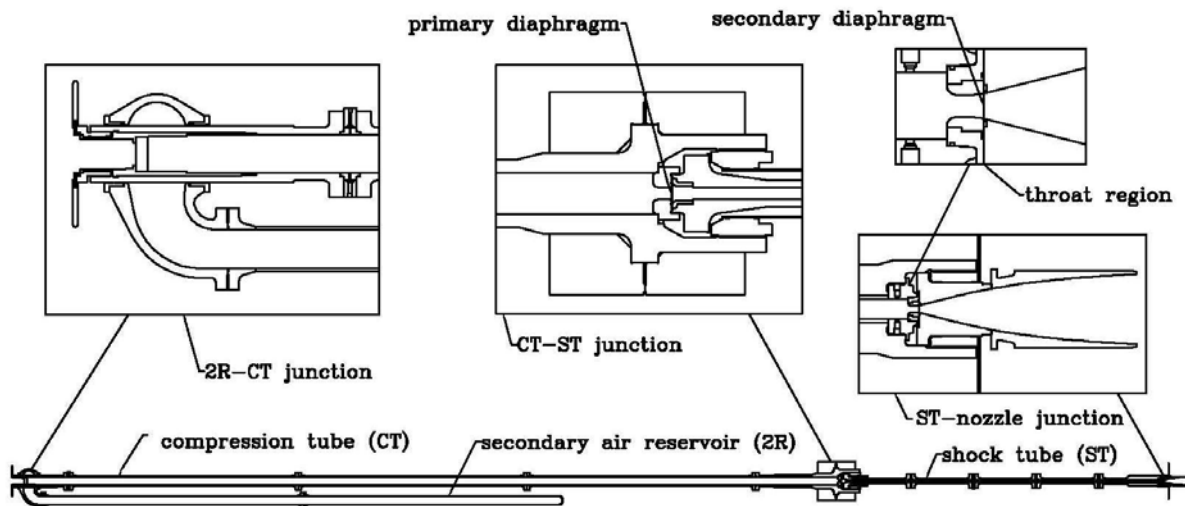


Figure 5: Schematic of the T5 hypervelocity shock tunnel facility.

The test flow is generated by driving a heavy (120 kg) piston down the CT with the release of high-pressure air from the 2R. The CT gas, a mixture of helium and argon, is compressed adiabatically by the advance of the piston until the pressure is sufficiently high to burst the primary diaphragm, located at the junction of the CT and ST. The primary diaphragm typically consists of a 0.187 to 0.270-inch thick stainless steel plate, etched with an X-shaped groove to control the burst pressure. The test gas is initially contained in the ST; the burst of the primary diaphragm produces a shock wave that travels the length of the ST and reflects from the end wall. Stagnation conditions are thus produced at the end of the ST, which then serves as the reservoir for the nozzle expansion. The incident shock also bursts the secondary diaphragm, consisting of a 0.002" mylar membrane located at the ST-nozzle junction. The test gas expands through the nozzle, flowing into the test section and finally into the dump tank. The test section and dump tank are initially evacuated, separated from the ST by the secondary diaphragm. Startup of the flow in the test section typically takes 1ms from the time of arrival of the incident shock at the nozzle throat; the test time is of the order of 1-2 ms. In all experiments in the present series, a contoured nozzle of area ratio 100 was used. The initial pressures in the 2R, CT, and ST were typically 800-1150 psi, 98-116 kPa, and 76-117 kPa, respectively. Test gases were N<sub>2</sub>, air, CO<sub>2</sub>, and combinations thereof.

The T5 facility is instrumented with various diagnostic tools. Most relevant for the present experiments are the accelerometer attached to the CT, used here to trigger the CO<sub>2</sub> injection, and several pressure transducers along the length of the ST. These transducers are used to measure the incident shock speed and reservoir pressure, from which the flow enthalpy is calculated using the ESTC program, and to trigger the T5 data acquisition system (DAS). The T5 DAS allows simultaneous recording of up to 80 data channels (in addition to the facility data) at a sampling rate of 200 kHz. The T5 optical setup is a typical Z-arrangement Schlieren system, capable of recording either a single frame or a sequence of high-speed images during the test period.

The model employed in the current experiments was the slender cone used in a number of previous experimental studies in T5, including that of Adam [8]. It is a 5 degree half-angle cone of approximately 1m in length and is composed of three sections: a sharp tip fabricated of molybdenum (to withstand the high heat fluxes), a mid-section, and the main body instrumented with 21 thermocouples. This shape was chosen because of the wealth of experimental and numerical data available, which will be used for comparison with the results from this program. A photograph of the cone model is shown in Figure 6.



**Figure 6. Cone model used for all experiments in this study. The solid mid-section, used in most experiments, has here been replaced by an injection tip.**

## IV. Experimental Results

### A. Freestream blends

In initial experiments, mixtures of  $N_2$  and  $CO_2$  in various ratios were used as the test gas, with no injection. These runs serve as a baseline, assessing the effect of the presence of  $CO_2$  in the boundary layer independent of any injection scheme. The average  $p_0$  for these runs was 51MPa and the average mixture  $h_0$  was 10.7 MJ/kg; the run conditions are given in the Appendix. The transition location for each shot was deduced from the heat transfer profile obtained along the length of the cone. Figure 7 shows a typical heat flux profile, plotted as the Stanton number versus the Reynolds number based on the thermocouple location and edge conditions. Lines corresponding to both laminar and turbulent theoretical (or semi-empirical) predictions are also shown. In the turbulent case, two of the more successful models are computed. In the case shown, the beginning of transition from laminar to turbulent flow in the boundary layer is seen. Good agreement between the initial experimental data points and the theoretical laminar prediction shows that the flow is initially laminar. Then, as the  $Re$  increases, a sharp increase in the heat flux is seen. The intersection between the laminar prediction line and a least-squares fit to these data can be used as a good approximation to the onset of transition. From this intersection, the transition Reynolds number,  $Re_{tr} = \rho_e U_{e,x_{tr}}/\mu_e$ , can be determined. As mentioned in the introduction of this paper, the transitional/turbulent heat flux values are significantly higher than those in the laminar regime, illustrating the potential value of suppressing such transition on a vehicle body.

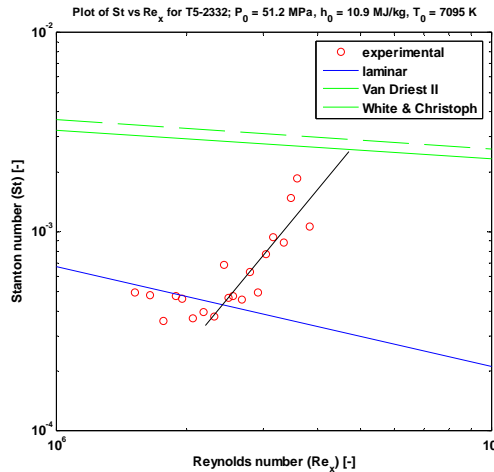


**Figure 7. Normalized heat transfer profile for a free-stream mixture of 95%  $N_2$  / 5%  $CO_2$  by mole fraction.**

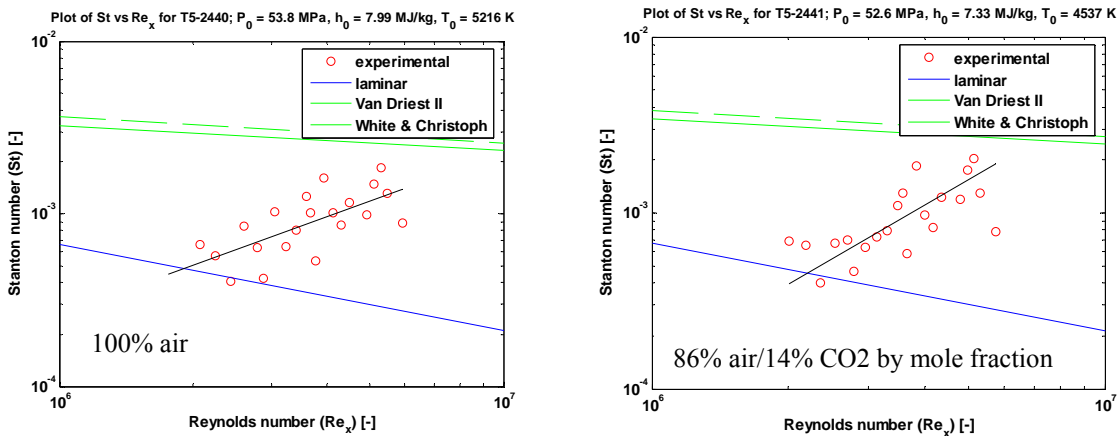


**Figure 8. Normalized heat transfer profile for free-stream mixtures of air and  $CO_2$**

Additional shots were run with mixtures of CO<sub>2</sub> and air, the results from which are shown in Figure 8. As with N<sub>2</sub>/CO<sub>2</sub> mixtures, the transition Reynolds number is seen to move to the right when CO<sub>2</sub> is added to the air test gas, even though it is only 14% by mole fraction. In figure 9, the transition data collected for CO<sub>2</sub> mixtures with both N<sub>2</sub> and air is plotted together. For this data, a switch has been made from the Reynolds number based on the edge conditions to  $Re_{tr}^* = \rho^* U_{e,x_{tr}} / \mu^*$  where the density and viscosity are evaluated at the conditions corresponding to Eckert's reference temperature, denoted by the \* superscript. As mentioned in the background section, the use of such conditions is more appropriate for discerning trends between different gases at different stagnation enthalpies. As might be expected, the minimum value of  $Re_{tr}^*$  occurs for 100% N<sub>2</sub> or air, but, as CO<sub>2</sub> is added,  $Re_{tr}^*$  increases significantly. In the case of N<sub>2</sub>, it has more than doubled by the time the CO<sub>2</sub> fraction reaches 40%. In the case of air,  $Re_{tr}^*$  also increases when the mole fraction of CO<sub>2</sub> is increased to 14%, but there are insufficient data points for quantitative conclusions to be drawn. The data pertaining to 100% CO<sub>2</sub> was inconclusive regarding the transition location: although suggestions of transition appear toward the end of the cone, there was not a clear trend. The data point plotted here thus signifies the minimum value that  $Re_{tr}^*$  could take, corresponding to the position of the last thermocouple. Previous experiments have shown  $Re_{tr}^*$  to be significantly higher in pure CO<sub>2</sub> flows than in either air or pure N<sub>2</sub> flows at the same enthalpy. This is the first time, however, that experiments have been performed in T5 that have shown CO<sub>2</sub> to be effective in delaying transition when present as a component of the free-stream gas. This result lends optimism to the efficacy of the transition delay technique being investigated here.

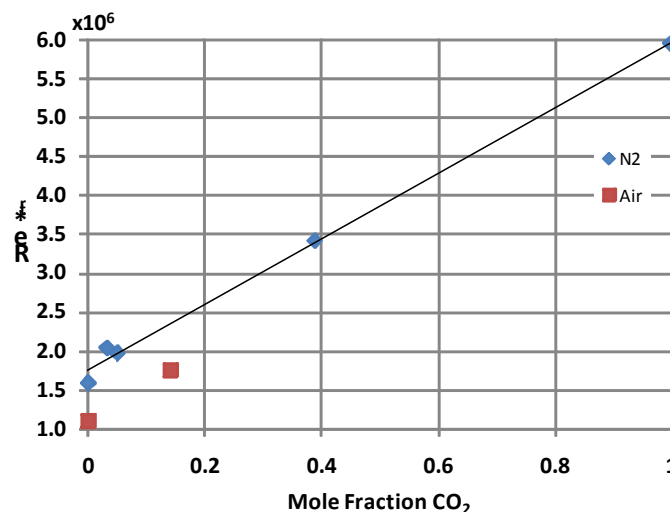


**Figure 9. The effect of CO<sub>2</sub> mole fraction in the test gas on  $Re_{tr}^*$  for flows over a 5 degree sharp cone, for a free-stream otherwise consisting of N<sub>2</sub> or air.**

## B. Injection Scheme

Several injector tip geometries were designed and built for this experimental series. A schematic of the initial design is shown in Figure 10; the CFD simulations discussed in the following section are based on this geometry. The CO<sub>2</sub> flows from a high-pressure run tank outside the test section, through a series of pipes into a reservoir in the tip, then exits to the surface of the cone through a series of holes. Only qualitative experimental data was able to be obtained with CO<sub>2</sub> injection since the instrumentation on the cone failed midway through testing (after about 10 years of use). However, based on this qualitative data and visualizations of the injected flow, it was decided to build a new injector tip for the next set of experiments. The new injector has twice as many holes and approximately double the flow area of the previous tip. This will allow lower injection pressures to be used for the same mass flow rate. A new cone model has also been constructed with 80 thermocouples uniformly distributed in the circumferential and axial directions. This will allow more precise determination of the transition location in comparison to the older model, which was restricted to 21 thermocouples located on only one side of the cone.

One of the principal engineering challenges of this project has been ensuring that the injected flow is adequately established by the time of arrival of the main flow in the test section, as there is only  $\sim 180$ ms from the earliest signal generated by the facility to the beginning of the test period. Through visualizations of the injected flow into ambient air, and comparisons of the run tank pressure traces with those obtained during experiments, it has been verified that the injected gas first arrives at the cone surface after  $\sim 70$ ms, and that injection is well established by the beginning of the test time (see Figure 10 B&C).

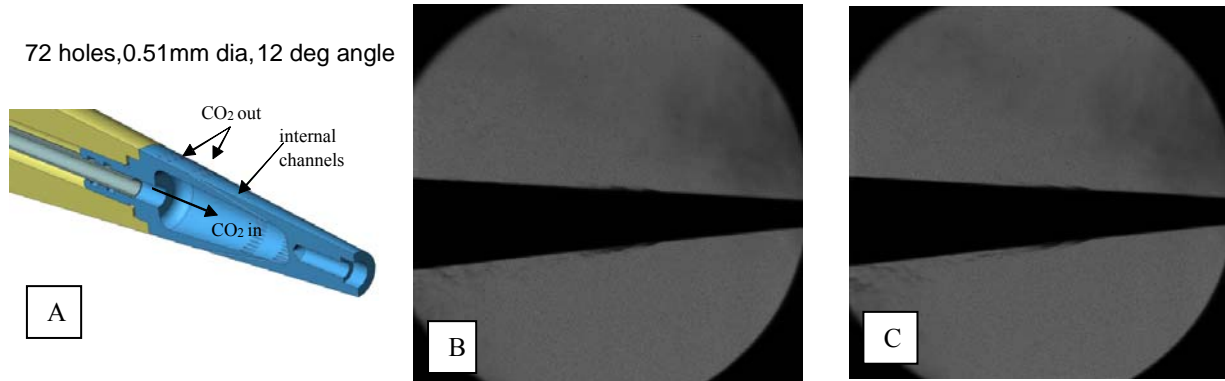


**Figure 10. A. Schematic of CO<sub>2</sub> injection section. Flow visualization of CO<sub>2</sub> injection from injector tip into ambient air. B: flow at 73 ms after trigger. C: flow at 78 ms after trigger.**

## V. Computational Results

Three injection cases were performed on a 5 degree cone with a single row of injector ports. These ports begin at an axial distance of approximately 13 cm from the nose and have a diameter of 0.762 mm. This is a simplified version of the actual tip used in the experiments. Each case had a different injection pressure in order to study the effect this has on the flow in the shock and boundary layers and the CO<sub>2</sub> distribution. All cases were run with the same freestream conditions. These conditions, as well as the injection pressures, are listed in table 2 of the appendix. A case without injection was also performed to evaluate the effect the injection has on the boundary layer height and also to quantify the improvement in stability.

### A. CFD Solvers

For these simulations, a finite volume formulation was used to solve the compressible Navier-Stokes equations. In the no-injection case, the structured solver DPLR was run on a two dimensional grid with an axi-symmetric formulation [19]. In the injection cases, a hybrid, unstructured solver [20] was used on a ten degree slice of the test body. In both cases, the inviscid fluxes were evaluated using a second-order accurate, modified Steger-Warming flux vector splitting method. For the viscous fluxes, gradient reconstruction was accomplished by using a weighted least-squares method. The time integration was a first-order accurate, implicit method. The implicit method is implemented in two different ways depending on the location in the grid. In the near-wall region, where the grid is clustered to the wall, the implicit method used was line relaxation, with lines being solved in the wall-normal direction. Where lines are not generated, a full matrix point relaxation was used. Both codes were run in parallel using MPI.

### B. Gas Properties

For these simulations, seven chemical species were used: CO<sub>2</sub>, CO, N<sub>2</sub>, O<sub>2</sub>, NO, N, and O. The viscosity for each species was calculated using the high temperature Blottner fits and the mixture viscosity was calculated using Wilke's semi-empirical mixing law. A Landau-Teller vibrational relaxation model was used for the translational-vibrational energy exchange with the jet-on cases using the characteristic relaxation times based on the Millikan and White semi-empirical curve fits [21-23]. The chemical reactions modeled in these simulations are listed in table 3 of the appendix. The forward reaction rate coefficients are taken from Park et al. [21], except for reactions five and

six, which are from Bose and Candler [24, 25]. The equilibrium coefficients are taken from Park [26], except for reactions one and seven, which are generated from fitting the data given in McBride et al. [27].

### C. Grid Generation

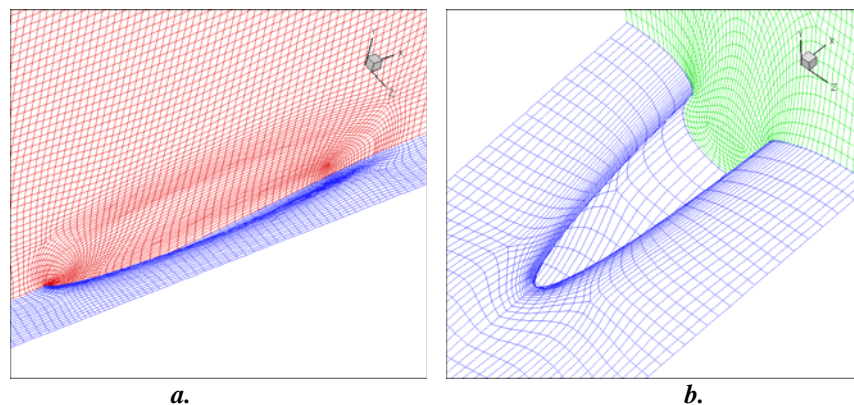
For the two dimensional, axi-symmetric case, a structured grid of quadrilateral elements was used. The grid was generated using a module in software suite STABL [28]. The three dimensional grid was composed of an unstructured set of hexahedral and triangular prism cells. It was generated using a combination of the commercial grid generation software packages Gridpro and Gridgen.

Only one of the injector ports was modeled to reduce the computation cost of the problem, resulting in a ten degree slice of the full test body. The topology around the port was designed to provide a continuous layer of cells normal to wall, in order to take advantage of the line relaxation method. An area of high cell density in the streamwise direction as well as a layer of cells were nested around the port to add additional refinement in order to capture the complexity of the flow in this region. This portion of the grid, created using gridpro, can be seen in Figure 11.

This grid was imported into Gridgen to create a mesh on the rest of the cone. At the nose, an initial cell spacing in the streamwise direction of approximately  $0.23 \mu\text{m}$  was used in order to resolve the sharp gradients at the nose. The sharp nose was approximated with hexahedral cells. It was found that using triangular prism cells at the nose created a significant amount of error for the isothermal wall condition. Due to the axisymmetric nature of flow before the injector port, only two cells were used in the spanwise direction to reduce the computational cost. A short distance before the injector port, the number of spanwise cells was increased from two to forty, by means of triangular prism cells, in order to resolve the shape of the port as well as the complexity of the flow in this region. Also, the streamwise cell spacing in the regions outside of the port had a sparser cell density, however the cell stretching maintained continuity through the use of a hyperbolic tangent distribution. The total number of cells for the grid was approximately 2.2 million cells.

Another requirement for an injection flow is to model the plenum chamber. It has been shown [29] that to correctly model the mass and momentum flux out of the port that both a subsonic, plenum condition must be applied and any geometry that could reduce the discharge coefficient must be modeled. For the jet-on case, a slightly modified version of the plenum chamber was modeled. This shape is displayed in Figure 11.

The clustering near the wall allowed for an initial cell spacing of less than one viscous wall unit for the entire cone surface. This was not the case inside the injector port near the plenum, where the value was on the order of one wall unit. However, due to the small velocities in this region, the effect on the flow field is not significant.



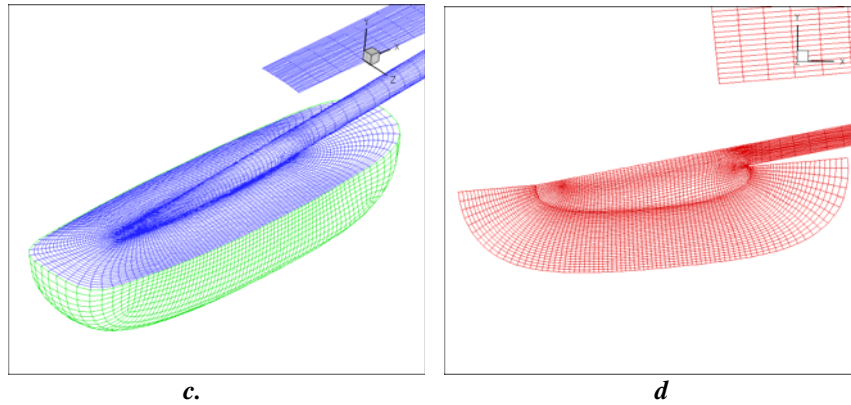


**Figure 11. The grid geometry. Pictures a and b are views of the injector port on the surface of the cone. Pictures c and d are views of the plenum chamber. These views were taken before clustering was applied to the grid.**

#### D. Results

A typical contour plot of Mach number at the location of injection is shown in figure 12. The surface of the cone is colored in gray and the black lines are fluid streamlines. In all cases tested, the pressure in the reservoir causes the injection gas to reach sonic speed near the exit of the injector port. This provides the injection gas with enough momentum to displace the boundary layer and penetrate into the shock layer. A higher injection pressure results in a larger height of penetration. This action results in a shock that develops in front of the injection stream and is transmitted to the oblique shock off the nose of the cone, causing the oblique shock to change its angle to the surface. Due to the displacement of the shock layer, the fluid that encounters the injection stream is diverted around the injection gas plume, as seen in some of the streamlines drawn in figure 12. This causes a vortex to form near the wall upstream of the injector port; this vortex wraps around both sides of the injection stream. These vortices play a major role in the distribution of the injection gas downstream. Secondly, they aid in heating the cold injection gas.

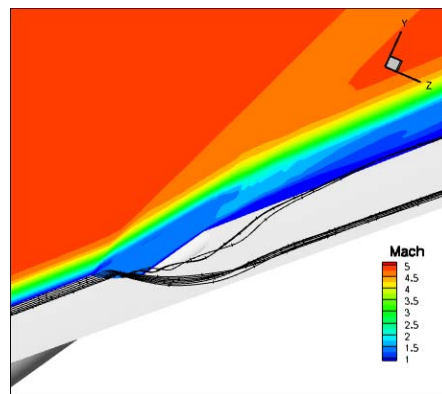


**Figure 12. Mach contours of the gas injection. The cone surface is colored in gray and the black lines represent fluid streamlines. This image was taken from the data obtained in case 1.**

Downstream of the injection, the core of injection gas starts mixing in the spanwise direction, due to both diffusion and convection. For case 1 with the lowest injection pressure (32.2 psia), at a distance of 30 cm from the nose of the cone, there is  $\text{CO}_2$  present over the whole surface of the cone, as seen in figure 13. From the plot of temperature contours, it can be seen that  $\text{CO}_2$  is being heated by the higher temperature fluid that sits on top of the  $\text{CO}_2$ . At this location, a large portion of the  $\text{CO}_2$  has reached a temperature of approximately 2000 K. The data show that the vibrational temperature is approximately equal to the translational temperature. This temperature is high enough to allow activation of three of the four vibrational modes of  $\text{CO}_2$ . As previously stated, this is beneficial to the stability of the boundary layer. The boundary layer edge is approximately 1.2 mm from the cone

surface. At this location in the no-injection case, the boundary layer edge is about 0.8 mm thick, implying that the injection of CO<sub>2</sub> has made the boundary layer grow.

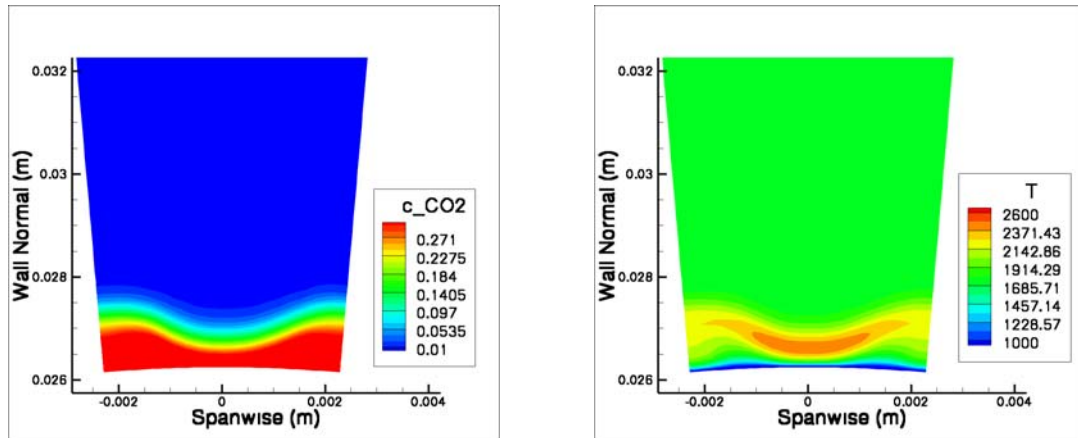


**Figure 13. Concentration and Temperatures profiles at 30 cm from the cone tip. These images are taken from case 1**

Further down the cone, the distribution of CO<sub>2</sub> has smoothed out and it has become a smaller constituent of the mixture, as seen in figure 14. However, areas exist where the mass fraction is above 10%, which is a large enough percentage to allow for increased stability, as inferred from figure 9. Looking at the temperature contours, a large portion of the CO<sub>2</sub> is now being heated to approximately 2200 K, which brings it within range of starting to dissociate. As stated in the discussion of figure 4, this can be advantageous due to ability of the dissociation to absorb energy of disturbances in the boundary layer. Also important to note, the height of the boundary layer at this location is approximately 1.3 mm. This is relatively larger than the no-injection case, which has a boundary layer height of approximately 1.05 mm.

Profiles such as those in figures 13 and 14 are seen in the other two cases tested, with the only difference being the amount of CO<sub>2</sub> in the boundary layer and the height of the high temperature zone. This is to be expected from adding more mass and more wall normal momentum into the boundary layer, however minimizing this effect is one of the goals of the project. It would seem that the low pressure case (case 1) would have the advantage over the higher pressure cases in that CO<sub>2</sub> is successfully added to the full surface of the cone with the smallest impact on the boundary layer.

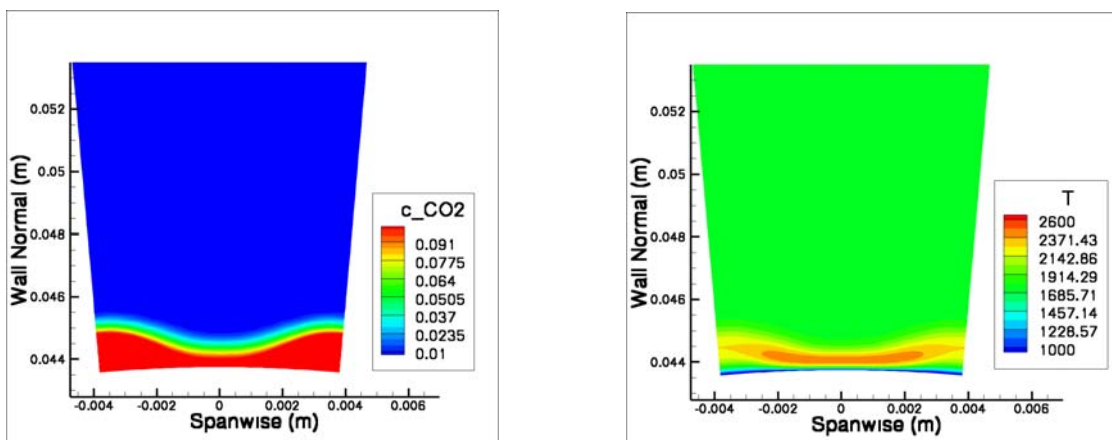


**Figure 14. Concentration and Temperatures profiles at 50 cm from the cone tip. These images are taken from case 1.**

It is important to note that injecting CO<sub>2</sub> with a single row of injectors may not be the best suited to achieve the goal of an even distribution of CO<sub>2</sub> over the cone's surface. This is best demonstrated by the wavy distribution of CO<sub>2</sub> as seen in figure 13. A possible solution to this is to use the model seen in figure 10. With two rows of offset injector ports, the second row could fill in the gaps in the distribution caused by the flow field of the first row. Simulations of this method of injection will be run in the future to confirm this.

## VI. Conclusion

In this project, a new technique to delay the transition in hypervelocity flows by injecting CO<sub>2</sub> into the boundary layer of interest has been proposed and investigated. A series of experiments have been conducted at Caltech's T5 to test this technique in high enthalpy flows over a 5 degree sharp cone. This geometry was chosen due to its relevance to axisymmetric vehicle configurations and to the wealth of previous data available for comparison with the obtained  $Re^*_{tr}$  data. Initial experiments used mixtures of CO<sub>2</sub>/N<sub>2</sub> as the test gas, rather than introducing CO<sub>2</sub> directly to the boundary layer of the cone. The obtained results demonstrate that the addition of CO<sub>2</sub> delays the onset of transition. For example, in the case of 60%N<sub>2</sub>/40%CO<sub>2</sub> by mole fraction, the value of  $Re^*_{tr}$  was more than double that of the case of 100% N<sub>2</sub>. A similar effect was noted in experiments using mixtures of air and CO<sub>2</sub> as the test gas. A small number of experiments were subsequently carried out with CO<sub>2</sub> injection into an air freestream, but questionable thermocouple readings meant that no quantitative conclusions could be drawn from these. However, tests were carried out in which the injected flow was visualized, providing confirmation that the triggering of the injection system is appropriately timed to provide adequate injected CO<sub>2</sub> during the test time. In fact, the CO<sub>2</sub> flow starts approximately 100ms before the main flow arrives, providing enough time for the injection flow to be fully established. This injection timing system will be used in upcoming experiments.

A series of numerical simulations were also completed with comparable freestream conditions to those obtained in T5 and a simplified injection geometry based on the experimental model. From the numerical results, it was found that the CO<sub>2</sub> reaches a temperature of about 2000K after 30 cm from the cone tip. This is encouraging since the lowest vibrational characteristic temperature for this gas is 960K. Also, the mass fraction contours of CO<sub>2</sub> showed that it is being rapidly mixed along the lateral direction of the cone, which is desired. The CFD results for the different reservoir pressures show that the lowest pressure tried (32 psia) might be most suitable as a start point for the next series of experiments since this shows the least disruption to the boundary layer.

## Appendix

Table 1. Run Conditions

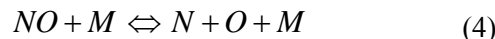
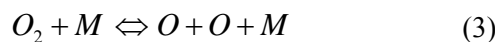
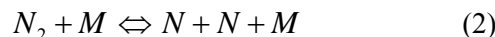
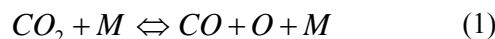
Shot No.	P <sub>0</sub> (MPa)	T <sub>0</sub> (K)	h <sub>0</sub> (MJ/kg)	[N <sub>2</sub> ] or [air] (mol/mol)	[CO <sub>2</sub> ] (mol/mol)
2331	52.2	7375	10.75	1.00 N2	0.00
2332	51.2	7095	10.90	0.95 N2	0.05
2333	50.0	4434	9.43	0.00 N2	1.00
2334	50.1	5380	10.89	0.61 N2	0.39
2337	51.2	7379	11.37	0.97 N2	0.03
2440	53.8	5216	7.99	1.00 air	0.00
2441	52.6	4537	7.33	0.86 air	0.14

**Table 2. Conditions used for CFD simulations**

Stagnation Conditions		Freestream Conditions	
Pressure (MPa)	58.5	Density kg/m <sup>3</sup>	0.06032
Temperature (K)	6305.3	Temperature (K)	1564
Enthalpy (MJ/kg)	10.47	Velocity (m/s)	4080
		Wall Temperature (K)	293
		Minf	5.1

Gas Composition (by mass fraction)	
N2	0.7345
O2	0.1844
NO	0.0654
N	0.0
O	0.0157

All at 300 K	Case 1	Case 2	Case 3
Pressure (psia)	32.2	64.4	107
Mass Flux (g/s)/hole	0.213	0.438	0.746

**Table 3. Reaction set used for the CFD simulations**

### Acknowledgments

The authors would like to thank Bahram Valiferdowski for helping with the design of the injection pieces and with the maintenance of the facility. Financial support for this work was provided in part by the Air Force Office of Scientific Research, USAF, under grant/contract number F49620-IHOUSE07E0000. The program manager is Dr. John Schmisser to whom the authors are grateful for his continued support throughout this project.

### References

- 1 Anderson Jr., J.D., *Hypersonic and High Temperature Gas Dynamics*, McGraw-Hill 1989.
- 2 Heisner, W.H., Pratt, D.T., "Hypersonic Airbreathing Propulsion," AIAA Education Series, 1994.

- 3 Mack, L.M., "Boundary-layer stability theory," In Special Course on Stability and Transition of Laminar Flow, AGARD Report Number 709, 1984.
- 4 Schlichting, H., Boundary Layer Theory. McGraw-Hill Company, 1987.
- 5 Hornung, H.G., Adam, P.H., Germain, P., Fujii, K., Rasheed, A., "On transition and transition control in hypervelocity flows," Proceedings of the Ninth Asian Congress of Fluid Mechanics, Isfahan, Iran, 2002
- 6 Eckert, E.R.G., "Engineering relations for friction and heat transfer to surfaces in high velocity flow," Journal of the Aeronautical Sciences, 22:585-587, Aug. 1955.
- 7 Johnson, H.B., Seipp, T.G., Candler, G.V., "Numerical study of hypersonic reacting boundary layer transition on cones," Physics of Fluids, 10 (10): 2676-2685 Oct. 1998.
- 8 Adam P.H. and Hornung, H.G., "Enthalpy effects on hypervelocity boundary-layer transition: Ground test and flight data," J. Spacecraft and Rockets 34, 614 (1997).
- 9 Fujii, K., Hornung, H.G., "An experiment of high-enthalpy effect on attachment line transition," AIAA 2001-2779, 2001.
- 10 Fujii, K., Hornung, H.G., "Experimental investigation of high-enthalpy effects on attachment-line boundary layer transition," AIAA Journal, Vol. 41, No. 7, July 2003.
- 11 Fujii, K., Hornung, H.G., "A Procedure to Estimate the Absorption Rate of Sound Propagating Through High Temperature Gas", GALCIT Report FM 2001.004, August 8, 2001.
- 12 Reshotko, E., Beckwith, I.E., "Compressible laminar boundary layer over a yawed infinite cylinder with heat transfer and arbitrary Prandtl number," Technical Report NACA Report 1379, National Advisory Committee for Aeronautics (NACA), 1958.
- 13 Lighthill, M.J., Viscosity effects in sound waves of finite amplitude. In G.K. Batchelor and R.M. Davies, editors, Surveys in Mechanics, pages 250-351. Cambridge University Press, 1956.
- 14 Herzfeld, K.F., and Litovitz T.A., Absorption and Dispersion of Ultrasonic Waves, New York, Academic Press 1959.
- 15 Clarke J.F. and McChesney M., The Dynamics of Real Gases. Butterworths, 1964.
- 16 Vincenti W.G. and Kruger C.H.. Introduction to Physical Gas Dynamics. Krieger Publishing Company, 1965.
- 17 Hornung, H., Belanger, J., "Role and techniques of ground testing simulation of flows up to orbital speeds", AIAA 90-1377.
- 18 Hornung, H., "Performance data of the new free-piston shock tunnel at GALCIT", AIAA 92-3943.
- 19 Wright, M. J., Candler, G. V., and Bose, D. "A Data-Parallel Line-Relaxation Method for the Navier-Stokes Equations," Paper 97-2046CP, AIAA, June 1997.
- 20 Nompelis, I., Drayna, T., Candler, G. V., "Development of a Hybrid Unstructured Implicit Solver for the Simulation of Reacting Flow over Complex Geometries," AIAA Paper No. 2004-2227, June 2004.
- 21 Park, C., "Review of Chemical-Kinetics Problems of Future NASA Missions, I: Earth Entries," Journal of Thermophysics and Heat Transfer, Vol. 7, No. 3, 1993, pp. 385-398.
- 22 Park, C., Howe, J.T., Jaffe, R.J., and Candler, G.V., "Review of Chemical-Kinetics Problems of Future NASA Missions, II: Mars Entries," Journal of Thermophysics and Heat Transfer, Vol. 8, No. 1, 1994, pp. 9-23.
- 23 Camac, M., "CO<sub>2</sub> Relaxation Processes in Shock Waves," Fundamental Phenomena in Hypersonic Flow, Ed. J.G. Hall, Cornell University Press, Ithaca, NY, 1966, pp. 195-215.
- 24 Bose, D. and Candler, G. V. "Thermal Rate Constants of the N<sub>2</sub> + O -> NO + N Reaction Using Ab Initio 3a' and 3a' Potential Energy Surfaces," Journal of Chemical Physics, vol. 104, No. 8, pp. 2825-2833, 1996.
- 25 Bose, D. and Candler, G. V. "Thermal Rate Constants of the O<sub>2</sub> + N -> NO + O Reaction Based on the 2a' and 4a' Potential Energy Surfaces," Journal of Chemical Physics, vol. 107, No. 16, pp. 6136-6145, 1997.
- 26 Park, C., Nonequilibrium Hypersonic Aerodynamics, Wiley, 1990

- 27 McBride, B. J., Zehe, M. J., and Gordon, S. "NASA Glenn Coefficients for Calculating Thermodynamic Properties of Individual Species," Tech. Rep. 2002-211556, NASA, September 2002.
- 28 Johnson, H. B. and Candler, G. V., "Hypersonic Boundary Layer Stability Analysis Using PSE-Chem," AIAA Paper No. 2005-5023, June 2005
- 29 Peterson, D. M., Subbareddy, P., and Candler, G. V., "Detached Eddy Simulations of Flush Wall Injection into a Supersonic Freestream," 42nd AIAA/ASME/SAE/ASEE Joint Propulsion Conference and Exhibit, Sacramento, CA, July 9-12, 2006, AIAA Paper No. 2006-4576.

# On the impact of injection schemes on transition in hypersonic boundary layers

Ivett A Leyva<sup>1</sup>,

*Air Force Research Laboratory, Edwards AFB, Ca, 93536*

Joseph S. Jewell<sup>2</sup>, Stuart Laurence<sup>3</sup>, Hans G. Hornung<sup>4</sup>, Joseph E. Shepherd<sup>5</sup>

*Caltech, Pasadena, Ca, 91125*

Three geometries are explored for injecting CO<sub>2</sub> into the boundary layer of a sharp five degree half-angle cone. The impact of the injection geometry, namely discrete injection holes or a porous conical section, on tripping the boundary layer is examined, both with and without injected flow. The experiments are conducted at Caltech's T5 reflected shock tunnel. Two different air free-stream conditions are explored. For the discrete-hole injectors, the diameter for the injection holes is 0.76 mm nominally and the length to diameter ratio is about 30. One injector has a single row of holes and the other has four rows. With the 4-row geometry fully turbulent heat transfer values are measured within 5.5 centimeters of the last injection row for both free-stream conditions. The 1-row injector results on a reduction of more than 50% in the transition Reynolds number. The porous injector does not move the transition Reynolds number upstream by itself with no injection flow.

## Nomenclature

$k$  = trip height  
 $\delta$  = boundary layer thickness  
 $\delta^*$  = boundary layer displacement thickness

## Subscripts

$o$  = stagnation  
 $e$  = edge  
 $\infty$  = free-stream

## I. Introduction

Designers of scramjet engines prefer to have turbulent flow at the entrance to the engine inlet for several reasons, including reduced susceptibility to flow separation inside the engine and improved fuel mixing and mass capture [1]. While transition to turbulence occurs naturally on a full-scale vehicle, it is more difficult to ensure turbulent flow at the entrance to the inlet in a sub-scale model due to its reduced size [1]. Therefore a considerable amount of work has been done to examine different passive and active trip schemes for this application [1-4]. Berry et al. [1] examined many active or blowing trip configurations on a 33% scale Hyper-X forebody model (71.1 cm),

<sup>1</sup> Lead, Combustion Devices Group, AFRL, Edwards AFB, CA, AIAA Senior Member

<sup>2</sup> Graduate Student, Caltech, Pasadena, CA, AIAA Student Member

<sup>3</sup> Former Postdoctoral Researcher, Caltech, Pasadena, CA now at DLR, Gottingen, Germany

<sup>4</sup> Professor Emeritus, Caltech, Pasadena, CA, AIAA Fellow

<sup>5</sup> Professor, Caltech, Pasadena, CA, AIAA Senior Member

including a single small hole ( $d=0.254\text{mm}$ ), single to triple rows with holes of the same size and 3.2 mm spacing, a single row of holes with  $d=0.5\text{mm}$ ; a straight and a saw-tooth slot (0.13 mm in width) and two porous configurations, one continuous and one with discrete plugs. In all these cases the injection flow was normal to the test article surface at 0.19 m from the leading edge. The tests were conducted at  $M=6, 7.3,$  and 10 with stagnation pressures of 0.87, 10.0, and 13.8 MPa, and stagnation enthalpies of 0.5, 1.1, 2.5 MJ/kg, respectively. The boundary layer thicknesses at the injection location for the above conditions were 2.1, 1.9, and 3.2 mm respectively. It was found that for a given mass flow rate (from about  $4.54\text{e-}5$  to  $4.54\text{e-}4$  kg/s) the continuous porous section and the straight slot were the least efficient to trip the boundary layer while the single row of small holes was among the most efficient configurations for  $4.54\text{e-}6$  to  $4.54\text{e-}5$  kg/s. For the single row of 17 of the larger holes, at a ratio of about 20 between the reservoir and the free-stream pressure the trip location moved substantially closer to the inlet. In all cases, choked flow was produced through the orifices or porous media. However, when no flow was injected there was no disturbance to the flow for most or all of the discrete hole configurations. Later Bathel et al. [2] performed NO PLIF measurements of the one row ( $d=0.5\text{mm}$ ) and single ( $d=0.254$  mm) hole configurations at the  $M=10$  conditions. This work provided a qualitative comparison with the results of Berry et al., who had used phosphor thermography for visualization. There were some differences in the estimates of the transition locations between the two visualization techniques. These experiments highlighted the importance of the flow separation region established upstream of the blowing jets. It was postulated that for low flow rates the gas trapped in the separation region, which is heated by virtue of being in the stagnation region, passes around the jets and propagates downstream, convecting with it higher heating loads. However as the flow rate is increased, the jets' cross section becomes larger and the gas from the separation region can no longer pass around the jets; instead the hot gas is forced around the ends of the orifice row. As it passes around the outer jets, it forms vortices and subsequently distributes the heat downstream.

Another area of interest for tripping mechanisms is transition control. For example, for the shuttle heat shield it is essential to know when in the trajectory the flow will become turbulent. Danehy et al [3] studied boundary layer trips using NO PLIF at the 31 inch Mach 10 wind tunnel at NASA Langley. Their main motivation was to be able to evaluate the consequences of given damage to the shuttle thermal protection system. Rectangular and triangular trips, typically oriented at 45 deg with respect to the flow, were installed on a flat plate 92.1 mm downstream from the leading edge. For these trips,  $k/\delta$  was 0.51, 1.32, and 1.89 for angles of 0, 10 and 20 deg, between the flat plate and the flow, respectively. Their stagnation conditions were  $P_o=4.96$  MPa and  $T_o=1000\text{K}$ . The Reynolds Number was  $3.28\text{e}6$  per meter. They found that at zero angle of attack the flow remained laminar with both trip geometries. The flow was laminar and transitional at 10 degrees; at 20 degrees the flow was laminar with no trip but turbulent for the two trip geometries.

Recently, Holden et al [5] reviewed experimental programs conducted at CUBRC from the 1970's to early 1990's to examine the effects of blowing and roughness on heating and skin friction on blunt nosetips, slender conical shapes and capsule heat shields. For rough slender cones at  $M=11, 13,$  and 15, blowing rates of 0.5 to 4.5 were found to decrease the heating loads and skin friction as compared to a smooth-walled cone. Here the blowing rate is defined as  $m/r_a u_e C_{Ho}$ . It was also found that surface blowing was more effective in reducing heat transfer than in previous experiments performed at supersonic Mach numbers. At Mach number 11 and Reynolds numbers up to  $10\text{e}6$ , roughness elements of 0.38 mm height produced more than double the heat enhancement of 0.254 mm roughness elements as compared to a baseline value of the turbulent heat transfer obtained on a smooth cone.

Work from Korkegi [6] in 1956 showed that for a flat plate at Mach 5.8 with  $P_o$  of 0.65 MPa,  $T_o$  of 380K and Reynolds number of  $8.5\text{e}6$  per meter, a fully developed turbulent boundary layer is not obtained below Reynolds numbers of  $2\text{e}6$  for normalized air injection rates of up to 4.5%. Here the mass flow rate of the jets per unit span has been normalized by the boundary layer mass defect per unit span. Finally, Coles [7] in 1954 obtained early measurements of the local skin friction over a smooth flat plate at  $M=4.54$  with and without passive trips and air jets. The passive trips consisted of a sand strip and a leading edge fence. The fence consisted of  $d=0.014''$  wires, spaced  $0.25''$  apart and projected about  $0.10''$  above the surface of the plate. The air jets consisted of a row of holes with  $d=0.014''$ , spaced  $0.25''$  apart and positioned  $0.75''$  downstream from the leading edge. At  $M=4.54$  the boundary layer was less sensitive to injection than at lower  $M$  values. Coles found that upon crossing a critical value of the mass flow rate, the effect on surface friction was large but did not change appreciably for higher mass flow rates. For  $M=4.54$  the critical value was a decrement of about 25 in the parameter  $u_\infty \delta^*/v_\infty$  for initial values between 3000 and 5000. Regarding experiments at high enthalpy and the effect of cavities on transition, Germain [8]

conducted several experiments with the same geometry used in the current study (sharp 5 degree half-angle cone). In these experiments a circumferential gap or cavity was created at  $x=0.203$  m. The gap was 5 mm deep with 0.127, 0.254, 0.508, and 0.889 mm widths. The test condition was  $P_o = 55$  MPa and  $h_o = 12$  MJ/kg. He observed no significant effects on transition.

In this paper we investigate three injection schemes designed originally to introduce  $\text{CO}_2$  into a supersonic boundary layer. The aim of injecting  $\text{CO}_2$  is to delay transition at high Mach numbers for slender bodies, as explained in detail in Leyva et al [9]. Briefly, the idea explored in that paper rests on the fact that at high enthalpies  $\text{CO}_2$  becomes vibrationally excited and absorbs energy from acoustic disturbances which are responsible for transition in the second or Mack mode. In the process of designing appropriate injection schemes for  $\text{CO}_2$ , however, we observed that our early injection schemes were in fact effective trips. This paper reports experimental results obtained on the impact of three injection schemes on transition. Two designs consist of discrete injection orifices and one has a porous section instead. The injection schemes were studied as passive trips, with no flow, and as active trips, with  $\text{CO}_2$  flow through the orifices or porous section.

## II. Experimental Setup

The facility used in all experiments in the current study was the T5 hypervelocity shock tunnel at the California Institute of Technology. It is the fifth in a series of free-piston driven, reflected shock tunnels built by R.J. Stalker, H.G. Hornung and colleagues [10-11]. The T5 facility consists of four major components: the secondary air reservoir (2R), the compression tube (CT), the shock tube (ST), and the test section/dump tank. The first three of these components are illustrated in Figure 1.

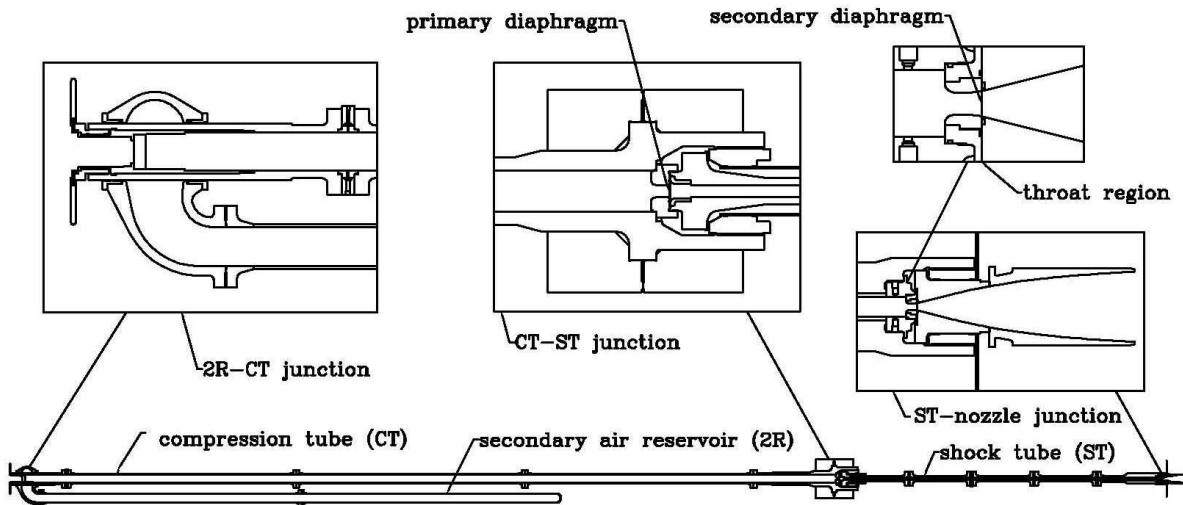


Figure 1. Schematic of the T5 hypervelocity shock tunnel facility.

The test flow is generated by driving a heavy (120 kg) piston down the CT with the release of high-pressure air from the 2R. The CT gas, a mixture of helium and argon, is compressed adiabatically by the advance of the piston until the pressure is sufficiently high to burst the primary diaphragm, located at the junction of the CT and ST. The primary diaphragm typically consists of a 4.75 to 6.9-mm thick stainless steel plate, indented with an X-shaped groove to aid petal formation. The test gas is initially contained in the ST; the burst of the primary diaphragm produces a shock wave that travels the length of the ST and reflects from the end wall. Stagnation conditions are thus produced at the end of the ST, which then serves as the reservoir for the nozzle expansion. The incident shock also bursts the secondary diaphragm, consisting of a 0.051 mm mylar membrane located at the ST-nozzle junction. The test gas expands through the nozzle, flowing into the test section and finally into the dump tank. The test section and dump tank are initially evacuated, separated from the ST by the secondary diaphragm. Startup of the flow in the test section typically takes 0.5 ms from the time of arrival of the incident shock at the nozzle throat; the test time is of the order of 1-2 ms. In all experiments in the present series, a contoured nozzle of area ratio 100 was used. The

initial pressures in the 2R, CT, and ST were typically 5.5-7.6 MPa, 98-116 kPa, and 76-117 kPa, respectively. The test gas for these experiments was air.

The T5 facility is instrumented with various diagnostic tools. An accelerometer attached to the CT is used here to trigger the CO<sub>2</sub> injection when needed. There are also several pressure transducers along the length of the ST. These transducers are used to measure the incident shock speed and reservoir pressure, from which the flow enthalpy is calculated using the ESTC program, and to trigger the T5 data acquisition system (DAS). The T5 DAS allows simultaneous recording of up to 80 data channels (in addition to the facility data) at a sampling rate of 200 kHz. The T5 optical setup is a typical Z-arrangement Schlieren system, capable of recording either a single frame or a sequence of high-speed images during the test period. A typical exposure time for each frame is 2  $\mu$ s.

The model employed in the current experiments was a sharp slender cone similar to that used in a number of previous experimental studies in T5. It is a 5 degree half-angle cone of approximately 1m in length and is composed of three sections: a sharp tip fabricated of molybdenum (to withstand the high heat fluxes), a mid-section, and the main body instrumented with 79 thermocouples. These thermocouples have a response time in the order of a few  $\mu$ s and have been successfully used for almost twenty years. For a complete description of the design see Sanderson [12]. The conical model geometry was chosen because of the wealth of experimental and numerical data available with which to compare the results from this program. A photograph of the cone model is shown in Figure 2.

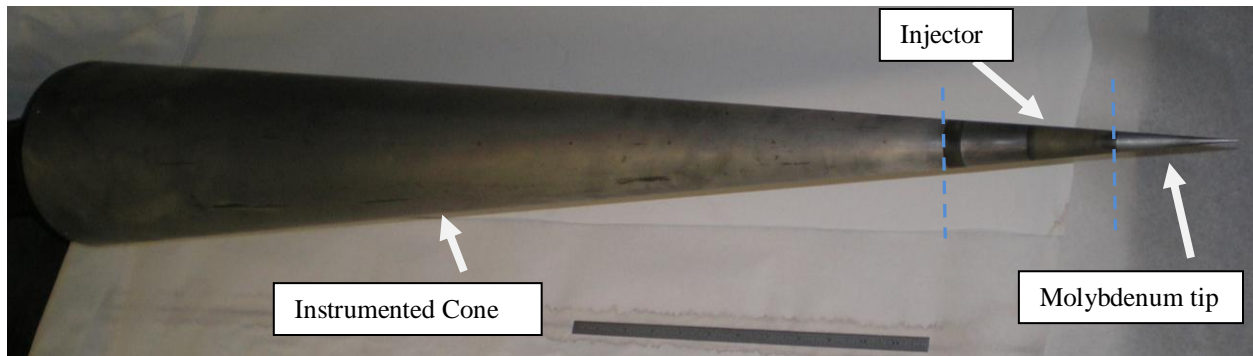


**Figure 2. Cone model used for all experiments. In this case the injector shown is the porous injector.**

### III. Experimental Results

#### A. 4-Row Injector

In these experiments two free-stream conditions were used. Condition A had  $P_o \sim 51$  MPa,  $h_o \sim 10$  MJ/kg,  $T_o \sim 6000$ K and Condition B had mean values of  $P_o \sim 44$  MPa,  $h_o \sim 6.5$  MJ/kg,  $T_o \sim 4550$ K. The first injection scheme consisted of 4 rows of injection holes. The diameter of the holes is  $\sim 0.8$  mm, the minimum diameter which could be reliably manufactured using the chosen technique. These pieces were fabricated using a rapid prototyping technique and the accuracy on the diameter of the holes is not as high as if the holes had been drilled or made using EDM. However, these models were made of a polymer vs. metal which is an advantage because the turnaround time was only a few days, and the cost was much cheaper than regular machining. As an aside, the polymer material survived repeated shots in T5 well, since during the short test times (1-2ms) the cone surface temperature does not rise more than 20 K or so for the conditions used here.

The 4-row injector is shown in Figure 3. The holes were made as close to tangential to the surface as possible; the actual angle between the holes and the surface is 6 degrees. The first row of holes is at 12.9 cm from the tip (along the surface of the cone) and the last row is at 16.5 cm. Each row has 36 orifices. Note that because the holes exit at an angle, the cross sectional area at the exit plane is elliptical. The holes have a length to diameter ratio of about 30. The orifices are connected to a plenum as seen in Figure 3. During a shot this plenum is either under vacuum, if there is no injection or is at a prescribed plenum pressure when injection occurs.

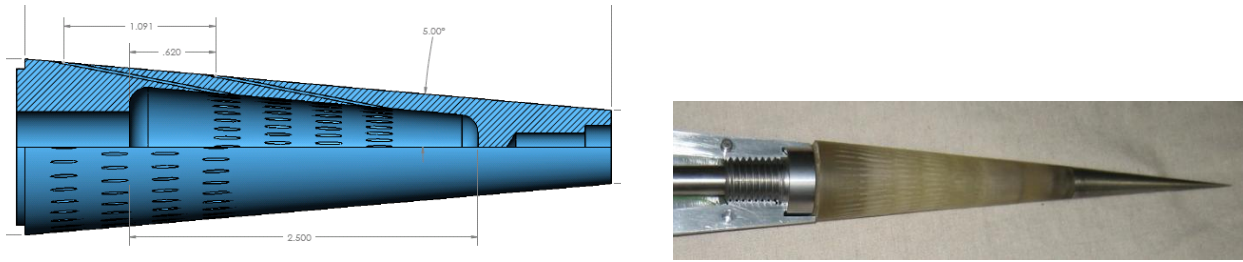


**Figure 3. Partial drawing and picture of injector with four rows of holes.**

To provide a comparison for the results with the injection schemes, a baseline case was run with a smooth conical midsection (made of the same polymer as the injectors) and the results are shown in Figure 4. Heat flux values are extracted from the 79 temperature readings using the method described in Sanderson [12]. The heat transfer  $q(x)$  is then normalized into a Stanton number (St) as follows:

$$St(x) = q(x) / (\rho_e u_e [h_0 - 0.5 u_e^2 (1 - r) - C_p T_w]) \quad [1]$$

where  $r$  is the recovery factor. For laminar flows,  $r_{lam} = Pr^{1/2}$ , and for turbulent flows,  $r_{turb} \sim Pr^{1/3}$ , where  $Pr$  is the Prandtl number.  $Pr$  is assumed to be constant, which is a reasonable approximation under the conditions of interest. The Reynolds number is evaluated at the edge conditions,  $Re(x) = \rho_e u_e x / \mu_e$ . In all the data to be presented here the experimental data is compared with laminar and turbulent heat transfer estimates for a slender cone. An estimate of the location for the onset of transition is obtained by the intersection of the laminar estimate and the line fit obtained from the rising heat transfer points, as indicated in figure 4. In this case natural transition occurs at  $Re(x) \sim 3.17e6$ .

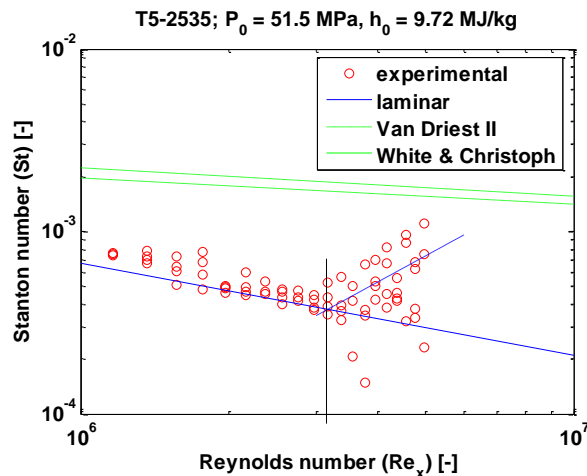


**Figure 4. Baseline results with a smooth cone for free-stream condition A.**

The results obtained with the 4-row injector are shown in Figure 5. As can be seen in the left plot, the holes induced an early transition by themselves without injection. Transition to fully turbulent values has occurred by the first temperature readings, which are located about 5.5 cm downstream of the last row of injection holes. Since the holes themselves are sufficient to induce early transition, injection of  $CO_2$  at 0.3MPa, as shown in the right plot, does not change the flow in any appreciable manner. The flow is still fully turbulent as measured by the most upstream thermocouples. Before we obtained the data shown in Figures 4 and 5, we observed a forward facing step between the molybdenum tip and the injector piece. That is, at the junction between the tip and the injector the diameter of the injector was larger than the molybdenum tip by 0.5 mm. The data obtained with the step is shown in

Figure 6. The traces obtained with the step look very similar to the corresponding traces without it. Therefore, the injection holes are sufficient to result on the early transition observed in both cases (Figures 5 & 6).

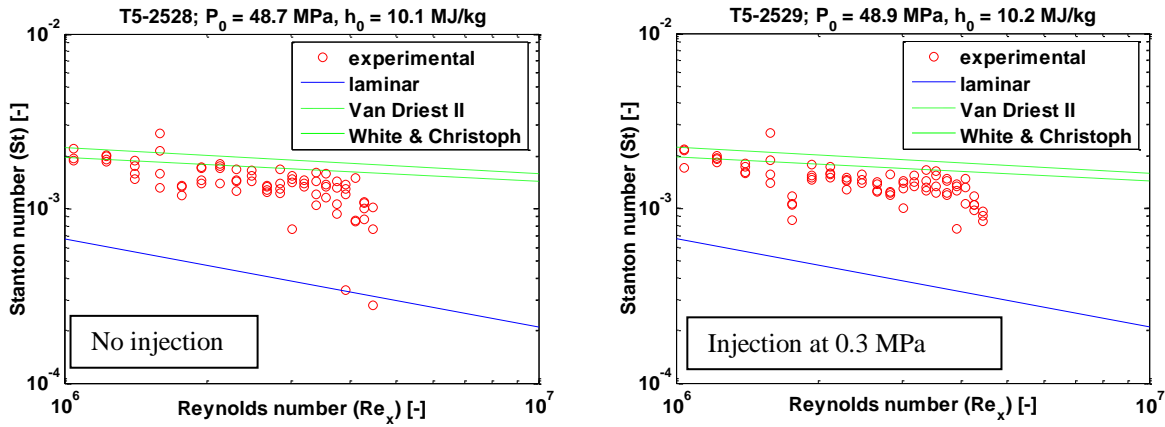


Figure 5. Normalized heat transfer for 4-row injector with and without CO<sub>2</sub> injection.

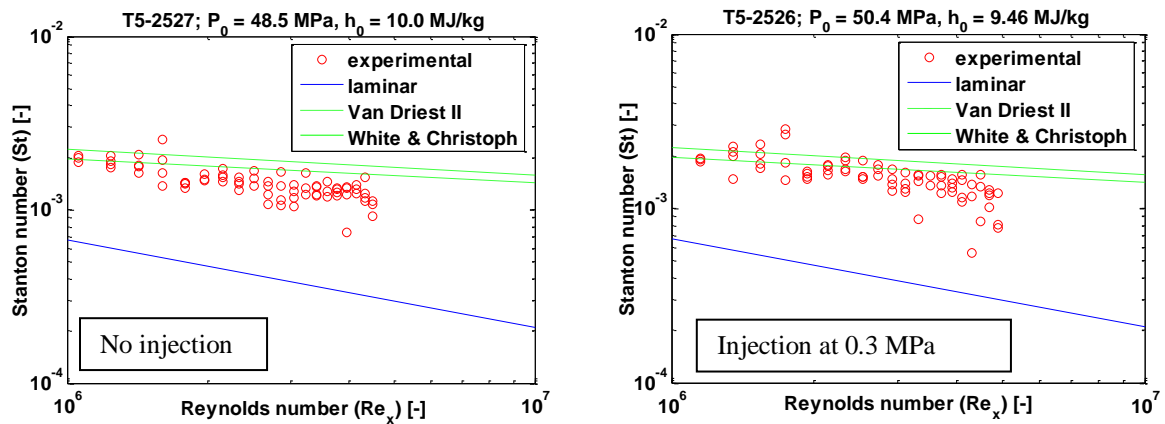


Figure 6. Normalized heat transfer for 4-row injector with and without CO<sub>2</sub> injection with a step between the injector and the molybdenum tip (condition A).

A different free-stream condition was run to assess the effect of the injection holes at a lower stagnation pressure and enthalpy condition (Condition B). As seen in Figure 7, the smooth cone (left) now has an earlier natural transition point which was estimated at  $Re(x)$  of  $\sim 2.17e6$ . The case with the 4-row injector (right), with CO<sub>2</sub> injected at 0.2MPa, shows fully turbulent heat transfer values at the most upstream location at which the temperature is measured – 22 cm from the tip. However, one should be cautious to interpret these results since in order to visualize the flow the cone had to be moved downstream so the injection piece would be aligned with the T5 windows. In the new location, the expansion fan from the nozzle is incident upon the back of the cone. In this position the results are not meaningful for transition location measurements. However, it is likely that the flow would have transitioned even if the cone were in the regular position (upstream). A visualization of the flow during the test time is shown in Figure 8. The visualizations allow one to obtain a sense of the injection process. The left picture in Figure 8 shows injection into vacuum and one can see the expansion fans from the jets. During the test time (right) weak shocks are visible originating from each row of holes.

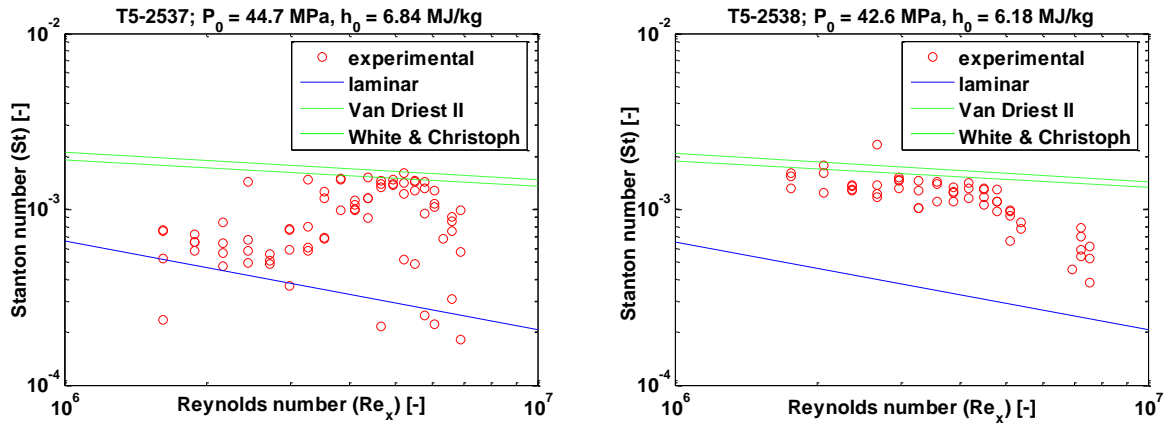


Figure 7. Normalized heat transfer for a smooth cone (left) and a 4-row injector (right) with 0.2 MPa injection pressure (condition B).

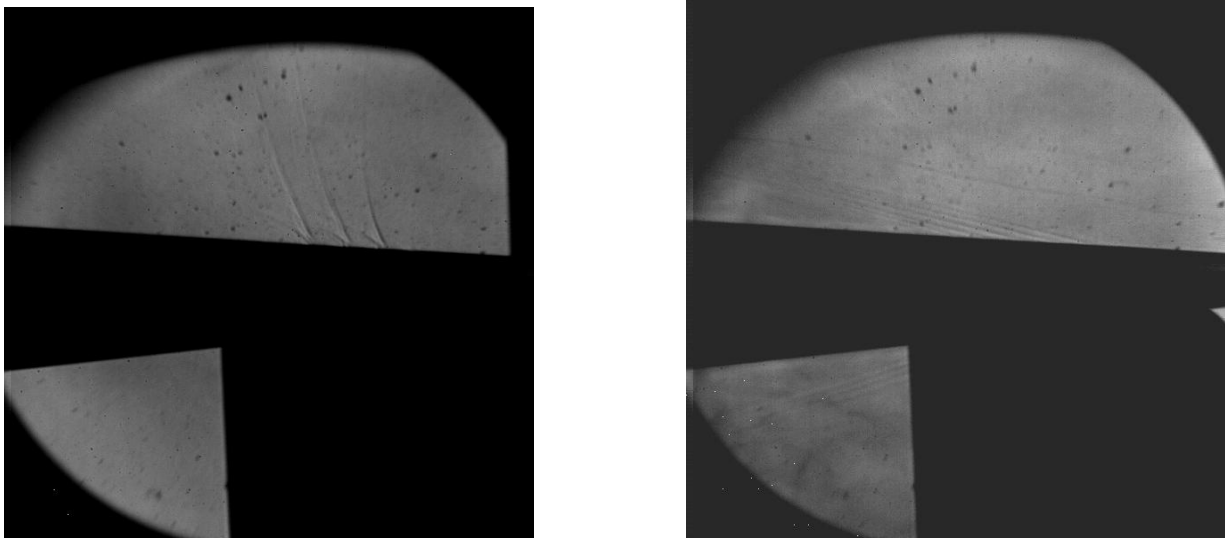


Figure 8. Visualization of flow field with 4-row injector injecting into vacuum (left) and with 0.2MPa injection pressure during shot 2538 (Figure 7 right).

## B. 1-Row Injector

To decrease the impact of the holes on transition, a new injector was built with only one row of holes. The design basically consisted of the previous injector with only the last row of holes. This injector was tested at condition A and the results are shown in Figure 9. When compared to the baseline case with a fully smooth cone (shot 2535, shown in Figure 4) the transition onset is seen to have been moved forward to a Re(x) of  $\sim 1.5e6$ . Thus, though the transition was not accomplished within 5.5 cm from the last injection row, as with the 4-row injector, it was still moved upstream significantly.

As has been seen from the previous cases for both the 1-row and the 4-row injectors, the tangential orifices are very effective at promoting transitions at the conditions studied. A rough estimate of the boundary layer height at the location of the first row of holes is approximately 0.5 mm, which would make the ratio of the orifice diameter to the boundary layer height 1.6. One possible explanation for the way in which the holes induce transition is through

the wake mode discussed in Rowley et al. [13]. This mode is observed in longer cavities (with respect to the boundary layer thickness) and higher Mach numbers compared to the Rositter or shear layer mode which is observed for shorter cavities and lower Mach numbers. The wake mode is characterized by a large-scale vortex shedding, in which a Kelvin-Helmholtz instability grows and produces a strong recirculation flow in the cavity. The flow is absolutely unstable and the Strouhal number is independent of Mach number [13]. Further studies would be needed to confirm this idea.

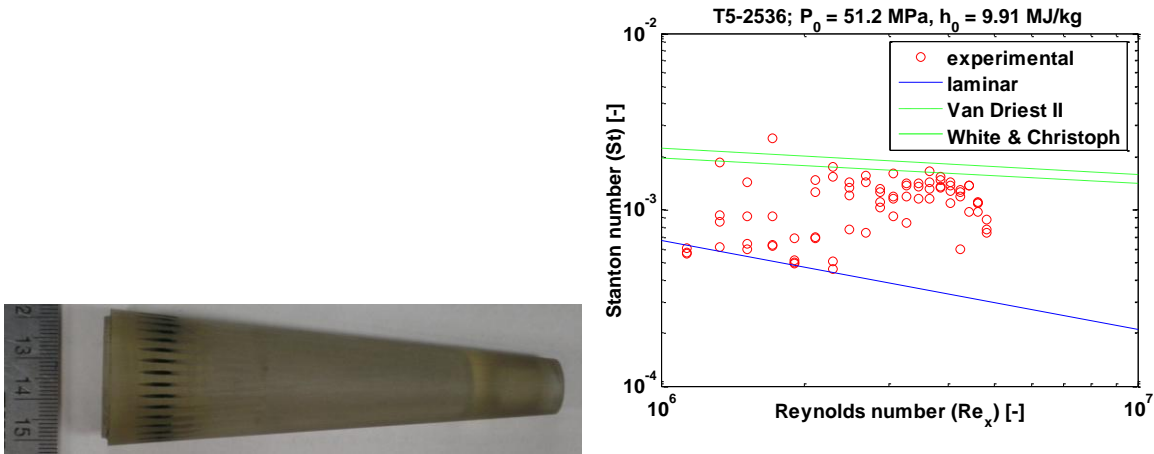


**Figure 9. Left: 1-Row injector design. Right: Normalized heat transfer for the 1-row injector with no injection.**

### C. Porous Injector

A porous injector was designed with the purpose of achieving a more spatially uniform injection flow, similar to transpiration cooling, instead of the discrete jets created with the designs discussed earlier. The piece chosen has 10 $\mu$ m porosity and is fabricated from sintered stainless steel [14]. The manufactured injector is shown in Figure 10. Porous injector. The thickness of the porous media is 1.6 mm. It starts at 12.8 cm from the tip and is 41 mm in length.



**Figure 10. Porous injector.**

Results for this geometry are shown in Figure 11. The free-stream conditions are similar to those of shot 2535 presented in Figure 4. The fact that the transition Reynolds numbers are very similar in the two cases indicates that the porous material does not itself cause transition. This is in contrast with the previous injector designs. A run was also conducted for the purpose of visualizing the injection of CO<sub>2</sub> through the porous material. Again, the cone was moved backward so that we could visualize the injector section. The results are presented in Figure 12. The CO<sub>2</sub> flow is evident in frames b-e. It is worth pointing out that a Schlieren setup is sufficiently sensitive for qualitative visualization of the CO<sub>2</sub> injection process. There is a shock emanating from the interface between the molybdenum tip and the injector due to a small discontinuity which was smoothed out prior to the following shot. The heat transfer traces show transition to fully turbulent flow by the third or fourth thermocouple location as seen in Figure

13. Therefore, it is likely that the flow would also be turbulent if the cone would be moved to its normal position. This is the only case studied in which injection was necessary to produce early transition. If the aim is to delay transition, as in the present case, it seems the injection pressure should be kept lower than 0.55 MPa. With this in mind, a preliminary shot was conducted with CO<sub>2</sub> injection at 0.16MPa (approximately 13.5 g/s) and it appeared that the transition Reynolds number was not affected as compared to the smooth case. This condition as well as other conditions with higher injection pressures will be completed in the next couple of months to find the practical range of CO<sub>2</sub> supply pressures which do not result in early transition.

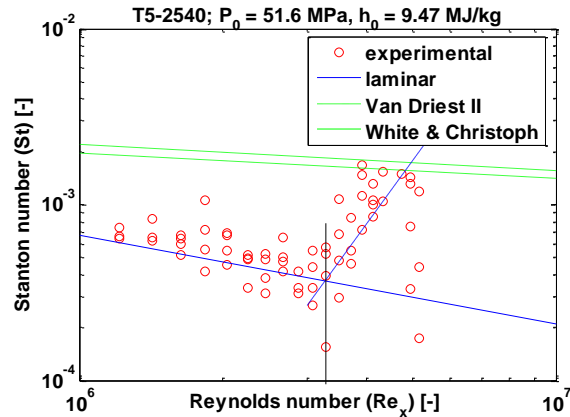


Figure 11. Normalized heat transfer for porous injector with no injection.

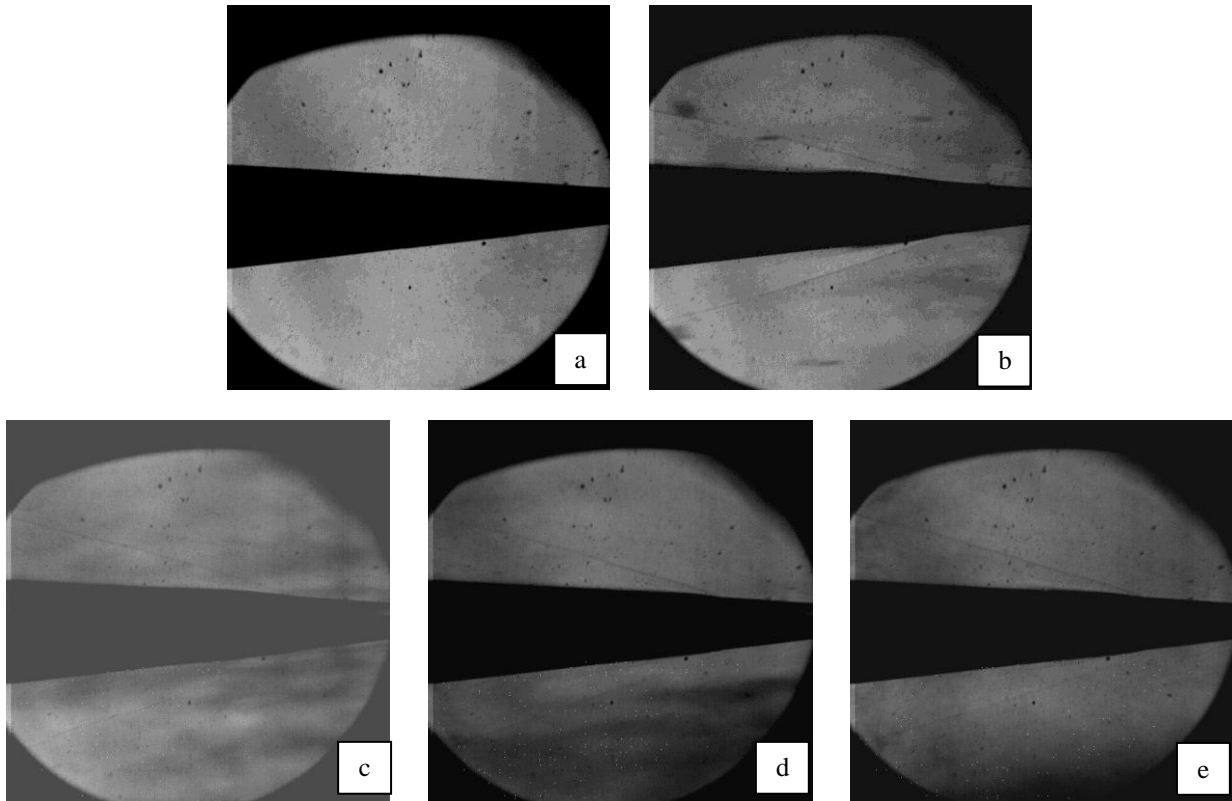


Figure 12. Shot 2539. Consecutive frames of a high-speed movie of the flow over the cone with the porous injector and 0.55 MPa CO<sub>2</sub> injection. The stagnation conditions were  $P_0=48.8$  MPa and  $h_0=10.1$  MJ/kg.

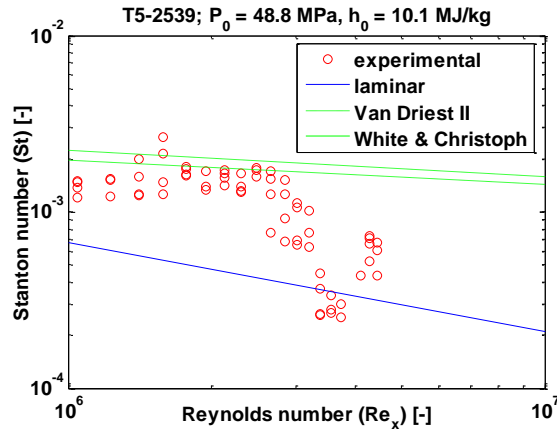


Figure 13. Normalized heat transfer for Shot 2539 with the porous injector and 0.55 MPa CO<sub>2</sub> injection.

#### IV. Conclusion

Three injection schemes were studied both as passive trips with no injection and as active trips with CO<sub>2</sub> injection. The first design had four rows of 36 orifices with nominal diameters of 0.76 mm. The second injector was derived from the former one by only keeping the fourth or most downstream row of orifices. The third injector consisted of a section with 10 μm porosity. The 4-row injector tripped the boundary layer to fully turbulent values within 5.5 cm from the last row of orifices for the two free-stream conditions studied. The transition Reynolds number with the 1-row injector was decreased by more than 50% as compared to the smooth cone. Therefore, while not as efficient as the 4-row injector, one row of holes still caused early transition. The 4-row injector was also tested with CO<sub>2</sub> injection pressure of 0.2-0.3MPa but the injection did not change the experimental results obtained. A porous injector was also tested and did not result in early transition when tested without injection. Injecting CO<sub>2</sub> at 0.55 MPa through the porous media is likely to cause early transition.

#### Acknowledgments

The authors would like to thank Bahram Valiferdowsi for helping with the design of the injection pieces and with the maintenance of the facility. Financial support for this work was provided in part by the Air Force Office of Scientific Research, USAF, under grant/contract number F49620-IHOUSE07E0000. The program manager is Dr. John Schmisser to whom the authors are grateful for his continued support throughout this project.

#### References

- 1 Berry, S. A., Nowak, R. J., Horvath, T. J., "Boundary Layer Control for Hypersonic Airbreathing Vehicles", AIAA 2004-2246.
- 2 Bathel, B.F., Danehy, P.M., Inman J.A., Alderfer, D.W., Berry, S.A., "PLIF Visualization of Active Control of Hypersonic Boundary Layers Using Blowing", AIAA 2008-4266.
- 3 Danehy, P.M., Garcia, A. P., Borg, S., Dyakonov, A.A., Berry, S.A., (Wilkes) Inman J.A., Alderfer, D.W., "Fluorescence Visualization of Hypersonic Flow Past Triangular and Rectangular Boundary-Layer Trips", AIAA 2007-536.
- 4 Berry, S.A., Auslender, A.H., Dille, A.D., Calleja, J.F., "Hypersonic Boundary Layer Development for Hyper-X", *J. Spacecraft and Rockets*, Vol. 38, No. 6, pp. 853-864, 2001.
- 5 Holden, M.S., Mundy, E.P., Wadhams, T.P., "A Review of Experimental Studies of Surface Roughness and Blowing on the Heat Transfer and Skin Friction to Nostetips and Slender Cones in High Mach Number Flows", AIAA 2008-3907.

- 6 Korkegi, R., H., "Transition Studies and Skin-Friction Measurements on an Insulated Flat Plate at a Mach Number of 5.8", *J. of the Aeronautical Sciences*, Vol. 23, No. 2, February 1956.
- 7 Coles, D., "Measurements of Turbulent Friction on a Smooth Flat Plate in Supersonic Flow", *J. of the Aeronautical Sciences*, Vol. 21, No. 7, July 1954.
- 8 Germain, P., "The Boundary Layer on a Sharp Cone in High-Enthalpy Flow", GALCIT, Caltech, Ph.D. thesis, 1994.
- 9 Leyva, I.A., Laurence, S., War-Kei Beierholm A., Hornung H.G., Wagnild R., Candler, G., "Transition delay in hypervelocity boundary layers by means of CO<sub>2</sub>/acoustic instability interactions", AIAA 2009-1287
- 10 Hornung, H., Belanger, J., "Role and techniques of ground testing simulation of flows up to orbital speeds", AIAA 90-1377.
- 11 Hornung, H., "Performance data of the new free-piston shock tunnel at GALCIT", AIAA 92-3943.
- 12 Sanderson, S., "Shock Wave Interaction in Hypervelocity Flow", GALCIT, Caltech, Ph.D. thesis, 1995.
- 13 Rowley. C. W., Colonius, T., Basu, A. J., "On self-sustained oscillations in two-dimensional compressible flow over rectangular cavities", *J. Fluid Mech.*, Vol. 455, pp. 315-346, 2002.
- 14 <http://www.mottcorp.com/sitemap/sitemap.htm>

# Carbon Dioxide Injection for Hypervelocity Boundary Layer Stability

Ross M. Wagnild<sup>1</sup> and Graham V. Candler<sup>2</sup>  
*University of Minnesota, Minneapolis, Minnesota, 55455*

Ivett A. Leyva<sup>3</sup>  
*Air Force Research Laboratory, Edwards AFB, California, 93536*

Joseph S. Jewell<sup>4</sup> and Hans G. Hornung<sup>5</sup>  
*Caltech, Pasadena, California, 91125*

**An approach for introducing carbon dioxide as a means of stabilizing a hypervelocity boundary layer over a slender bodied vehicle is investigated through the use of numerical simulations. In the current study, two different test bodies are examined. The first is a five-degree-half-angle cone currently under research at the GALCIT T5 Shock Tunnel with a 4 cm porous wall insert used to transpire gas into the boundary layer. The second test body is a similar cone with a porous wall over a majority of cone surface. Computationally, the transpiration is performed using an axi-symmetric flow simulation with wall-normal blowing. The effect of the injection and the transition location are gauged by solving the parabolized stability equations and using the semi-empirical  $e^N$  method. The results show transition due to the injection for the first test body and a delay in the transition location for the second test body as compared to a cone without injection under the same flight conditions. The mechanism for the stabilizing effect of carbon dioxide is also explored through selectively applying non-equilibrium processes to the stability analysis. The results show that vibrational non-equilibrium plays a role in reducing disturbance amplification; however, other factors also contribute.**

## I. Introduction

In the study of hypersonic vehicles, when a boundary layer transitions from a laminar to a turbulent state, both the skin friction and surface heat transfer rate on the vehicle increase in magnitude. The implications for high speed vehicle design are increased drag and greater thermal protection thickness, which require a greater vehicle weight and result in a reduction of fuel efficiency.

The purpose of the current study is to further investigate the stabilizing effect of carbon dioxide on hypervelocity boundary layers. The concept for this work is derived from combining three findings from past research. First, transition on slender bodies in hypervelocity flows is caused by amplification of acoustic waves trapped in the boundary layer<sup>1</sup>. Second, non-equilibrium effects such as molecular vibration and dissociation can damp acoustic waves<sup>2,3</sup>. Lastly, carbon dioxide has been found to be well suited to absorb acoustic energy in an enthalpy range relevant to realistic applications<sup>4</sup>. These findings point to the potential beneficial application of adding carbon dioxide into a boundary layer in order to delay transition onset. Experimentally, this is attempted by introducing carbon dioxide into the boundary layer by transpiring it through a porous material. The experiments are being performed on a five-degree-half-angle cone in the Graduate Aerospace Laboratories at California Institute of Technology (GALCIT) Free-Piston Shock Tunnel, T5. A computational fluid dynamics (CFD) simulation that

<sup>1</sup> Graduate Student, University of Minnesota, Minneapolis, Minnesota, AIAA Student Member.

<sup>2</sup> Professor, University of Minnesota, Minneapolis, Minnesota, AIAA Fellow.

<sup>3</sup> Lead, Combustion Devices Group, AFRL, Edwards AFB, California, AIAA Senior Member,

<sup>4</sup> Graduate Student, Caltech, Pasadena, California, AIAA Student Member.

<sup>5</sup> Professor Emeritus, Caltech, Pasadena, California, AIAA Fellow.

solves the reacting, compressible Navier-Stokes equations is used to recreate the experiment. The simulations are solved such that the boundary layer is laminar. These data are then used to provide the mean flow to be analyzed with the software suite STABL (Stability and Transition Analysis for hypersonic Boundary Layers), which solves the linear set of parabolized stability equations. A cone without injection is also studied in order to calibrate this method to the T5 tunnel environment and to form a baseline for determining transition delay. A similar study is performed on a theoretical cone with a longer interval of transpiration in order to isolate non-equilibrium effects. The objective is to show that adding carbon dioxide delays transition on the test body. This work leads to further analysis on variations on the design to gain insight into using chemical reactions and vibrational degrees of freedom to stabilize boundary layers. This research is part of a continuing effort to actively control boundary layer transition by means of carbon dioxide gas injection, which, to the authors' knowledge is a new technology.

## II. Background

A summary of the theoretical basis of this research is first laid out by Leyva et al.<sup>5</sup>, however, a brief review of the essential concepts follows. For slender bodies in hypervelocity flow, transition occurs due to second mode disturbances, also known as a Mack mode, which is an inviscid effect caused by acoustic waves trapped in the boundary layer. Once these disturbances are sufficiently amplified, the flow in the boundary layer transitions from laminar to turbulent. Hornung et al.<sup>6</sup> summarizes the work that has been done to characterize transition on slender bodies using the GALCIT Free-Piston Shock Tunnel, T5. Hornung's study begins with the measurement of transition on a five-degree-half-angle cone with free-stream compositions of nitrogen, air, and carbon dioxide. Their results show that carbon dioxide had higher transition Reynolds number evaluated at Eckert's reference conditions<sup>7</sup> as compared to that of nitrogen and air. However, this difference was not seen in experiments at lower total enthalpies. Hornung attributes the difference in transition behavior at different enthalpies to the acoustic damping of non-equilibrium processes such as molecular vibration and dissociation.

The effect of non-equilibrium has also been studied using numerical simulations as a means for delaying transition. Analyses, such as that of Johnson et al.<sup>8</sup>, prove that adding chemical and thermal non-equilibria to a simulation increase the stability of a boundary layer. This increase in stability is due to endothermic reactions and vibrational modes absorbing the energy of the disturbances. In addition, these analyses find that the stabilizing effect is greater when the fluid consists of carbon dioxide rather than air, which is a result of various properties of carbon dioxide. First, carbon dioxide has a relatively low dissociation temperature compared to that of diatomic oxygen and nitrogen. Second, carbon dioxide has three vibrational modes, whereas oxygen and nitrogen have only one. Lastly, carbon dioxide most efficiently absorbs acoustic energy at frequencies similar to those that cause transition for high Mach numbers.

A more in-depth analysis of carbon dioxide's stabilizing effect was done by Fujii and Hornung<sup>4</sup>, which found that carbon dioxide most efficiently absorbs acoustic frequencies in the same range as those that cause transition, typically around 1-10 MHz, displayed in Figure 1. In general, carbon dioxide most efficiently absorbs acoustic energy in this frequency range near 2000 K, as seen in Figure 2. Fujii also notes that when two peaks are present in the absorption rate versus frequency curve they correspond to a particular relaxation mode. The first peak, at a lower frequency, is due to dissociation, and the second peak, at a higher frequency, is due to vibrational relaxation. Fujii's data show that vibrational relaxation will be the dominant mechanism for disturbance energy absorption for the current study. As the temperature increases, more carbon dioxide dissociates, resulting in fewer molecular vibrators and thus a weaker peak in the vibrational absorption rate. However, if the temperature is sufficiently high, the chemical relaxation can begin to have significant acoustic energy absorption.

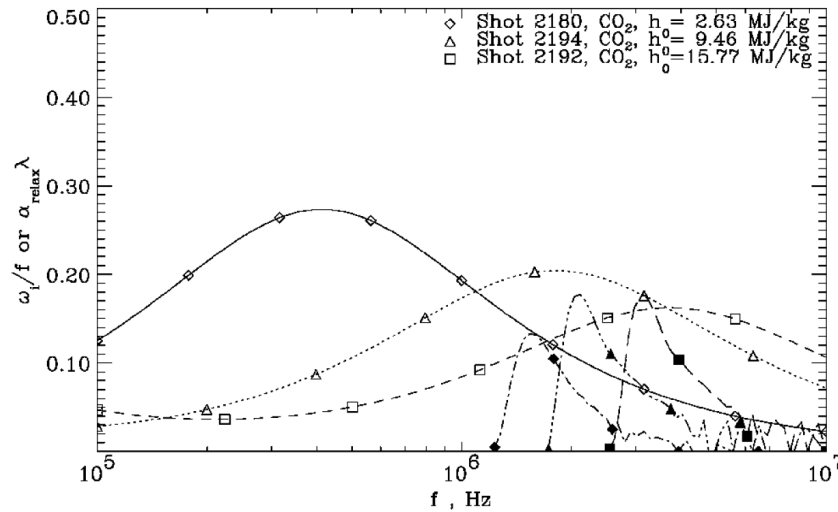


**Figure 1.** This plot compares the disturbance frequencies calculated using a linear stability analysis against the absorption rate of carbon dioxide on a 45-degree, swept cylinder. The disturbance frequencies are in the range of 1-10 MHz, which is typical for the second mode. This plot is taken from Fujii and Hornung<sup>4</sup>.

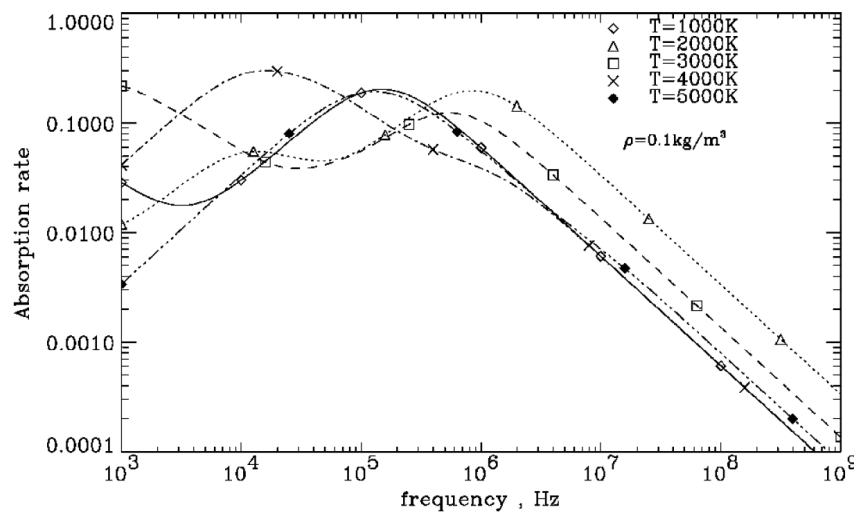


**Figure 2.** Sound absorption rate based on frequency for carbon dioxide at various temperatures. Carbon dioxide absorbs disturbance energy most effectively at 2000 K for the range of 1-10 MHz. This plot is taken from Fujii and Hornung<sup>4</sup>.

The previous work by Leyva et al.<sup>5</sup> included a preliminary study to test the feasibility of injecting carbon dioxide to delay boundary layer transition by altering the free-stream mixture. As inferred from Figure 3, increasing the mole fraction of carbon dioxide increases the transition Reynolds' number, reinforcing the findings of Hornung et al.<sup>6</sup> These tests could be considered the result from an optimal addition, mixing, and heating of carbon dioxide in a free-stream composed of air or nitrogen. Though the tests with air as the primary free-stream component are limited, a mole fraction of fourteen percent would have a noticeable delay in transition.

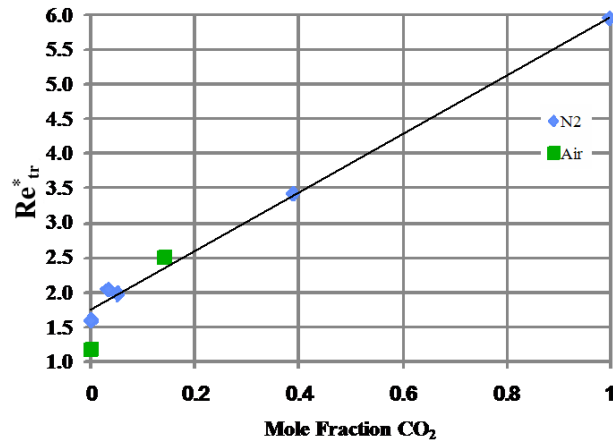


**Figure 3.** This plot summarizes preliminary work performed at the T5 tunnel. An increase in the amount of carbon dioxide delays transition further down the cone. This plot is taken from Leyva et al.<sup>5</sup>

Over the last year the injector models proposed in Leyva et al.<sup>5</sup> were tested more thoroughly experimentally and numerically. These models include a number of rows, ranging from one to four, of evenly spaced injector ports at a shallow angle to surface. The objective of this low angle injection was to add carbon dioxide while minimizing the disturbance caused to the boundary layer, with regards to the penetration height and the loss of stream-wise momentum. At the T5 tunnel, experiments revealed that the flow was transitioning at the location of injection, indicating that the injection was causing too large of a disturbance to the boundary layer. Further testing also showed that the presence of the ports alone, without gas injection, was causing a disturbance large enough to transition the boundary layer<sup>9</sup>, seen in Figure 4. Numerical testing of a simplified model of the experiment showed promise; however, upon completion of a grid convergence study, it was found that the shear layer that develops between the shock layer and jet gas became unstable and began to breakdown, shown in Figure 5. Due to the tendency of the discrete jets to cause transition, a model using an axi-symmetric transpiration was built and is currently under research.

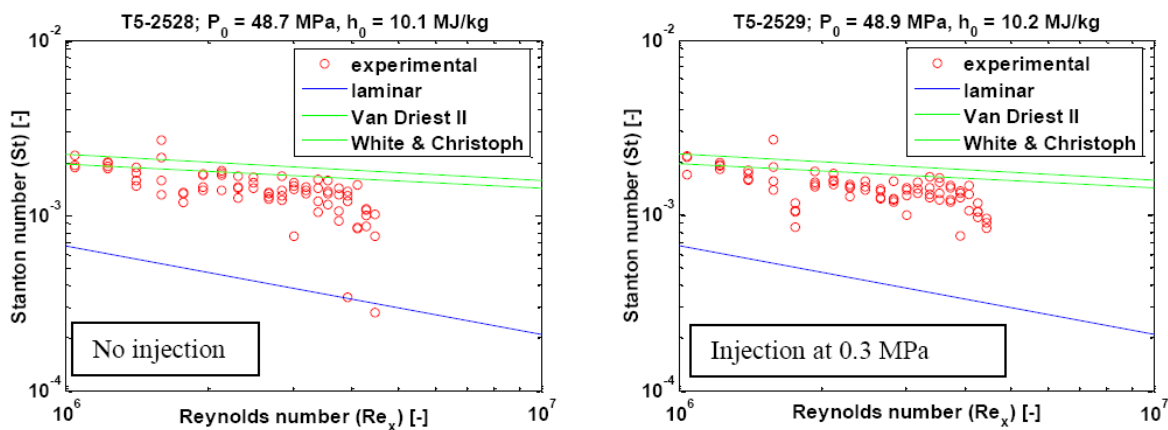


**Figure 4.** These plots are data from the thermocouples for two shots at the T5 tunnel. Both shots have four rows of discrete injector ports and both show fully turbulent heating. This plot is taken from Leyva et al.<sup>9</sup>

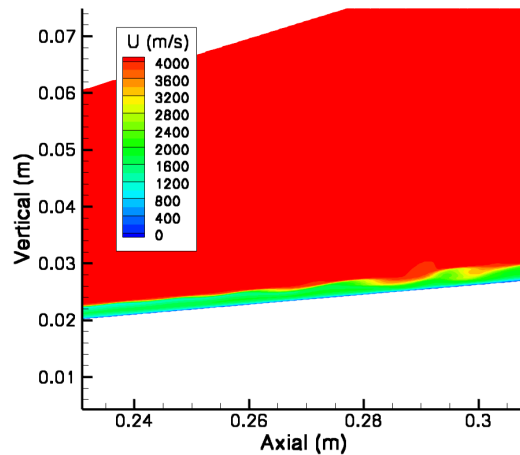


**Figure 5. This plot shows contours of stream-wise velocity from a simulation of carbon dioxide injection through a discrete port at 0.58 MPa. The injection resulted in shear-layer breakdown.**

### III. Computational Model

Due to the axi-symmetric nature of the injection scheme, the axi-symmetric, reacting, compressible Navier-Stokes equations are solved using a structured, optimized, 2D/axi-symmetric CFD solver based on the implicit Data-Parallel, Line-Relaxation (DPLR) method<sup>10</sup>. The solutions are laminar and provide a mean flow for the stability analysis. The inviscid fluxes are evaluated using the second-order accurate, modified Steger-Warming flux vector splitting method. The viscous fluxes are calculated using a second-order central method. The time integration is the first-order accurate, implicit, line-relaxation method. Solutions are calculated in parallel using MPI to handle inter-processor communication. This solver is contained in the software suite called STABL<sup>11</sup>, written by Dr. Heath Johnson.

The stability analysis is performed with the PSE-Chem solver, also a part of STABL. PSE-Chem solves the two-dimensional linear parabolized stability equations, which are derived from the Navier-Stokes equations. The PSE-Chem solver also includes the effects of finite-rate chemical reactions and translational-vibrational energy exchange. The parabolized stability equations predict the amplification of disturbances as they interact with the boundary layer. The transition location is then predicted using the semi-empirical  $e^N$  approach, in which transition is assumed to occur when a disturbance has grown by a factor of  $e^N$  from its initial amplitude. The critical value of  $N$  should depend on the disturbance environment and other features such as surface roughness. Therefore,  $N$  must be calibrated for a particular wind tunnel facility; usually conventional non-quiet supersonic wind tunnels have been shown to have a critical  $N$  factor of about 6. For a more detailed explanation of the stability analysis, the reader is referred to the works by Johnson and Candler<sup>11</sup> and Johnson et al.<sup>12</sup>.

These analyses are performed using a seven species chemistry set which includes  $\text{CO}_2$ ,  $\text{CO}$ ,  $\text{N}_2$ ,  $\text{O}_2$ ,  $\text{NO}$ ,  $\text{N}$ , and  $\text{O}$ . For simulations involving the injection of nitrogen or air, a simplified version of this set including only  $\text{N}_2$ ,  $\text{O}_2$ ,  $\text{NO}$ ,  $\text{N}$ , and  $\text{O}$  is used. The viscosity for each species is calculated using a composition of various models, each appropriate for a different temperature range. The models are unified using blending functions to maintain continuity for both the value and derivative value of viscosity. The conductivity is calculated using Eucken's relation. The mixture quantities are then calculated using Wilke's semi-empirical mixing law. It is assumed that vibrational-vibrational energy exchanges happen on a relatively short time scale and thus are in equilibrium and governed by a single temperature,  $T_v$ . It is also assumed that rotation and translation are coupled and are governed by the translational temperature. The translational-vibrational energy exchanges are governed by the Laudau-Teller model. The characteristic relaxation times are based on the Millikan and White model, except for the relaxation times involving  $\text{CO}_2$ , which are based on those determined by Camac<sup>13</sup>. The chemical reactions used for these simulations are given in Table 4 in the appendix. The forward reaction rate coefficients are taken from Park et al.<sup>14</sup>, except reactions five and six, which are taken from Bose and Candler<sup>15, 16</sup>, respectively. The equilibrium coefficients

are taken from Park<sup>17</sup>, except for reactions one and seven, which result from fitting the data given by McBride et al.<sup>18</sup>.

#### IV. T5 Tunnel Test Body

The T5 tunnel test body is a sharp, five-degree-half-angle cone. The surface of the cone is smooth with the exception of a porous material between 12.8 cm and 16.9 cm from the nose of the cone. This material has pores with a diameter of approximately 10  $\mu\text{m}$ . In the numerical simulations, the porous wall transpiration is modeled through the use of the wall-blowing condition contained in the CFD solver. It is assumed that mass flow rate through the porous material is a constant over a given area. In an axi-symmetric simulation, this results in a top hat distribution of mass flux per meter across the length of the injection region. To maintain continuity of the mass flux of injection gas through the wall between the solid and porous surfaces, a function based on hyperbolic tangent is generated to approximate the top hat distribution.

The grid used in these simulations is generated by a module included in STABL. Due to the structured nature of the CFD solver, all cells of the grid are quadrilateral. The wall-normal direction has 300 cells and the cells are clustered near the wall to guarantee that the  $y^+$  values are all less than one and have a maximum geometric growth rate of 2.7 percent in order to properly resolve the boundary layer gradients. The wall-tangential direction has 1249 total cells. A majority of these cells are clustered near the nose and have a maximum geometric growth rate of 5.8 percent until the injection region. At this location, 100 cells are distributed across the porous wall surface. From the end of the injection region until the end of the cone the cell sizes have a maximum geometric growth rate of 2.4 percent.

The conditions for the current injection simulations are chosen to be similar to shot 2541 performed in the T5 tunnel and consist of a partially dissociated mixture of air with the physical properties listed in Table 1 as both the reservoir for the tunnel and the free-stream. The free-stream Mach number is approximately 5.3. The wall condition for this experiment is considered to be isothermal with a temperature of 293 K.

**Table 1. Free-stream Conditions Used for the T5 Tunnel Simulations.**

Stagnation Conditions		Free-stream Conditions	
Pressure (MPa)	50.92	Density ( $\text{kg/m}^3$ )	0.05572
Temperature (K)	5968.5	Temperature (K)	1369.4
Entalpy (MJ/kg)	9.51	Velocity (m/s)	3957.9

A number of cases are run using carbon dioxide as the injection gas with a total mass flow rate ranging from 3 grams per second (g/s) to 13.5 g/s. Air and nitrogen are also injected to determine the effectiveness of injection gases with different vibrational and chemical parameters. For these cases the injection gas temperature is assumed to be equal to the wall temperature. To gauge the effect of heating the carbon dioxide before injection, four cases are run with injection temperatures of 1000, 1500, 2000, and 2500 K. These last six cases all have different mass flow rates in order to match the penetration height of transpiration for the cold carbon dioxide case with a total mass flow rate of 13.5 g/s. A summary of these test cases is provided in Table 5 in the appendix.

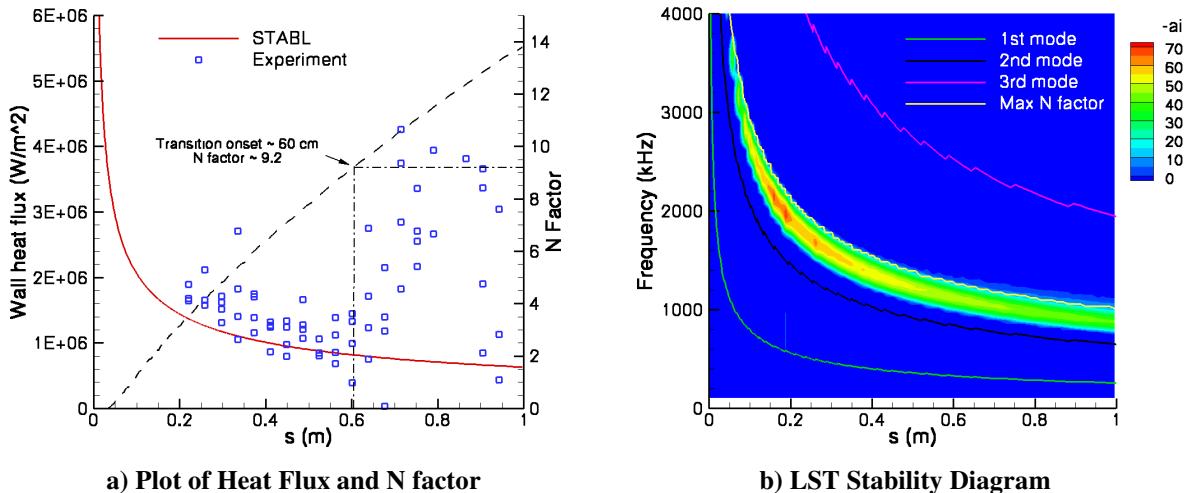
##### A. Smooth Cone

As previously mentioned, the semi-empirical  $e^N$  method requires calibration to the environment of the test facility to determine the growth rate that will cause transition. A stability analysis is performed on a cone without injection to provide this calibration and also to serve as a baseline from which a potential delay in transition will be measured. The experimental data are taken from the shot 2540 and the comparison of these and the computational data are seen in Figure 6a. The free-stream conditions are similar to those of the injection cases and are listed in Table 2. The gas composition is a partially dissociated mixture of air and the Mach number is approximately 5.3. Transition onset occurs at approximately 60 cm along the cone's surface, which corresponds to an N factor of approximately 9.2. This differs from previously published data<sup>8</sup> and requires more thorough investigation to ensure the accuracy of this result for the T5 facility. However, this is the N factor that will be used for the current study. The accuracy of the mean flow can also be gauged from Figure 6a by the similarity in the laminar heating rates on the cone surface.

The stability diagram produced by the LST analysis, seen in Figure 6b, plots contours of amplification rate over a range of frequencies and distances along the cone. The 1<sup>st</sup>, 2<sup>nd</sup>, and 3<sup>rd</sup> mode estimates are plotted as well as the most-amplified frequency. The diagram shows that the disturbances that cause transition are second mode, demonstrating that this case is well-suited to test the injection of carbon dioxide.

**Table 2. Free-stream Conditions for the Shot 2540.**

Stagnation Conditions		Free-stream Conditions	
Pressure (MPa)	51.61	Density (kg/m <sup>3</sup> )	0.05788
Temperature (K)	5857.77	Temperature (K)	1323.77
Entalpy (MJ/kg)	9.47	Velocity (m/s)	3909.74



**a) Plot of Heat Flux and N factor** **b) LST Stability Diagram**  
**Figure 6.** These plots show the results from the stability analysis of a smooth cone. The free-stream conditions for this case are contained in Table 2. The plot on the left, a), shows the comparison of heat flux between the simulation and experiment. Transition onset is gauged by the rapid increase in heat flux and the N factor at that location is measured. The plot on the right, b), is the LST stability diagram, disturbance mode frequency estimates, and the most-amplified frequency.

## B. Cold Carbon Dioxide Injection

Wall-blowing usually has a destabilizing effect on a boundary layer, so it is expected that increasing mass flow rate of blowing would cause a decrease in stability. The stability analyses of cases with injection of 3 g/s through 7.5 g/s follow this trend, seen in Figure 7a. Transition is predicted in the post-injection region for the 3 g/s case; however, it may not due to the variability in the amplification required for transition. All other cases show sufficient amplification to transition immediately following the injection region. The N factor plots for cases of 6 g/s and 7.5 g/s are truncated toward the nose of the vehicle due to the presence of a recirculation zone at the front of the transpiration. It is unknown if this recirculation exists in the experimental flow field and also the effect the recirculation has on the boundary layer stability. Some conditions in the PSE analysis were not calculated in order to avoid integrating through a recirculation zone and therefore the data in this region have been omitted from the results. All of the N factor profiles are similar in the region immediately following injection, indicating that the flow features such as the penetration height of the injection and distance of the boundary layer recovery are also similar, with their amplitudes dependent on the total mass injected.

For the cases with injection of 10 g/s to 12 g/s, the stability analyses show a further increase in amplification with injection rate, seen in Figure 7b. The cases with injection of 13 g/s and 13.5 g/s show an increase in stability, however, all cases in this range have sufficient amplification after the injection to transition.

One feature common to all injection cases simulated is the growth of N factor is more rapid than in the smooth cone case on the later part of the cone. The reason for this is best demonstrated by the stability diagram from the case with injection of 6 g/s, seen in Figure 8. The second mode disturbances continue to experience the largest amplification; therefore it is expected that the most-amplified frequencies will follow the boundary layer thickness. During the injection, the boundary layer thickness increases from the injection gas, thus resulting in a drop in the frequencies being amplified. After the injection, the boundary layer thickness decreases until resuming its natural growth. The distance where this growth begins represents a recovery distance for the boundary layer. The change in

slope of the boundary layer thickness allows for a band of frequencies to be continuously amplified for a greater length than in the smooth cone case. Due to this flow feature, the recovery distance is a factor that could cause transition for all simulations after the flow has absorbed the disturbance the injection. Also visible on the stability diagram is the amplification of higher modes of disturbances.

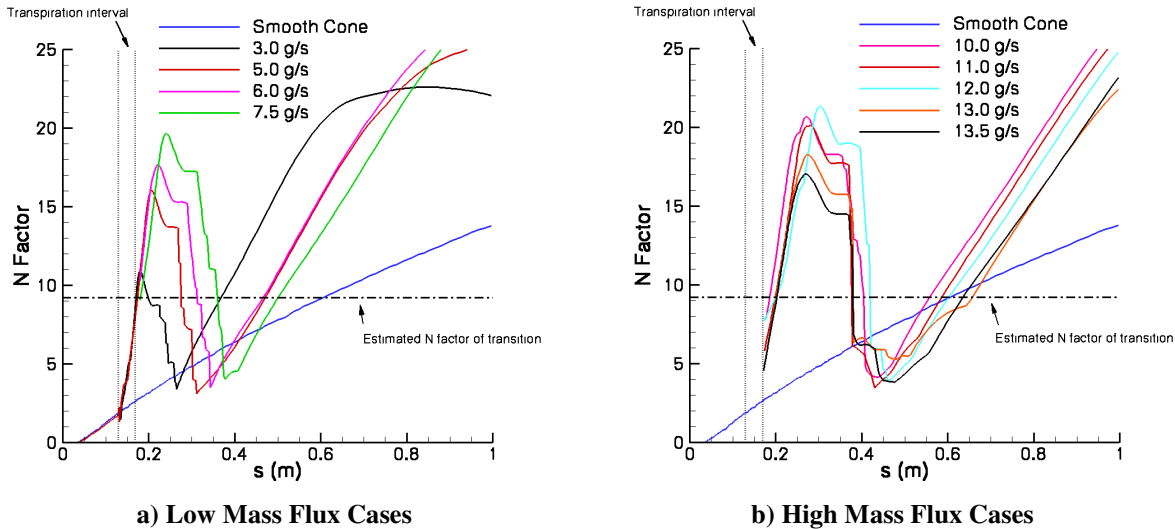


**Figure 7.** These plots show the results from the stability analyses of cold carbon dioxide injection. The free-stream conditions for these cases are contained in Table 1. The low mass flux cases are shown in a). The high mass flux cases are shown in b). The 3 g/s case is in a borderline state of transition, while all other cases reach an N factor sufficient to cause transition immediately following the injection region.

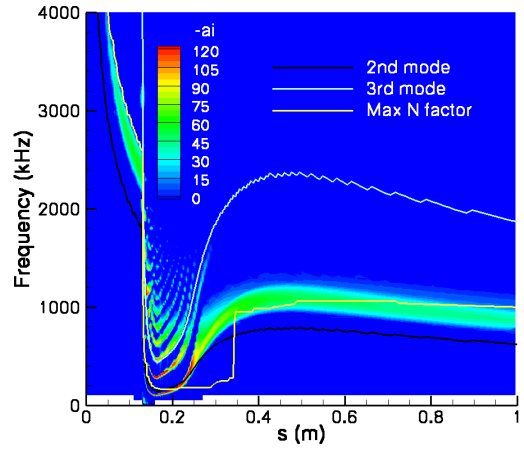


**Figure 8.** This plot shows the LST stability diagram for the case of cold carbon dioxide injection at a rate of 6 g/s. The sharp drop in amplified frequencies is due to the rapid increase in boundary layer thickness. The frequencies rise as the boundary layer recovers from the injection until resuming its natural growth. Also visible is the amplification of higher modes of disturbances.

**C. Alternate Injection Gases**

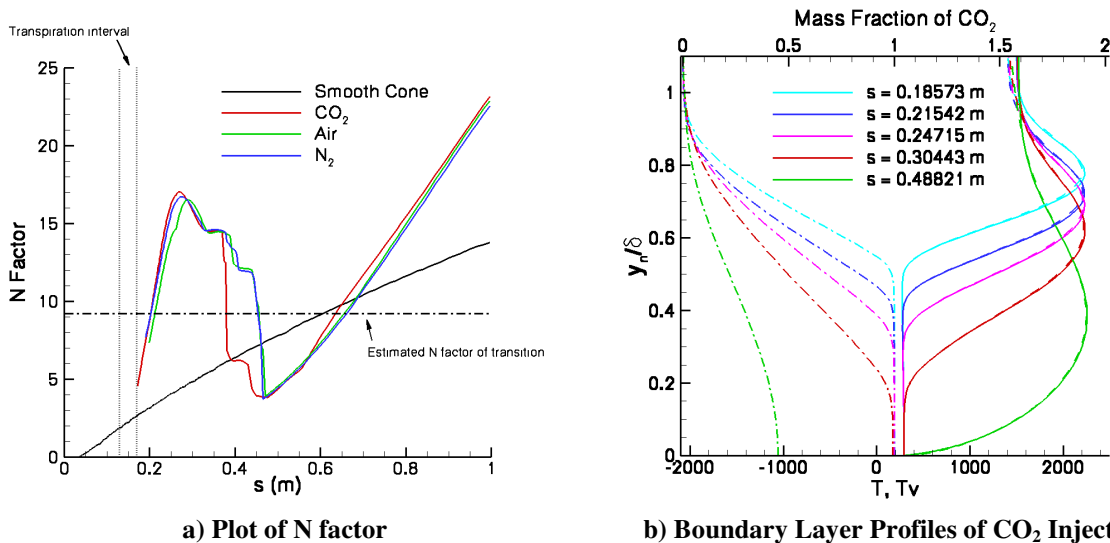
From previous experiments at the T5 tunnel, it is known that flows involving air and pure nitrogen will transition at a lower Reynolds number for stagnation enthalpies ranging from 4 MJ/kg to 10 MJ/kg than flows involving carbon dioxide. Due to this knowledge, it is expected that injection of carbon dioxide would result in a more stable

Downloaded by AFRL/DII on November 27, 2013 | http://arc.aiaa.org | DOI: 10.2514/6.2010-1244

boundary layer relative to a boundary layer of air or nitrogen, if carbon dioxide has a high enough temperature to be vibrationally excited. For the alternate injection gas cases the momentum of injection is matched to the carbon dioxide injection with a total mass flow rate of 13.5 g/s, requiring a different total mass flow rate for each case. The similarity of amplification, seen in Figure 9a, suggests that the momentum of injection is more important in determining the stability when the injection gases are cold. It is easiest to understand a possible reason for these similarities by inspecting the boundary layer profiles of the case with carbon dioxide injection, seen in Figure 9b. These profiles show that a majority of the injected carbon dioxide remains relatively cold. At these low temperatures, the carbon dioxide does not have the ability to absorb disturbance energy with the same capacity that it does at higher temperatures.

#### D. Heated Carbon Dioxide Injection

In order to ensure the effectiveness of the injected carbon dioxide to absorb energy from acoustic disturbances, the gas is heated before injection to a temperature range where the effects of non-equilibrium occur. The carbon dioxide is assumed to be in chemical and thermal equilibrium before injection. For the case of 2500K this results in approximately twenty percent, by mass, of the carbon dioxide being dissociated. This implies that fewer molecules are present to absorb energy from disturbances, however, as shown in Figure 2, the carbon dioxide is more efficient around 2000 K than it is below 1000 K. For these cases, the momentum of injection has been matched with the 13.5 g/s case of cold carbon dioxide injection. The effect of injecting less mass has not been separated from injecting heated gas. The stability analyses in Figure 10 show a reduction in amplification with an increase in temperature of the injection gas in the post-injection region. For the case where the injection gas is 1000 K, the boundary layer is in a borderline state of transition following the injection. If this case does not transition at this distance on the cone, then transition is expected at approximately the same location as the smooth cone case. However, all other cases are expected to transition earlier than the smooth cone case due the amplification that occurs where the boundary layer recovers.



**a) Plot of N factor** **b) Boundary Layer Profiles of CO<sub>2</sub> Injection**  
**Figure 9.** The plot on the left, a), shows the N factors that result from the injection of various gases while preserving the penetration height of transpiration. The plot on the right, b), shows the normalized boundary layer profiles of mass fraction of carbon dioxide (dashed dot), translational temperature (solid), and vibrational temperature (dashed). This plot shows a layer of cold carbon dioxide that is inefficient for absorbing energy from acoustic disturbances. The free-stream conditions for these cases are contained in Table 1. Each case has a different total mass flux in order to match the penetration height of the injection. The variable  $y_n$  indicates the wall-normal direction.

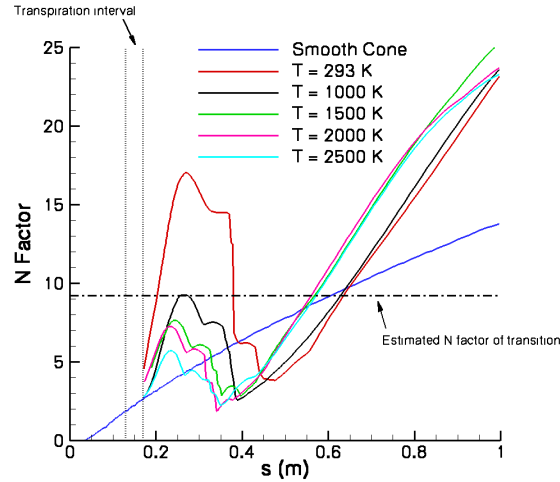


**Figure 10.** This plot shows the results from the stability analyses of heated carbon dioxide injection. The free-stream conditions for these cases are contained in Table 1. As expected, an increase in temperature of the injected gas further reduces the amplification experienced in the post-injection region.

## V. Theoretical Injection

The analyses of the previous cases predict that injecting a beneficial amount of carbon dioxide over a short interval without causing transition will be difficult. Based on these results, a second, purely theoretical, test body is simulated in order to isolate the effects of non-equilibrium processes. The test body is also a sharp, five-degree-half-angle cone. The free-stream is composed of only nitrogen in an attempt to reduce the influence of the free-stream gas. Based on the work by Fujii and Hornung<sup>4</sup>, nitrogen has a lower absorption rate of acoustic energy as compared to air, which will further reduce the free-stream gas's ability to damp second mode disturbances. The free-stream total enthalpy is similar to the previous cases in order to maintain a similar heating environment for the injected gas in the boundary layer. Rather than reduce the mass flux through the short interval, the theoretical injection cases have a similar amount of mass transpired over a longer interval, starting at 10 cm and ending at 90 cm from the nose of the cone. The injection profile is more gradual and is based on a wall-suction model suggested by Malik<sup>19</sup> and further investigated by Johnson et al.<sup>20</sup>. The mass flux through the wall is specified by edge properties and a dimensionless wall blowing parameter,  $f_w$ , seen in Eq. (1).

$$f_w = \frac{\sqrt{2\text{Re}_x} \rho_w v_w}{\rho_e v_e} \quad (1)$$

In this equation,  $\text{Re}_x$  is the Reynolds number based on the surface distance along the cone,  $\rho$  is the fluid density,  $v$  is the fluid velocity, the subscript  $e$  denotes boundary layer edge properties, and the subscript  $w$  denotes wall properties. For these cases the parameter  $f_w$  is held constant, making the mass flux vary along the length of the cone. Using this model, the dominant factors of rapid boundary layer thickness increase and also the boundary layer recovery seen in the previous cases have been eliminated. It should now be possible to see the effects of non-equilibrium processes that support previous work.

The grid for these simulations is composed of a structured set of quadrilaterals. The wall-normal direction has 300 cells with the spacing at the wall set such that the  $y^+$  value is less than one and the maximum geometric growth rate is 2.7 percent. The wall-tangential direction has 1000 cells, which are clustered to the nose of the cone and have a maximum growth rate of 4.4 percent.

The conditions for the following simulations are chosen to be similar to shot 548 performed in the T5 tunnel, with the properties contained in Table 3. As previously stated, the free-stream consists of a partially dissociated mixture of nitrogen. The free-stream Mach number is 6.5 and the wall condition is isothermal with a temperature of

293 K. Six cases of cold carbon dioxide injection are run with  $f_w$  ranging from 0.05 to 0.6. Nitrogen is tested in three cases as the injection gas with  $f_w$  ranging from 0.05 to 0.2 and air is also tested with  $f_w$  set to 0.1. Finally, the effect of pre-heating the carbon dioxide to a temperature of 1000 K is also tested in five cases with  $f_w$  ranging from 0.05 to 0.4. A summary of these test cases, as well as total mass flux for each case, is included in the appendix in Table 6.

**Table 3. Free-stream Conditions Used for the Theoretical Injection Simulations.**

Stagnation Conditions		Free-stream Conditions		Edge Conditions	
Pressure (MPa)	55.0	Density ( $\text{kg/m}^3$ )	0.051855	Unit Reynolds (1/m)	6.0003e+6
Temperature (K)	6958	Temperature (K)	925.5	Density ( $\text{kg/m}^3$ )	0.072
Entalpy (MJ/kg)	9.39	Velocity (m/s)	4039.7	Velocity (m/s)	3975

#### A. Smooth Cone

A cone without injection is also tested and the stability analysis results in a similar curve as the previous set of free-stream conditions, shown in Figure 11a. Using the same critical N factor as the previous cases, transition is expected to occur near 63 cm from the nose of the cone. This will serve as the baseline to gauge transition delay.

#### B. Cold Carbon Dioxide Injection

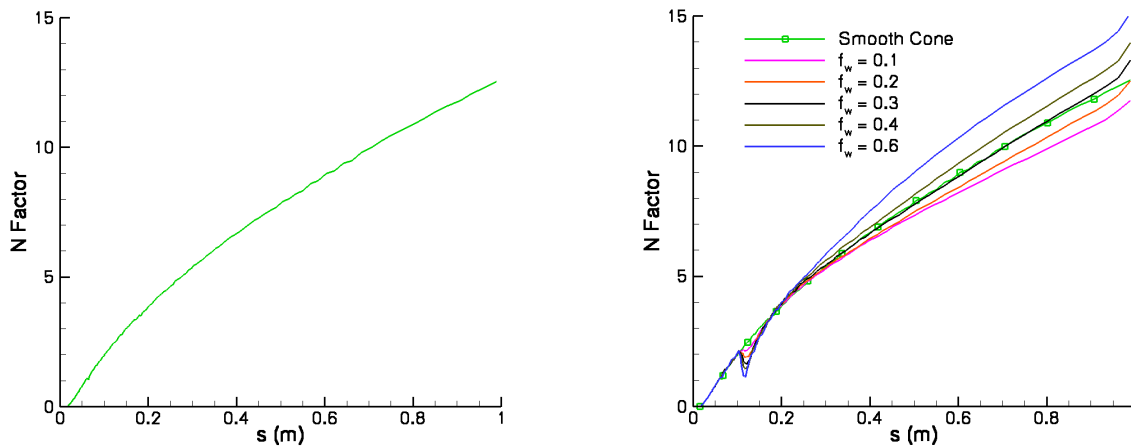
The stability results for the cold carbon dioxide injection are as expected and are contained in Figure 11b. Since the injection profile is more gradual than the injection in the T5 tunnel cases, the rapid growth of the boundary layer thickness and rapid amplification is not present for these cases. Initially, the injection of carbon dioxide increases the stability moving transition back to 72 cm. As the mass flux increases the amplification increases, indicating an optimum amount of injection. When  $f_w$  is 0.3, the stabilizing effect of the carbon dioxide is offset by the destabilizing effect of blowing. For the higher values of  $f_w$  this destabilizing trend continues.

#### C. Alternate Injection Gases

The results from the injection of air and nitrogen are as expected. The stability analyses, seen in Figure 12a, show that only a small difference exists between the injection of air and nitrogen and that blowing for either of these two gases only destabilizes the boundary layer. These qualities suggest that the stagnation enthalpy of the free-stream is too low to take advantage of the non-equilibrium effects for these gases and are in agreement with the previous experiments at T5.

#### D. Heated Carbon Dioxide Injection

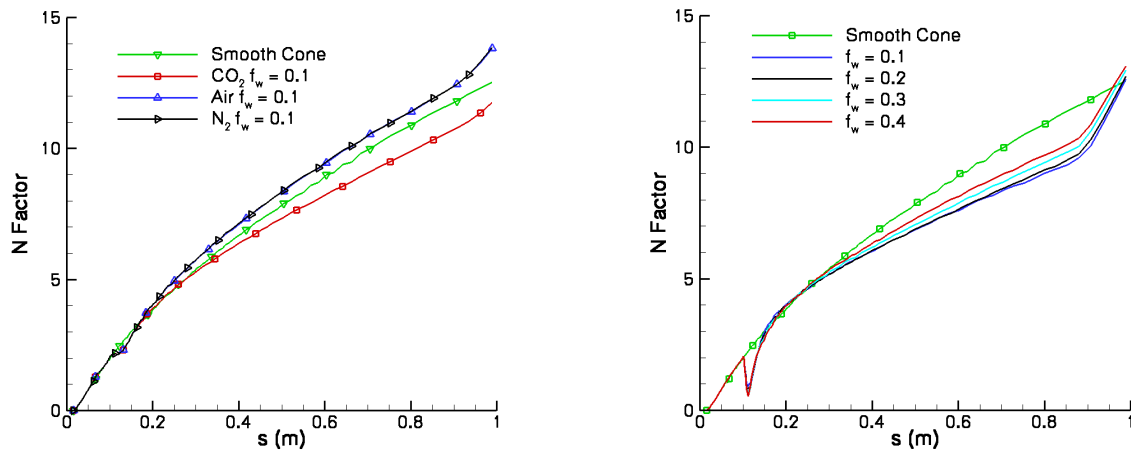
Pre-heating the injected carbon dioxide has a similar effect as in the T5 tunnel cases. The stability analyses, seen in Figure 12b, show transition delay for all cases tested with heated carbon dioxide injection. In the cold injection cases, the carbon dioxide needs some distance along the cone to absorb heat to be in a temperature range where it will more effectively absorb energy from acoustic disturbances. When the carbon dioxide is pre-heated, it starts absorbing disturbance energy earlier, thus resulting in less amplification over the length of the cone. Higher temperature gas, not necessarily carbon dioxide, could also contribute to the reduction in amplification of second mode disturbances. This effect is discussed in more detail by Malik<sup>19</sup>. Using a critical N factor of 9.2, the estimated transition location can be measured. A summary of these locations for all of the theoretical cases tested is plotted in Figure 13.



a) Smooth Cone with  $N_2$  free-stream

b) N Factors for Cold  $CO_2$  Injection

Figure 11. These plots show the stability analysis results for the smooth cone, a), and cold carbon dioxide injection, b), with a free-stream composed of nitrogen. The free-stream conditions for these cases are contained in Table 3. The case with  $f_w$  set to 0.1 shows the maximum transition delay. Cases with higher mass flux result in more amplification.



a) N factors for Alternate Injection Gases

b) N Factors for Heated Carbon Dioxide Injection

Figure 12. These plots show the stability analysis results for select cases of alternate gas injection, a), and heated carbon dioxide injection, b). The temperature of the injection gas for plot b) is 1000 K. The free-stream conditions for these cases are contained in Table 3. Transition delay does not occur for the alternate gases, while the delay is increased for the heated carbon dioxide cases.

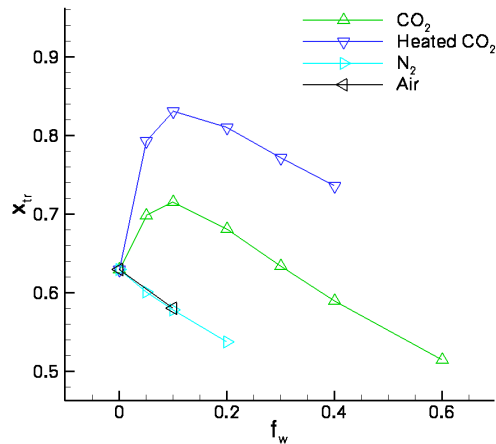


**Figure 13.** This plot is a summary of the transition locations for the theoretical injection cases based on the critical N factor of 9.2. The injection of carbon dioxide shows an optimum amount of mass injected.

## VI. Effects of Relaxation Processes

A unique feature of computational analysis is the ability to freeze both the chemical and vibrational modes of disturbance energy absorption. The effect on boundary layer transition delay of each of these modes can then be assessed. The freezing of each relaxation process is done with PSE-chem analysis, while the mean flow has both vibration and chemistry active. This test is performed for the injection of cold carbon dioxide, heated carbon dioxide and nitrogen all with  $f_w$  set to 0.1. As seen in Figure 14, both the full relaxation and vibrational relaxation from the injection of cold carbon dioxide follow the same curve, indicating that the vibrational relaxation is responsible for absorbing energy from disturbances. To verify this, a stability analysis with only chemical relaxation is compared to one with no relaxation processes active and is found to be identical. For this temperature range, the vibrational mode is expected to be the dominant mechanism for reducing the amplification of acoustic disturbances, as discussed in Fujii and Hornung<sup>4</sup>. It is interesting that a reduction of amplification still occurs when non-equilibrium effects in the disturbances are frozen. These data suggest that the gain in stability is also due to other aspects of injecting carbon dioxide. For the heated carbon dioxide case, a similar trend occurs with the only difference being the amplitude with which the N factors are increased without vibrational relaxation. The case with nitrogen shows no difference in amplification, verifying that the non-equilibrium in the disturbances has no effect for nitrogen for this temperature range.

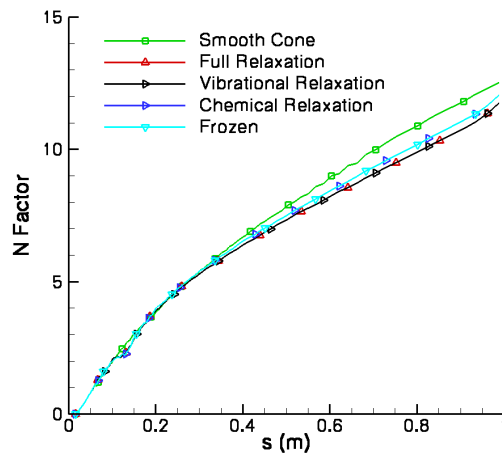


**Figure 14.** This plot shows the effect of non-equilibrium processes on the disturbances for cold carbon dioxide with  $f_w$  set to 0.1. It is interesting that a reduction in amplification still occurs despite these processes being frozen. The free-stream conditions for these cases are contained in Table 3.

## VII. Conclusion

This study tested the feasibility of injecting carbon dioxide as a means of boundary layer transition delay through the use of numerical simulations for two different test bodies. The first test case was a five-degree-half-angle cone with a 4 cm interval of transpiration and was modeled after an experimental test body that will be used in the GALCIT T5 Shock Tunnel at Caltech. The simulations predicted that transition will occur immediately following the injection of cold carbon dioxide. The test cases with air and nitrogen as the test gas suggested the momentum of the injection plays a dominant role in the amount of amplification seen immediately downstream due to the inefficient heating of the injected carbon dioxide. To remedy this, the injected carbon dioxide was pre-heated, resulting in a reduction of amplification in the post-injection region. Despite this reduction, the stability analyses still predicted transition to occur earlier on the cone as compared to a case without injection.

To isolate the effects of non-equilibrium processes on the disturbances, a second case involving a similar cone with a longer transpiration interval was tested. For this case, the stability analyses predicted a window of carbon dioxide injection resulting in a reduction of amplification and thus a delay in boundary layer transition. The cold carbon dioxide injected experienced sufficient heating to cause transition delay. Pre-heating the carbon dioxide showed a further delay in transition. The analyses further indicated an optimum amount of carbon dioxide injection as a balance between the stabilizing effects of carbon dioxide and the destabilizing effect of wall-blowing. Testing on the injection of air and nitrogen predicted no transition delay would occur and an increase in wall-blowing simply causes more amplification.

Finally, the effect of specific non-equilibrium processes was tested in order to investigate the contribution of each of these modes. Stability analyses predicted that vibrational relaxation contributes to damping acoustic disturbances, while chemical relaxation does not for the enthalpy range tested.

Further work includes experimental testing of the first test body in the T5 Shock Tunnel. This work will be very important to validate all of the models used to simulate these experiments, as well as the application of stability analysis for this type of flow. Should the results of these analyses prove to be accurate, an alternative means of injection will be explored.

## VIII. Acknowledgments

This work was sponsored by the Air Force Office of Scientific Research under grant FA9550-04-1-0341 and by the Department of Defense National Security Science & Engineering Faculty Fellowship. The views and conclusions contained herein are those of the author and should not be interpreted as necessarily representing the official policies or endorsements, either expressed or implied, of the AFOSR or the U.S. Government.

## IX. References

- <sup>1</sup>Mack, L.M., "Boundary-layer stability theory," In Special Course on Stability and Transition of Laminar Flow, AGARD Report Number 709, 1984.
- <sup>2</sup>Lighthill, M.J., Viscosity effects in sound waves of finite amplitude. In G.K. Batchelor and R.M. Davies, editors, *Surveys in Mechanics*, pages 250-351. Cambridge University Press, 1956.
- <sup>3</sup>Vincenti, W.G. and Kruger, C.H. *Introduction to Physical Gas Dynamics*, Krieger Publishing Company, 1965.
- <sup>4</sup>Fujii, K., and Hornung, H. G., "Experimental Investigation of High Enthalpy Effects on Attachment-line Boundary Layer Transition," AIAA, vol. 41, no. 7, July 2003.
- <sup>5</sup>Leyva, I. A., Laurence, S., Beierholm, A. W., Hornung, H.G., Wagnild, R. W., and Candler, G. V., "Transition Delay in Hypervelocity Boundary Layers by Means of CO<sub>2</sub>/acoustic Instability Interactions," AIAA Paper 2009-1287, January 2009.
- <sup>6</sup>Hornung, H. G., Adam, P. H., Germain, P., Fujii, K., and Rasheed, A., "On Transition and Transition Control in Hypervelocity Flows," Proceedings of the Ninth Asian Congress of Fluid Mechanics, Isfahan, Iran, 2002.
- <sup>7</sup>Eckert, E.R.G., "Engineering relations for friction and heat transfer to surfaces in high velocity flow," *Journal of the Aeronautical Sciences*, 22:585-587, Aug. 1955.
- <sup>8</sup>Johnson, H. B., Seipp, T. G., and Candler, G. V., "Numerical Study of Hypersonic Reacting Boundary Layer Transition on Cones," *Physics of Fluids*, vol. 10, No. 10, October 1998.
- <sup>9</sup>Leyva, I. A., Jewell, J. S., Laurence, S., Hornung, H. G., Shepherd, J. E., "On the impact of injection schemes on transition in hypersonic boundary layers," AIAA Paper 2009-7204, October 2009.
- <sup>10</sup>Wright, M. J., Candler, G. V., and Bose, D., "A Data-Parallel Line-Relaxation Method for the Navier-Stokes Equations," AIAA Paper 97-2046CP, June 1997.
- <sup>11</sup>Johnson, H. B., and Candler, G. V., "Hypersonic Boundary Layer Stability Analysis Using PSE-Chem," AIAA Paper 2005-5023, June 2005.
- <sup>12</sup>Johnson, H. B., Candler, G. V., and Wright, M. J., "Boundary Layer Stability Analysis of Mars Science Laboratory Aeroshell," AIAA Paper 2006-0920, January 2006.
- <sup>13</sup>Camac, M., "CO<sub>2</sub> Relaxation Processes in Shock Waves," *Fundamental Phenomena in Hypersonic Flow*, Ed. J.G. Hall, Cornell University Press, Ithaca, NY, 1966, pp. 195-215.
- <sup>14</sup>Park, C., Howe, J.T., Jaffe, R.J., and Candler, G.V., "Review of Chemical-Kinetic Problems of Future NASA Missions, II: Mars Entries," *Journal of Thermophysics and Heat Transfer*, Vol. 8, No. 1, 1994, pp. 9-23.
- <sup>15</sup>Bose, D. and Candler, G. V. "Thermal Rate Constants of the N<sub>2</sub> + O → NO + N Reaction Using Ab Initio 3a' and 3a' Potential Energy Surfaces," *Journal of Chemical Physics*, vol. 104, No. 8, pp. 2825-2833, 1996.
- <sup>16</sup>Bose, D. and Candler, G. V. "Thermal Rate Constants of the O<sub>2</sub> + N → NO + O Reaction Based on the 2a' and 4a' Potential Energy Surfaces," *Journal of Chemical Physics*, vol. 107, No. 16, pp. 6136-6145, 1997.
- <sup>17</sup>Park, C., *Nonequilibrium Hypersonic Aerodynamics*, Wiley, 1990.
- <sup>18</sup>McBride, B. J., Zehe, M. J., and Gordon, S. "NASA Glenn Coefficients for Calculating Thermodynamic Properties of Individual Species," Tech. Rep. 2002-211556, NASA, September 2002.
- <sup>19</sup>Malik, M. R., "Prediction and Control of Transition in Supersonic and Hypersonic Boundary Layers," *AIAA Journal*, vol. 27, no. 11, November 1989, pp. 1487-1493.
- <sup>20</sup>Johnson, H. B., Gronvall, J. E., Candler, G. V., "Reacting Hypersonic Boundary Layer Stability with Blowing and Suction," AIAA Paper 2009-938, January 2009.

## X. Appendix

**Table 4. Reaction set used for the CFD simulations**

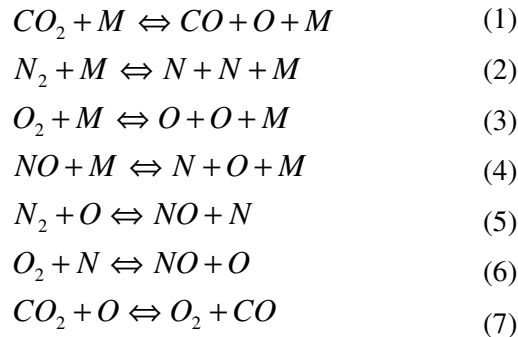


**Table 5. Summary of cases tested for the T5 tunnel test body**

Case	Injection Gas	Temperature (K)	Mass Flux (g/s)
1	CO <sub>2</sub>	293	3.0
2	CO <sub>2</sub>	293	5.0
3	CO <sub>2</sub>	293	6.0
4	CO <sub>2</sub>	293	7.5
5	CO <sub>2</sub>	293	10.0
6	CO <sub>2</sub>	293	11.0
7	CO <sub>2</sub>	293	12.0
8	CO <sub>2</sub>	293	13.0
9	CO <sub>2</sub>	293	13.5
10	Air	293	10.93
11	N <sub>2</sub>	293	10.77
12	CO <sub>2</sub>	1000	9.43
13	CO <sub>2</sub>	1500	7.7
14	CO <sub>2</sub>	2000	6.9
15	CO <sub>2</sub>	2500	6.3

**Table 6. Summary of cases tested for the theoretical test body**

Case	Injection Gas	Temperature (K)	$f_w$	Mass Flux (g/s)
1	CO <sub>2</sub>	293	0.05	1.24
2	CO <sub>2</sub>	293	0.1	2.47
3	CO <sub>2</sub>	293	0.2	4.96
4	CO <sub>2</sub>	293	0.3	7.43
5	CO <sub>2</sub>	293	0.4	9.92
6	CO <sub>2</sub>	293	0.6	14.88
7	N <sub>2</sub>	293	0.05	1.24
8	N <sub>2</sub>	293	0.1	2.47
9	N <sub>2</sub>	293	0.2	4.96
10	Air	293	0.1	2.47
11	CO <sub>2</sub>	1000	0.05	1.24
12	CO <sub>2</sub>	1000	0.1	2.47
13	CO <sub>2</sub>	1000	0.2	4.96
14	CO <sub>2</sub>	1000	0.3	7.43
15	CO <sub>2</sub>	1000	0.4	9.92

# Effect of gas injection on transition in hypervelocity boundary layers

J.S. Jewell<sup>1</sup>, I.A. Leyva<sup>2</sup>, N.J. Parziale<sup>1</sup>, and J.E. Shepherd<sup>1</sup>

## 1 Introduction

A novel method to delay transition in hypervelocity flows in air over slender bodies by injecting CO<sub>2</sub> into the boundary layer is presented. The dominant transition mechanism in hypersonic flow is the inviscid second (Mack) mode, which is associated with acoustic disturbances which are trapped and amplified inside the boundary layer [8]. In dissociated CO<sub>2</sub>-rich flows, nonequilibrium molecular vibration damps the acoustic instability, and for the high-temperature, high-pressure conditions associated with hypervelocity flows, the effect is most pronounced in the frequency bands amplified by the second mode [3]. Experimental data were obtained in Caltech's T5 reflected shock tunnel. The experimental model was a 5 degree half-angle sharp cone instrumented with 80 thermocouples, providing heat transfer measurements from which transition locations were from turbulent intermittency based upon laminar and turbulent heat flux correlations. An appropriate injector was designed and fabricated, and the efficacy of injecting CO<sub>2</sub> in delaying transition was gauged at various mass flow rates, and compared with both no injection and chemically inert Argon injection cases. Argon was chosen for its similar density to CO<sub>2</sub>. At an enthalpy of approximately 10 MJ/kg (Eckert's reference temperature  $T^* = 2550$  K), transition delays in terms of Reynolds number were documented. For Argon injection cases at similar mass flow rates, transition is promoted.

## 2 Acoustic delay

Turbulent heat transfer rates can be an order of magnitude higher than laminar rates at hypersonic Mach numbers. A reduction in heating loads by keeping the bound-

---

*California Institute of Technology, 1200 E. California Blvd., Pasadena, CA 91125, USA · Air Force Research Laboratory, 10 East Saturn Blvd., Edwards AFB, CA 93524, USA*

ary layer laminar longer means less thermal protection is necessary, and hence less weight to carry, or conversely more payload deliverable, for a given design.

The theory of how energy from acoustic disturbances is absorbed by relaxation processes is treated in, among others, Vincenti and Kruger [12] which provides the simplified Landau-Teller theory,

$$\tau = C \exp(K_2/T)^{1/3}/p, \quad (1)$$

where  $C$  and  $K_2$  are constants, which implies that the vibrational relaxation time  $\tau$  decreases with increasing pressure and temperature. This suggests that increased temperature, if pressure is constant, should generally permit acoustic absorption at higher frequencies, as shown computationally by Johnson et al. [6].

Fujii and Hornung [3] computed sound absorption spectra for flows of both air and CO<sub>2</sub>. While the air flow's sound absorption curve peak occurs at much lower frequencies than the calculated amplification peak, in CO<sub>2</sub> the broad sound absorption peak coincides with the calculated amplification peaks. This coincidence is most pronounced at enthalpies of approximately 10 MJ/kg. Thus, for flows around this enthalpy, we might expect increasing the fraction of CO<sub>2</sub> in the boundary layer to lead to significant acoustic damping, and therefore delay transition.

### 3 Experiments

The facility used in all experiments in the current study was the T5 hypervelocity reflected shock tunnel at the California Institute of Technology; see [5] and [4]. The model employed for all experiments was a sharp slender cone similar to that used in a number of previous experimental studies in T5. It is a 5 degree half-angle aluminum cone, 1m in length, and is composed of three sections: a sharp tip fabricated of molybdenum (to withstand the high stagnation heat fluxes), a mid-section containing a porous gas-injector section (interchangeable with a smooth, non-porous injector section for control shots), and the main body instrumented with a total of 80 thermocouples evenly spaced at 20 lengthwise locations. These thermocouples have a response time on the order of a few  $\mu$ s and have been successfully used for boundary layer transition location in Leyva et al. [7] among many others. For a complete description of the thermocouple design, see Sanderson [11]. The conical model geometry was chosen because of the wealth of experimental and numerical data available with which to compare the results from this program. A photograph of the cone model is shown in Figure 1. The porous injector section is 4.13 cm in length and consists of sintered 316L stainless steel, with an average pore size of 10 microns. A detail view of the tip and porous injector section is shown in the bottom of Figure 1. The porous injector design was chosen in favor of various injection schemes with macroscopic holes, all of which were found to trip the boundary layer and lead to immediate or near-immediate transition. The goal of the porous injector was to achieve more spatially uniform injection flow, as discussed in Leyva et al.

[7]. The injector section is mounted around a plenum which supplies gas from a tank instrumented with a pressure transducer used to compute mass flow rate.

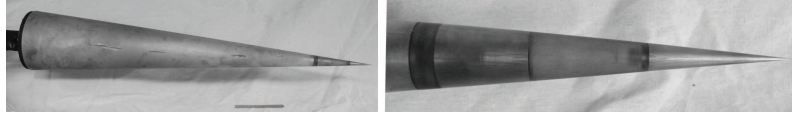


**Fig. 1** Left: Aluminum cone, 1m in length, instrumented with 80 thermocouples in 20 rows. Right, from right to left: molybdenum tip, plastic holder with 316L stainless steel 10 micron porous injector, aluminum cone body.

A total of 16 shots in T5 make up the data set for the present study. All were nominally intended to have the same flow conditions: air at 10 MJ/kg and 55 MPa in the reflected shock region. The measured tunnel conditions are presented in Table 1.

**Table 1** Similar tunnel conditions (nominally 10 MJ/kg, 55 MPa), and varied gas injection conditions, with resulting transition Reynolds numbers, determined with the intermittency method.

	$H_0$ [MJ/kg]	$p_0$ [MPa]	$\dot{m}$ [g/s]	$Re_t$
2587	9.94	51.9	8.1 (Ar)	2.09e6
2589	10.37	56.3	9.3 (CO <sub>2</sub> )	4.30e6
2590	9.92	55.9	11.6 (CO <sub>2</sub> )	4.59e6
2591	9.49	53.2	4.6 (CO <sub>2</sub> )	4.23e6
2592	9.89	52.5	6.9 (CO <sub>2</sub> )	4.35e6
2593	9.99	55.2	13.1 (CO <sub>2</sub> )	4.39e6
2594	9.84	56.1	16.2 (CO <sub>2</sub> )	3.54e6
2596	10.03	54.1	0	3.88e6
2597	10.09	55.6	13.9 (Ar)	3.07e6
2598	10.26	55.3	0	3.85e6
2600	9.88	54.7	11.6 (Ar)	1.79e6
2607	9.80	54.5	a	4.07e6
2608	9.75	55.2	a	4.27e6
2609	9.92	55.7	a	4.45e6
2610	10.37	54.9	a	3.63e6
2611	10.44	54.6	a	4.08e6

<sup>a</sup> Solid plastic injector section, no flow.

## 4 Results and Conclusions

The current study detected transition by analyzing the intermittency of the heat flux signals, as described in Clark et al. [2] and implemented for similar conditions in Mee and Goynes [9]. Intermittency represents the fraction of the run time during which flow over each gauge is turbulent. Gauge signals are considered turbulent when the signal is elevated above the predicted laminar value by more than 40% of the difference between the predicted laminar and turbulent values. Gauge signals are considered laminar when the signal is elevated above the predicted laminar value by less than 20% of the difference between the predicted laminar and turbulent values. For values between 20% and 40% above the laminar correlation, the numerical intermittency meter of Mee and Goynes [9] is employed. As Mee and Goynes suggest, similar data sets (from the repeated shots: five smooth and two porous non-injection) are combined for better intermittency determination. Sample intermittency plots for two different shots are presented in Figure 2. Transition location is determined from these plots by noting where the intermittency trend departs zero. Results are presented in the left-hand plot of Figure 4.

An alternate method of determining transition location averages the heat transfer rate from each gauge over the entire test time (see Figure 3). Transition is considered to have occurred when the trend departs the predicted laminar Stanton number, as in [1]. Results for this method are presented in the right-hand plot of Figure 4.

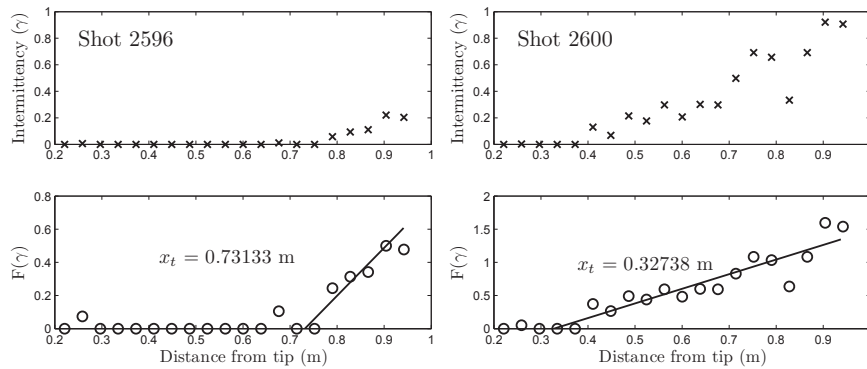


**Fig. 2** Top: Combined intermittency by gauge location. Bottom: The universal intermittency of Narasimha [10], used to find transition location.

Transition delays were documented in shots with CO<sub>2</sub> injection, compared both to shots with a porous injector but no injection, and control shots with a smooth injector section, as presented numerically in Table 1 and graphically in Figure 4. The data show a general trend of increasing delay with injection rate, before a sharp dropoff at the highest injection rate, which may be due to boundary layer detachment. All three Argon injection conditions transitioned far earlier than any CO<sub>2</sub>

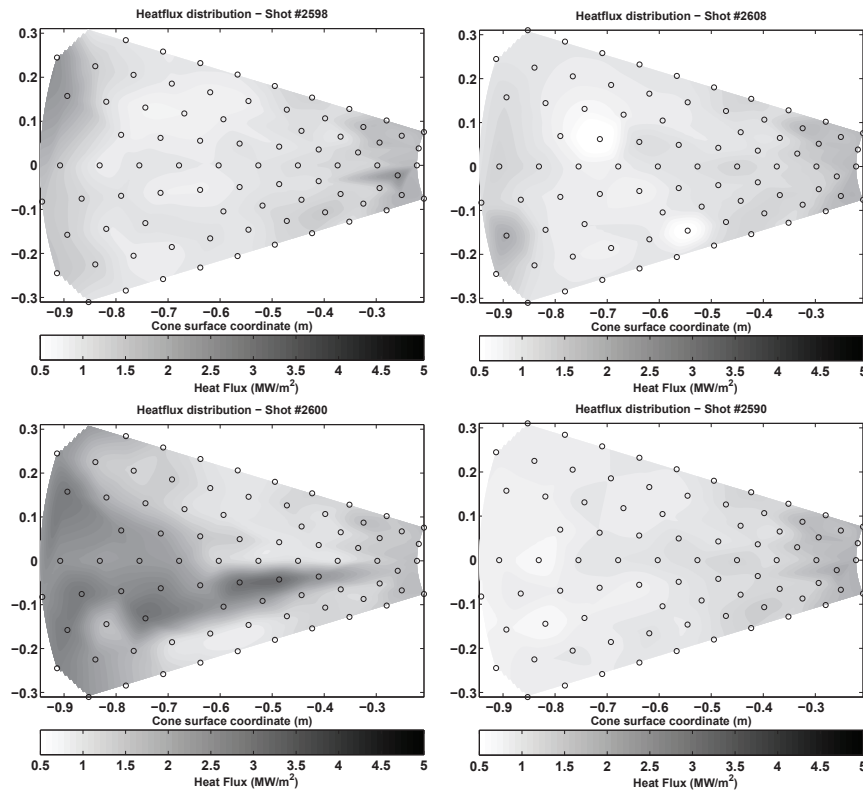


**Fig. 3** Heat flux contour plots on the developed cone surface. Top left: porous injector with no injection. Top right: solid injector section. Bottom left: Ar injection at 11.6 g/s. Bottom right: CO<sub>2</sub> injection at 11.6 g/s.

injection or no-injection conditions. Average heat fluxes for several exemplar conditions are presented in Figure 3.

Future work includes documenting transition delay due to gas injection at a greater variety of flow conditions, as well as more precise measurement of mass flow rate and measurements of CO<sub>2</sub> mass fractions in the boundary layer. Special emphasis will be placed upon finding a condition for which natural condition occurs closer to the center of the test article, so that larger delays may potentially be measured. Coordination with the numerical efforts of the G.V. Candler group will also continue, as described in Wagnild et al. [13].

**Acknowledgements:** The authors thank Prof. Hans G. Hornung for invaluable guidance, advice, and other contributions on both the conception and execution of this work, and Mr. Bahram Valiferdowsi for his work with design, fabrication, and maintenance. This project was sponsored by the Air Force Office of Scientific Research under award number FA9550-10-1-0491, for which Dr. John Schmisser is the program manager. The views expressed herein are those of the authors and

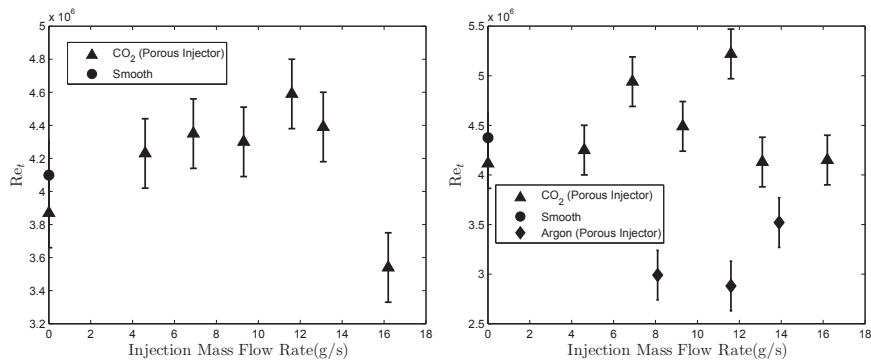


**Fig. 4** Left: Transition Reynolds number, determined with the intermittency method, plotted against injection mass flow rate. Argon injection data, which all lie far below this Reynolds number range, are omitted for clarity. Right: Transition Reynolds number, determined with the average Stanton number method, plotted against injection mass flow rate.

should not be interpreted as necessarily representing the official policies or endorsements, either expressed or implied, of AFOSR or the U.S. Government.

## References

1. Adam, P.H. (1997) Enthalpy Effects on Hypervelocity Boundary Layers. PhD Thesis, California Institute of Technology, Pasadena, CA 91125.
2. Clark J.P., Jones T.V. and LaGraff J.E. (1994) On the Propagation of Naturally-Occurring Turbulent Spots. *Journal of Engineering Mechanics*, Vol. 28, No. 1:1–19.
3. Fujii K. and Hornung H.G. (2003) Experimental investigation of high-enthalpy effects on attachment-line boundary layer transition. *AIAA Journal*, Vol. 41, No. 7.
4. Hornung H.G. and Belanger J. (1990) Role and techniques of ground testing simulation of flows up to orbital speeds. AIAA 90-1377.
5. Hornung H.G. (1992) Performance data of the new free-piston shock tunnel at GALCIT. AIAA 92-3943.
6. Johnson H.B., Seipp T.G. and Candler G.V. (1998) Numerical study of hypersonic reacting boundary layer transition on cones. *Physics of Fluids*, Vol. 10 No. 10: 2676–2685.
7. Leyva I.A., Jewell J.S., Laurence S., Hornung H.G. and Shepherd J.E. (2009) On the impact of injection schemes on transition in hypersonic boundary layers. AIAA 2009-7204.
8. Mack L.M. (1984) Boundary-layer stability theory. *Special Course on Stability and Transition of Laminar Flow*. AGARD Report 709.
9. Mee D.J. and Goynes C.P. (1996) Turbulent spots in boundary layers in a free-piston shock-tunnel flow. *Shock Waves*, Vol. 6, No. 6:337–343.
10. Narasimha R. (1985) The Laminar-Turbulent Transition Zone in the Boundary Layer. *Progress in Aerospace Sciences*, Vol. 22, 29–80.
11. Sanderson S. (1995) *Shock Wave Interaction in Hypervelocity Flow*, GALCIT, California Institute of Technology, Ph.D. thesis.
12. Vincenti W.G. and Kruger C.H. (1965) *Introduction to Physical Gas Dynamics*. Krieger.
13. Wagnild R.M., Candler G.V., Leyva I.A., Jewell J.S. and Hornung H.G. (2010) Carbon Dioxide Injection for Hypervelocity Boundary Layer Stability. AIAA 2010-1244.

42nd AIAA Fluid Dynamics Conference and Exhibit, 25–28 June 2012, New Orleans, Louisiana  
**HYPERSONICS**

# Turbulent Spot Observations within a Hypervelocity Boundary Layer on a 5-degree Half-Angle Cone

Joseph S. Jewell<sup>1</sup> and Nicholas J. Parziale<sup>2</sup>  
*California Institute of Technology, Pasadena, CA, 91125*

Ivett A. Leyva<sup>3</sup>  
*Air Force Research Laboratory, Edwards AFB, CA, 93536*

Joseph E. Shepherd<sup>4</sup>  
*California Institute of Technology, Pasadena, CA, 91125*

## Nomenclature

$C_{le}$	=	$U_{le}/U_e$	normalized turbulent spot leading edge propagation rate
$C_m$	=	$U_m/U_e$	normalized turbulent spot trailing edge propagation rate
$C_{ie}$	=	$U_{ie}/U_e$	normalized turbulent spot centroid/peak propagation rate
$M_e$	=		boundary layer edge Mach number
$\dot{q}$	=		heat flux (transfer rate)
$\dot{q}_L$	=		laminar heat flux
$\dot{q}_T$	=		turbulent heat flux
$Re_1$	=		unit Reynolds number
$Re_{1e}$	=		boundary layer edge unit Reynolds number
$T_e$	=		boundary layer edge temperature
$T_w$	=		wall temperature
$U_e$	=		boundary layer edge velocity
$\alpha$	=		turbulent spot spreading angle

## I. Introduction

Laminar to turbulent transition is a critically important process in hypersonic vehicle design. Higher thermal loads, by half an order of magnitude or more, result from the increased heat transfer due to turbulent flow. Drag, skin friction, and other flow properties are also significantly impacted. Transition to turbulence in initially laminar boundary layers can occur along many paths. In low-speed flow under ideal conditions (quiet freestream, nominally smooth surfaces with favorable or zero pressure gradient and minimal crossflow) transition occurs over a finite distance and is associated with the creation and growth of propagating patches of turbulent flow, known as turbulent spots. Spots may be due to the breakdown of linear instabilities or induced by “bypass mechanisms” associated with nonideal effects in the flow or model. H.W. Emmons (1951) was the first to propose that laminar boundary layers break down through the convergence of spots, after observations of a water-table analogy to air flow. Spot formation has been studied extensively in subsonic flows, a recent review of past and current work on spots in incompressible flows is given by Strand and Goldstein (2011).

The first turbulent spots in a supersonic boundary layer were detected by James (1958) on free-launched projectiles using spark shadowgraphs with a conical light field, characterizing both propagation speed and growth rate for free-stream Mach numbers from 2.7 to 10. James was able to surmise that the differences were likely to be small between turbulent-spot propagation in subsonic and supersonic flow. Around the same time, Deissler and

<sup>1</sup> PhD Candidate, GALCIT, MC 205-45, Caltech. AIAA Student Member.

<sup>2</sup> PhD Candidate, GALCIT, MC 205-45, Caltech. AIAA Student Member.

<sup>3</sup> Sr. Aerospace Engineer, Air Force Research Laboratory. AIAA Senior Member.

<sup>4</sup> Professor, GALCIT, MC 105-50, Caltech. AIAA Senior Member.

Loeffler (1958) studied supersonic transition on a flat plate. Since then, a number of studies of spots in supersonic and hypersonic flows have been carried out, with reviews given by Fiala et al. (2006) and Mee (2002).

## II. Recent Work on Supersonic Flows

Clark (1993) and Clark et al. (1994) studied the propagation of naturally-occurring turbulent spots in turbine-representative flows from Mach 0.24 to Mach 1.86 using thin-film heat transfer gauges to track individual spots. Clark characterized turbulent spot leading-edge, trailing-edge, and “mean” or centroid velocities, and also measured the spreading angle at several Mach numbers in this range. Clark also examined the propagation of turbulent spots in mild and strong pressure gradients both favorable and adverse.

Hofeldt (1996) and Hofeldt et al. (1998) also studied spots in flows from Mach 0.24 to Mach 1.86 using thin-film heat transfer gauges, examining the effect of gas-to-wall temperature ratios as well as the “overhang” region—the turbulent spot’s spatial extent in the downstream direction is greater further from the plate and observing “becalmed” regions behind turbulent spots. Hofeldt was able to show that the becalmed region behind a turbulent spot is in fact consistent with the re-establishment of a laminar boundary layer.

Mee and Goyne (1996) performed experiments to detect turbulent spots on a flat plate in free-piston shock tunnel flows of Mach 5.6 to 6.1 at low, mid-range, and high unit Reynolds numbers ( $Re_x$  between  $1.6 \times 10^6 \text{ m}^{-1}$  and  $4.9 \times 10^6 \text{ m}^{-1}$ ) using thin-film heat transfer gauges. They were able to detect turbulent spot activity and measure intermittency, and recommended further tests to measure convection speeds and spreading rate. Mee (2001) and Mee (2002), using the same facility as Mee and Goyne (1996) with new instrumentation, measured the effect of using 2 mm-high boundary layer “trips” behind the leading edge of a flat plate in Mach 5.5 to Mach 6.3 free-piston shock tunnel flow and found them to be capable of advancing the transition location. Mee measured a spot growth angle of  $3.5^\circ \pm 0.5^\circ$ .

Fiala et al. (2006) measured turbulent spots progressing on a blunt cylindrical body with spherical nose in hypersonic flow (Mach 8.9 free stream; Mach 3.74 at the edge of the boundary layer) using a series of thin-film heat transfer gauges. They were able to detect clear turbulent spot activity and measure intermittency by comparing heat transfer time histories from axial gauges in the intermittent region of the body, and also visualize the passing signals from individual spots with a circumferential array of gauges. Computational studies of spot propagation in supersonic flows have been carried out by Chong and Zhong (2005), Krishan and Sandham (2006), and Jocksch and Kleiser (2008). Sivasubramanian and Fasel (2010) have carried out DNS of turbulent spot evolution on a cone in Mach 6 cold flow and observed the breakdown of two-dimensional second mode disturbances into a three-dimensional wave packet or spot. Selected results of experiments and computations are given in Table 2.

## III. Experiment

The facility used in all experiments for the current study is the T5 hypervelocity reflected shock tunnel; see Hornung (1992) and Hornung and Belanger (1990). The model is a 5 degree half-angle aluminum cone similar to that used in a number of previous experimental studies in T5. The model is 1m in length, and is composed of three sections: a sharp tip fabricated of molybdenum, a mid-section containing a porous gas-injector section, and the main body instrumented with a total of 80 thermocouples in evenly spaced rows 38 mm apart at 20 lengthwise locations between 220.9 mm and 942.0 mm from the cone tip. These thermocouples have a response time (Marineau and Hornung 2009) on the order of a few microseconds and have been successfully used for boundary layer transition location in Adam (1997) and

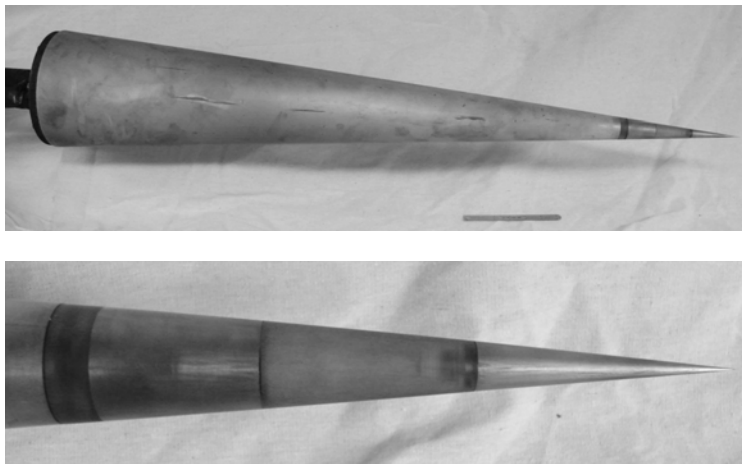


**Figure 1. Top: Aluminum cone, 1m in length, instrumented with 80 thermocouples in 20 rows. Bottom, from right to left: molybdenum tip, plastic holder with 316L stainless steel 10 micron porous section, aluminum cone body.**

Rasheed (2001). Previous studies in T5 have mainly used these gauges to measure mean heat transfer as an indicator

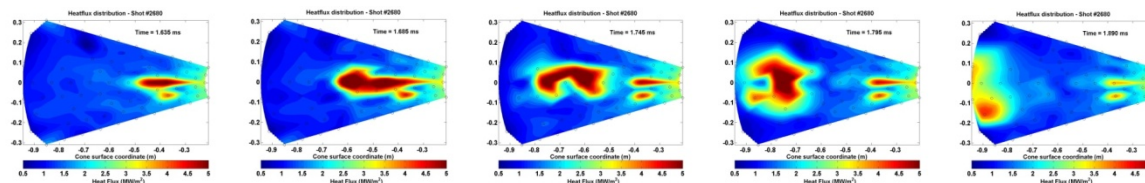


**Figure 2. Time-resolved heat transfer rate plots of the developed cone surface. In these frames from a heat flux “movie”, a turbulent spot can be seen growing as it propagates down the surface of the cone. Flow in each image goes from right to left.**

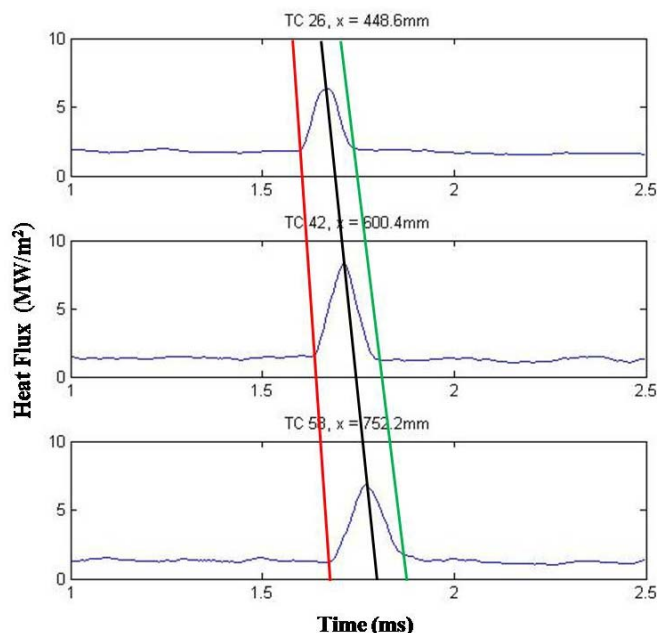


**Figure 3. Smoothed heat transfer traces from three colinear thermocouples, at  $x$ -displacements from the cone tip of 448.6mm, 600.4mm, and 752.2mm, respectively, under the propagating spot depicted in Figure 2. The spot’s leading edge (red), centroid (black), and trailing edge (green) velocities may be calculated from the signals.**

edge and centroid (peak) velocity. Measurements for six such spots, at a Mach number of about 5.1, are presented in Table 1 as fractions of the respective boundary layer edge velocities. The present results may be compared with other experimental and computational supersonic and hypersonic results at similar and disparate boundary layer edge conditions, presented in the same format in Table 2. The non-dimensionalized average heat flux gauge signals are plotted (Figures 4-9) for each of these six runs as Stanton number versus Reynolds number based on the distance of the gauge from the tip of the cone. In each case, the boundary layer is on average laminar over the majority of the length of cone, with some cases showing incipient transition near the end of the cone so that the spots we are observing are propagating as isolated turbulent patches within the surrounding laminar flow. The initiating events for these spots are unknown but may be due to the nonlinear breakdown of second mode instabilities, which have recently been observed within similar transitional boundary layers in T5 using a recently developed optical method for observing low-amplitude, high-frequency density fluctuations (Parziale et al 2012).

of average laminar to turbulent flow transition location. In the present study, a denser array of the gauges was used compared to the past studies and the high-speed data recordings were utilized more fully in order to visualize and quantify turbulence spot motion.

For simplicity and comparison with previous experimental and computational results, the cone axis was aligned with the tunnel axis as closely as possible to a zero degree angle of incidence to the flow. A photograph of the cone model is shown in Figure 1. The porous injector section is 4.13 cm in length and consists of sintered 316L stainless steel, with an average pore size of 10 microns. A detail view of the tip and porous injector section is shown in the bottom of Figure 1. Although the injector section was installed during the present tests, no injection was used. The section has been shown not to trip the boundary layer when gas is not injected.

A method of presenting time- and spatially-resolved heat flux data has been developed and implemented, which allows the presentation of a “movie” of heat flux over the entire instrumented surface of the cone during the test time (see Figure 2). A similar method has allowed the observation of turbulent “spots” observed in lower-speed flow (Clark 1994). Figure 3, depicts the results from shot 2680, and the trajectories shown indicate how we have characterized spots by leading edge, trailing

Shot	2645	2654	2680	2702	2706	2718
$H_0$ [MJ/kg]	10.26	10.68	9.48	8.74	9.53	10.44
$P_0$ [MPa]	54.3	74.1	71.2	49.9	49.0	70.1
$M_e$	5.07	5.04	5.11	5.20	5.11	5.04
$u_e$ [m/s]	3995	4087	3875	3732	3871	4034
$Re_{le}$ [1/m]	$5.18 \times 10^6$	$6.63 \times 10^6$	$7.42 \times 10^6$	$5.72 \times 10^6$	$5.15 \times 10^6$	$6.46 \times 10^6$
$T_w/T_e$	0.180	0.169	0.195	0.219	0.196	0.174
$C_{le}$	$0.92 \pm 0.04$	$0.93 \pm 0.08$	$0.96 \pm 0.07$	$0.92 \pm 0.03$	$0.79 \pm 0.04$	$0.87 \pm 0.04$
$C_m$	$0.82 \pm 0.04$	$0.77 \pm 0.08$	$0.78 \pm 0.07$	$0.58 \pm 0.03$	$0.69 \pm 0.04$	$0.88 \pm 0.04$
$C_{te}$	$0.69 \pm 0.04$	$0.56 \pm 0.08$	$0.55 \pm 0.07$	$0.50 \pm 0.03$	$0.57 \pm 0.04$	$0.77 \pm 0.04$

**Table 1. Results for turbulent spot propagation rates, presented in terms of the ratio of measured spot leading edge ( $C_{le}$ ), centroid ( $C_m$ ), and trailing edge ( $C_{te}$ ) velocities to the calculated velocity at the boundary layer edge,  $u_e$ . The reservoir enthalpy and reservoir pressure at the end of the shock tube are also provided. Free stream species and boundary layer edge conditions are calculated with an expansion through a contoured nozzle with area ratio 100, followed by a conical shock emanating from the tip of the cone.**

	Z & H 1996	Fiala 2006	Mee 2002	Clark 1994	K & S 2006	J & K 2008	J & K 2008	S & F 2010
Type	Exp.	Exp.	Exp.	Exp.	Comp.	Comp.	Comp.	Comp.
$M_e$	8.02 <sup>b</sup>	3.74	6.1	1.86	6	5	5	6
$u_e$ [m/s]	<sup>a</sup>	1300 <sup>b</sup>	3370	580 <sup>b</sup>	<sup>a</sup>	<sup>a</sup>	<sup>a</sup>	875
$Re_{le}$ [1/m]	<sup>a</sup>	$2.69 \times 10^6$	$4.9 \times 10^6$	$16.0 \times 10^6$	<sup>a</sup>	<sup>a</sup>	<sup>a</sup>	$11.0 \times 10^6$
$T_w/T_e$	4.38 <sup>b</sup>	0.97 <sup>b</sup>	0.371 <sup>b</sup>	1.23 <sup>b</sup>	7.00	5.19	1.00	5.7
$C_{le}$	0.98	0.81	$0.90 \pm 0.10$	$0.83 \pm 0.04$	0.89	0.96	0.89	0.91
$C_m$	–	–	–	$0.64 \pm 0.02$	0.76 <sup>c</sup>	–	–	–
$C_{te}$	0.68	0.40	$0.50 \pm 0.10$	$0.53 \pm 0.02$	0.53	0.54	0.23	0.79

a: value not reported  
b: calculated from other reported values  
c: spot “wing tip” convection velocity

**Table 2. The present experimental (Mach 5 cone) results may be compared with other supersonic and hypersonic experiments (Zanchetta and Hillier 1996, Fiala et al. 2006, Mee 1996, and Clark et al. 1994) and computations (Krishnan and Sandham 2006, two results from Jocksch and Kleiser 2008, and one from Sivasubramanian and Fasel 2010) reported for a range of conditions.**

At lower Mach numbers, such as the results of Clark et al. (1994), the subsonic (first) mode is the dominant linear boundary layer instability mechanism. At hypersonic Mach numbers (>4), instabilities in the second (Mack) acoustic mode dominate the boundary layer transition mechanism. For cold-wall hypervelocity flow with a hot freestream, which is characteristic of high-enthalpy shock tunnels like T5 and T4, the first mode is expected to be damped and the higher inviscid modes are amplified, so that the second mode would be expected to be the only mechanism of linear instability. The present results are thus most directly comparable, in terms of Mach number and wall temperature ratio, to those of Mee (2002), and indeed are largely within the uncertainty range of Mee’s measurements.

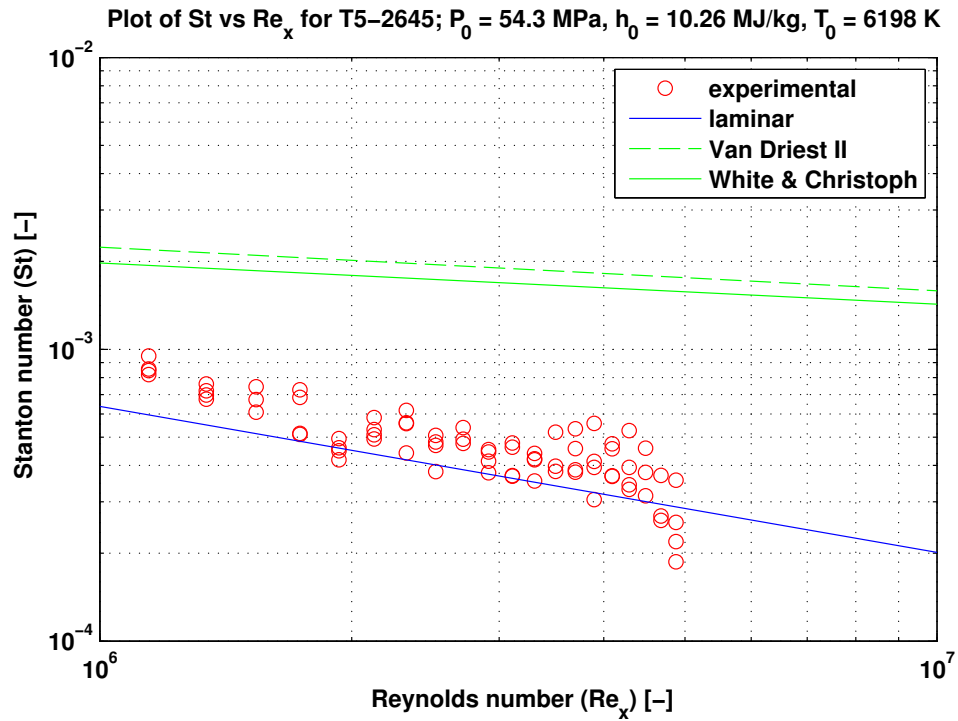


Figure 4. Stanton number versus Reynolds number plot for test 2645. See Table 1 for edge conditions.

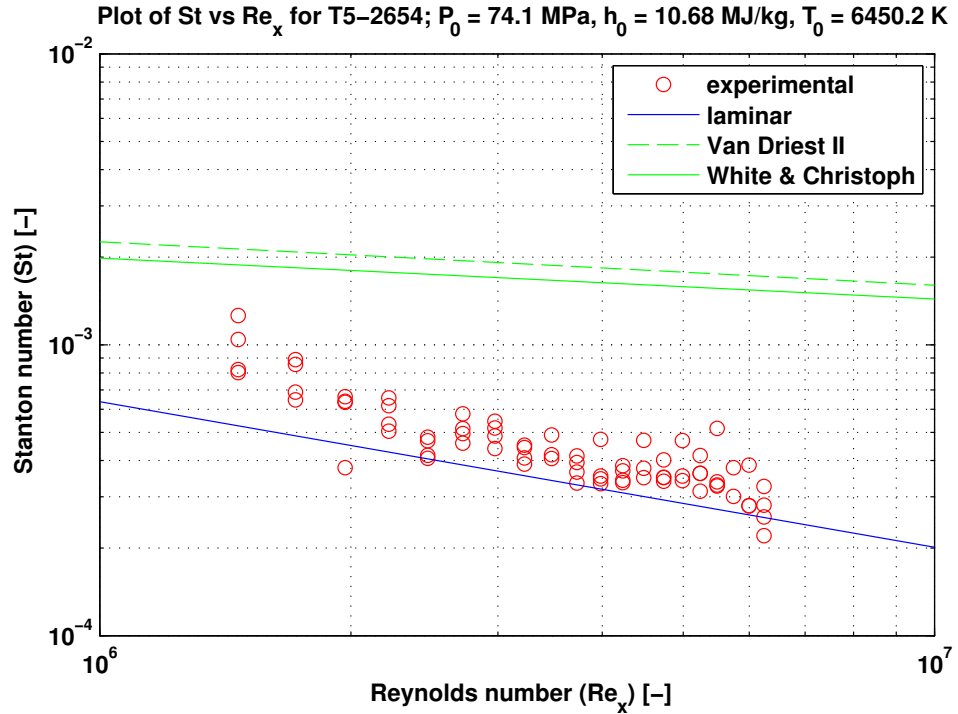


Figure 5. Stanton number versus Reynolds number plot for test 2654. See Table 1 for edge conditions.

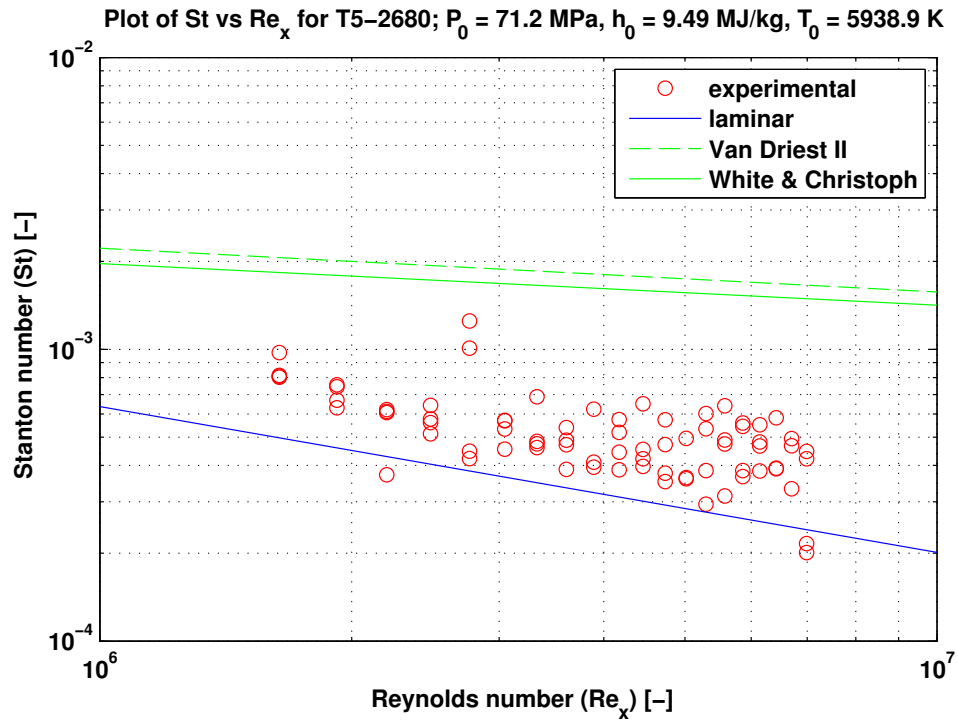


Figure 6. Stanton number versus Reynolds number plot for test 2680. See Table 1 for edge conditions.

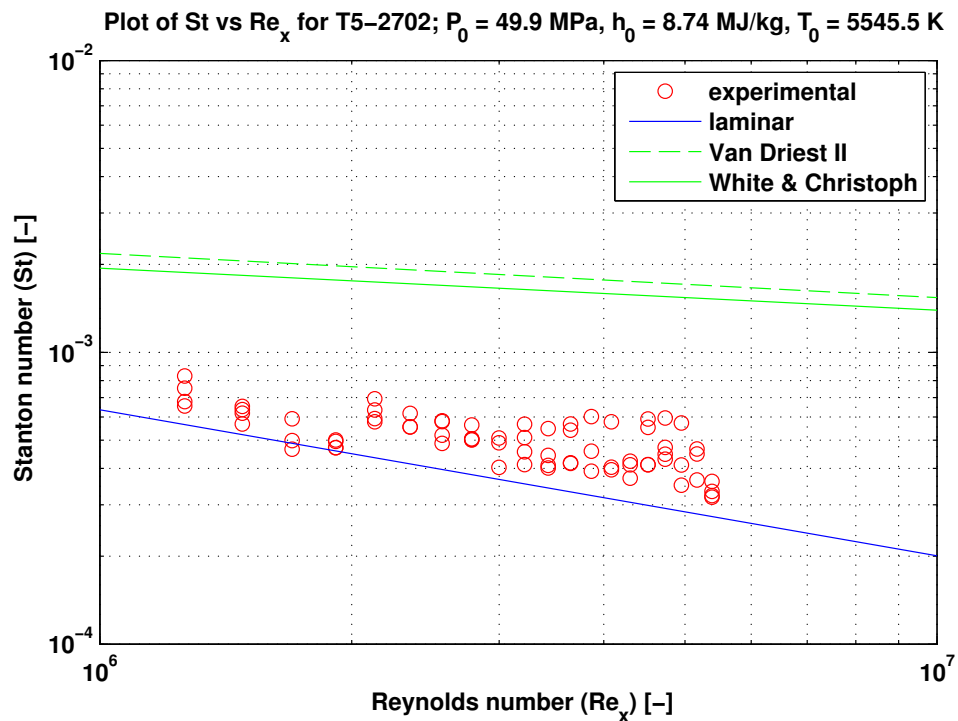


Figure 7. Stanton number versus Reynolds number plot for test 2702. See Table 1 for edge conditions.

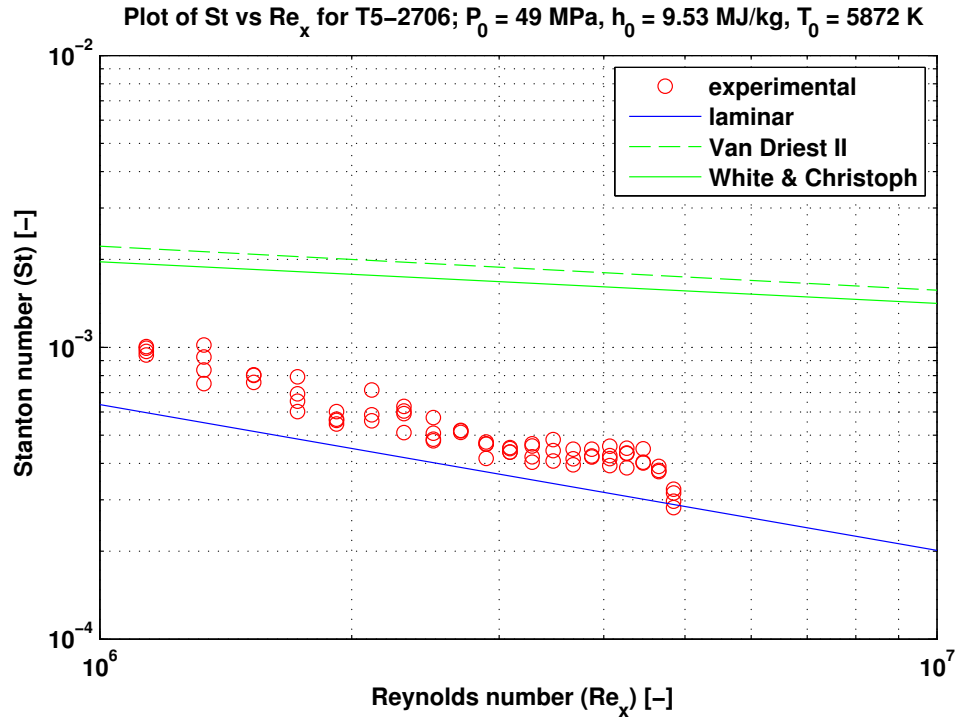


Figure 8. Stanton number versus Reynolds number plot for test 2706. See Table 1 for edge conditions.

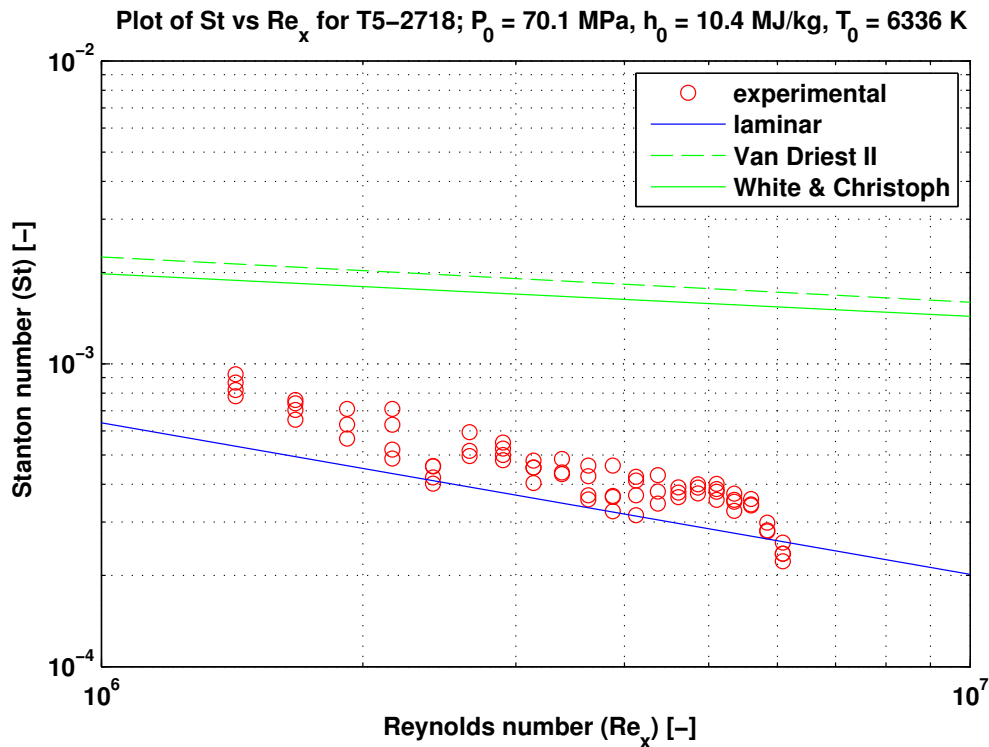


Figure 9. Stanton number versus Reynolds number plot for test 2645. See Table 1 for edge conditions.

#### IV. Conclusion

Time- and spatially-resolved heat transfer traces in a high-enthalpy hypervelocity flow on a 5-degree half angle cone are measured with thermocouples. Turbulent spots are observed propagating in both heat transfer traces and heat flux “movies” of the developed cone surface. These observations are used to calculate turbulent spot convection rates, which are compared with previous experimental and computational results. Although the present results were obtained at different conditions from past experiments, the normalized spot propagation results for Mach 5 flow appear to be generally consistent with past supersonic and hypersonic experiments, as well as with the computational results. However, all available computational results of spot propagation in hypersonic flow in the present literature survey simulated much higher wall temperature ratios  $T_w/T_e$  than actually occur in reflected shock tunnel experiments (see Tables 1 and 2). The computations of Sivasubramanian and Fasel (2010) are most representative of the present conditions and their spot propagation speeds are reasonably consistent with our experimental results. However, the flow conditions in all of these simulations are essentially nonreactive (cold flow with frozen composition) and the ratios of freestream to wall temperature in the simulations are far from our experimental conditions. The flow conditions in these T5 tests are designed to simulate hypervelocity atmospheric flight and the flow over the model is hot, partially-dissociated air with some amount of chemical and vibrational nonequilibrium due to the rapid expansion process in the nozzle. Because of the sparse number and nature of the thermocouple data, there is substantial uncertainty in defining the precise leading and trailing edges of the spot. Taking the results of all six examples together, the putative leading edge nominally propagates at about  $0.90U_e$ , the centroid at  $0.75U_e$ , and the trailing edge at  $0.60U_e$ , with an estimated uncertainty of  $\pm 0.05U_e$ . While the design of the experiment precludes precise measurement of spot spreading angle  $\alpha$ , preliminary bounding values for this parameter have been obtained. For example, for shot 2654, we estimate  $2^\circ < \alpha < 13^\circ$ , which brackets the reported value of  $3.5^\circ \pm 0.5^\circ$  of Mee (2002). More precise measurements of propagation speed and spreading angle would be possible with the addition of thermocouples in a more circumferentially dense pattern.

#### Acknowledgments

The authors thank Mr. Bahram Valiferdowski for his work with design, fabrication, and maintenance, and Prof. Hans Hornung for his advice and support. This project was sponsored by the Air Force Office of Scientific Research under award number FA9550-10-1-0491 and the NASA/AFOSR National Center for Hypersonic Research. The views expressed herein are those of the authors and should not be interpreted as necessarily representing the official policies or endorsements, either expressed or implied, of AFOSR or the U.S. Government.

#### References

- Adam, P.H., *Enthalpy Effects on Hypervelocity Boundary Layers*. PhD Thesis, California Institute of Technology, Pasadena, CA, 1997. See also Adam, P.H. and Hornung, H.G. “Enthalpy Effects on Hypervelocity Boundary-Layer Transition: Ground Test and Flight Data” *J. Spacecraft Rockets*, Vol. 34(5), 614-619, 1997.
- Chong, T.P. and Zhong, S. “On the Three-Dimensional Structure of Turbulent Spots,” *Journal of Turbomachinery*, Vol. 127, June 2005, pp. 545-551.
- Clark, J.P., *A Study of Turbulent-Spot Propagation in Turbine-Representative Flows*, D.Phil Thesis, Department of Engineering Science, University of Oxford, 1993.
- Clark, J.P., Jones, T.V., and LaGraff, J.E., “On the Propagation of Naturally-Occurring Turbulent Spots,” *Journal of Engineering Mathematics*, Vol. 28, 1994, pp. 1-19.
- Clark, J.P., Magari, P.J., and Jones, T.V., *On the Distribution of the Heat-Transfer Coefficient in Turbulent and ‘Transitional’ Wedges*, Department of Engineering Science, Oxford University, Parks Road, Oxford OX1 3PJ, United Kingdom, 1993.
- Deissler, H.G. and Loeffler, A.L. “Analysis of Turbulent Flow and Heat Transfer on a Flat Plate at High Mach Numbers with Variable Fluid Properties.” NACA TN 4262, Washington, April 1958.
- Emmons, H.W., “The Laminar-Turbulent Transition in a Boundary Layer—Part I,” *Journal of the Aeronautical Sciences*, Vol. 18, No. 7, 1951, pp. 490-498.

## 42nd AIAA Fluid Dynamics Conference and Exhibit, 25–28 June 2012, New Orleans, Louisiana HYPERSONICS

- Fiala, A., Hillier, R., Mallinson, S.G. and Wijesinghe, H.S., “Heat transfer measurement of turbulent spots in a hypersonic blunt-body boundary layer.” *Journal of Fluid Mechanics*, Vol. 555, 2006, pp. 81-111.
- Hofeldt Jr., A.J., *The Investigation of Naturally-Occurring Turbulent Spots Using Thin-Film Gauges*, D.Phil Thesis, Department of Engineering Science, University of Oxford, 1996.
- Hofeldt Jr., A.J., Jones, T.V., Clark, J.P., and LaGraff, J.E., *The BeCALMED Region of Naturally-Occurring Turbulent Spots*, Department of Engineering Science, Oxford University, Parks Road, Oxford OX1 3PJ, United Kingdom, 1998.
- Hornung, H.G. and Belanger, J. “Role and techniques of ground testing simulation of flows up to orbital speeds.” 1990. AIAA 90-1377.
- Hornung, H.G. “Performance data of the new free-piston shock tunnel at GALCIT.” 1992. AIAA 92-3943.
- James, C.S., “Observation of turbulent-burst geometry and growth in supersonic flow,” NACA TN 4235, 1958.
- Jocksch, A. and Kleiser, L. “Growth of turbulent spots in high-speed boundary layers on a flat plate.” *International Journal of Heat and Fluid Flow*, Vol. 29, 2008, 1543–1557.
- Krishnan, L. and Sandham, N.D. “Effect of Mach number on the structure of turbulent spots.” *Journal of Fluid Mechanics*, Vol. 556, 2006, pp. 225-234.
- Marineau, E., and Hornung, H., “Modeling and Calibration of Fast-Response Coaxial Heat Flux Gages,” AIAA Paper 2009-737, 47<sup>th</sup> AIAA Aerospace Sciences Meeting, Orlando, FL, Jan 2009
- Mee, D.J., “Boundary Layer Transition Measurements in Hypervelocity Flows in a Shock Tunnel,” *AIAA Journal*, Vol. 40, No. 8, August 2002, pp. 1542-1548.
- Mee, D.J., *Transition Measurements on a 5 Degree Cone in the T4 Shock Tunnel*, University of Queensland, Department of Mechanical Engineering, Research Report Number 2001-2.
- Mee, D.J. and Goynes, C.P., “Turbulent spots in boundary layers in a free-piston shock tunnel flow”, *Proceedings of the 20th International Symposium on Shock Waves*, Pasadena, USA, 24-28 July 1995. Edited by B. Sturtevant, J.E. Shepherd and H.G. Hornung. World Scientific, Singapore, 1996, pp. 771-776.
- Parziale, N., Shepherd, J.E., and Hornung, H.G. “Reflected Shock Tunnel Noise Measurement by Focused Differential Interferometry” 42nd AIAA Fluid Dynamics Conference and Exhibit, June, 2012, New Orleans, Louisiana.
- Rasheed, A., *Passive hypervelocity boundary layer control using an acoustically absorptive surface*. PhD Thesis, California Institute of Technology, Pasadena, CA, 2001. See also Rasheed, A., Hornung, H.G., Fedorov, A.V., and Malmouth, N.D. “Experiments on passive hypervelocity boundary-layer control using an ultrasonically absorptive surface” *AIAA J.*, Vol. 40(3), 481-489, 2002.
- Strand, J.S. and Goldstein, D.B. “Direct numerical simulations of riblets to constrain the growth of turbulent spots”, *J. Fluid Mech.* (2011), vol. 668, pp. 267–292
- Sivasubramanian, J. and Fasel, H. F. “Direct Numerical Simulation of a Turbulent Spot in a Cone Boundary Layer at Mach 6”. AIAA 40<sup>th</sup> Fluid Dynamics Conference, June 28-July 1, 2010. AIAA 2010-4599.
- Zanchetta, M. and Hillier, R. “Boundary Layer Transition on Slender Blunt Cones at Hypersonic Speeds.” *Proceedings of the 20th International Symposium on Shock Waves*, 1996, pp. 699-704.

# Transition Within a Hypervelocity Boundary Layer on a 5-Degree Half-Angle Cone in Air/CO<sub>2</sub> Mixtures

Joseph S. Jewell\*

*California Institute of Technology, Pasadena, CA, 91125*

Ross M. Wagnild†

*Sandia National Laboratories, Albuquerque, NM, 87185*

Ivett A. Leyva‡

*Air Force Research Laboratory, Edwards AFB, CA, 93536*

Graham V. Candler§

*University of Minnesota, Minneapolis, MN, 55455*

Joseph E. Shepherd¶

*California Institute of Technology, Pasadena, CA, 91125*

Laminar to turbulent transition on a smooth 5-degree half angle cone at zero angle of attack is investigated computationally and experimentally in hypervelocity flows of air, carbon dioxide, and a mixture of 50% air and carbon dioxide by mass. Transition N factors above 10 are observed for air flows. At comparable reservoir enthalpy and pressure, flows containing carbon dioxide are found to transition up to 30% further downstream on the cone than flows in pure air in terms of  $x$ -displacement, and up to 38% and 140%, respectively, in terms of the Reynolds numbers calculated at edge and reference conditions.

## Nomenclature

$f$	frequency
$h$	enthalpy
$M$	Mach number
$P$	pressure
$Pr$	Prandtl number
$R$	specific gas constant
$T$	temperature
$u$	velocity
$w$	mass fraction
$x$	displacement from the tip
$\gamma$	ratio of specific heats
$\delta$	boundary layer thickness
$\Theta$	characteristic vibrational temperature
$\mu$	dynamic viscosity
$\rho$	density
$\tau$	vibrational relaxation time

\*Ph.D. Candidate, GALCIT, MC 205-45, Caltech. AIAA Student Member.

†Senior Member, Technical Staff, Sandia National Laboratories. AIAA Member.

‡Sr. Aerospace Engineer, Air Force Research Laboratory. AIAA Associate Fellow.

§Professor, University of Minnesota. AIAA Fellow.

¶Professor, GALCIT, MC 105-50, Caltech. AIAA Senior Member.

### Subscript

e	condition at the boundary layer edge
res	condition in the reservoir
tr	condition at the location of transition
w	condition at the wall

### Superscript

*	condition at Dorrance reference temperature
---	---

## I. Introduction

IN hypervelocity flow over cold, slender bodies, the most significant instability mechanism is the so-called second or Mack mode. These flows are characteristic of high-enthalpy facilities like the T5 shock tunnel at Caltech. A second mode disturbance depends on the amplification of acoustic waves trapped in the boundary layer, as described by Mack.<sup>1</sup> Another potential disturbance is the first mode, which is the high speed equivalent of the viscous Tollmien–Schlichting instability.<sup>2</sup> However, at high Mach number ( $> 4$ ) and for cold walls, the first mode is damped and higher modes are amplified, so that the second mode would be expected to be the only mechanism of linear instability leading to transition for a slender cone at zero angle of attack.

Parametric studies in air and CO<sub>2</sub> in the T5 hypervelocity reflected shock tunnel by Germain<sup>3</sup> and Adam<sup>4</sup> on a smooth 5-degree half angle cones at zero angle of attack showed an increase in the reference Reynolds number  $Re^*$  (see Equation 6 on page 8) at the point of transition as reservoir enthalpy  $h_{res}$  increased. Germain and Adam also observed that flows of CO<sub>2</sub> transitioned at higher values of  $Re^*$  than flows of air for the same  $h_{res}$  and  $P_{res}$ . Johnson et al.<sup>5</sup> studied this effect with a linear stability analysis focused on the chemical composition of the flow, and found an increase in transition Reynolds number with freestream total enthalpy, and further found the increase to be greater for gases with lower dissociation energies and multiple vibrational modes, such as CO<sub>2</sub>. In fact, with the assumption of a transition N factor of 10 that was made at the time, none of the CO<sub>2</sub> cases computed by Johnson et al. predicted transition at all. These effects led Fujii and Hornung<sup>6</sup> to further investigate their hypothesis that the delay in transition was due to the damping of acoustic disturbances in non-equilibrium relaxing gases by vibrational absorption. Fujii and Hornung estimated the most strongly amplified frequencies for representative T5 conditions and found that these agreed well with the frequencies most effectively damped by non-equilibrium CO<sub>2</sub>. This suggests that the suppression of the second mode through the absorption of energy from acoustic disturbances through vibrational relaxation is the dominant effect in delaying transition for high-enthalpy carbon dioxide flows.

Numerous studies have been made on inhibiting the second mode, and therefore preventing or delaying transition through the suppression of acoustic disturbances within the boundary layer; see Fedorov et al.<sup>7</sup> and Rasheed<sup>8</sup> for work focused on absorbing acoustic energy using porous walls. Another approach to suppression of the pressure waves that lead to transition centers around altering the chemical composition within the boundary layer to include species capable of absorbing acoustic energy at the appropriate frequencies. Efforts in this area to date have included preliminary experimental work on mixed freestream flows, e.g. Leyva et al.,<sup>9</sup> computations, e.g. Wagnild et al.,<sup>10,11</sup> and experiments with direct injection of absorptive gases into the boundary layer, e.g. Jewell et al.<sup>12</sup> The present aim is to confirm and extend these studies both computationally and experimentally by considering transition within a hypervelocity boundary layer on a 5-degree half-angle cone in freestream mixtures of air and carbon dioxide.

## II. Background

By assuming that the boundary layer acts as an acoustic waveguide for disturbances (see Fedorov<sup>13</sup> for a schematic illustration of this effect), the frequency of the most strongly-amplified second-mode disturbances in the boundary layer may be estimated as Equation (1), as shown in Stetson.<sup>14</sup>

$$f \approx 0.8 \frac{u_e}{2\delta} \quad (1)$$

Here  $\delta$  is the boundary layer thickness and  $u_e$  is the velocity at the boundary layer edge. For a typical T5 condition in air, with enthalpy of 10 MJ/kg and reservoir pressure of 50 MPa, the boundary layer thickness is on the order of 1.5 mm and the edge velocity is 4000 m/s. This indicates that the most

strongly amplified frequencies are in the 1 MHz range. This is broadly consistent with the results of Fujii and Hornung.<sup>6</sup> Kinsler et al.<sup>15</sup> provide a good general description of the mechanisms of attenuation of sound waves in fluids due to molecular exchanges of energy within the medium. The relevant exchange of energy for carbon dioxide in the boundary layer of a thin cone at T5-like conditions is the conversion of molecular kinetic energy (e.g. from compression due to acoustic waves) into internal vibrational energy. In real gases, molecular vibrational relaxation is a non-equilibrium process, and therefore irreversible. This absorption process has a characteristic relaxation time. The problem of sound propagation, absorption, and dispersion in a dissociating gas has been treated from slightly different perspectives by Clarke and McChesney,<sup>16</sup> Zeldovich and Raizer,<sup>17</sup> and Kinsler et al.<sup>15</sup> However, in non-equilibrium flows when the acoustic characteristic time scale and relaxation time scale are similar, some finite time is required for molecular collisions to achieve a new density under an acoustic pressure disturbance. This results in a limit cycle, as the density changes lag the pressure changes. The area encompassed by the limit cycle's trajectory is related to energy absorbed by relaxation. Energy absorbed in this way is transformed into heat and does not contribute to the growth of acoustic waves.<sup>9</sup> Carbon dioxide, a linear molecule, has four normal vibrational modes. The first two, which correspond to transverse bending, are equal to each other, and have characteristic vibrational temperatures  $\Theta_1 = \Theta_2 = 959.66$  K. The third mode, corresponding to symmetric longitudinal stretching, has  $\Theta_3 = 1918.7$  K, and the fourth mode, corresponding to asymmetric longitudinal stretching, has  $\Theta_4 = 3382.1$  K. Camac<sup>18</sup> showed that the four vibrational modes for carbon dioxide all relax at the same rate, and proposed a simplified formula, Equation (2), to calculate vibrational relaxation time, which was reproduced in Fujii and Hornung.<sup>6</sup>

$$\ln(A_4\tau_{CO_2}P) = A_5T^{-1/3} \quad (2)$$

Here  $A_4$  and  $A_5$  are constants given by Camac for carbon dioxide as  $A_4 = 4.8488 \times 10^2 \text{ Pa}^{-1}\text{s}^{-1}$  and  $A_5 = 36.5 \text{ K}^{1/3}$ . Using the constants suggested by Camac, with  $P = 35\text{kPa}$  and  $T = 1500$  K, which are consistent with a typical T5 condition with enthalpy 10 MJ/kg and stagnation pressure 50 MPa, we find vibrational relaxation time =  $1.43 \times 10^{-6}$  s, which indicates that frequencies around 700 KHz should be most strongly absorbed at these conditions. This is, again, broadly similar to the results of Fujii and Hornung,<sup>6</sup> who computed curves at 1000 K and 2000 K with peaks bracketing 700 kHz.

Thus, in a flow of gas that absorbs energy most efficiently at frequencies similar to the most strongly amplified frequencies implied by the geometry of the boundary layer, laminar to turbulent transition is expected to be delayed. Using computations, we show that the flow of carbon dioxide/air mixtures over a slender cone at T5 conditions allows for such a match in frequencies. We then perform a series of experiments to confirm this effect.

### III. Experimental Model

The facility used in all experiments for the current study is the T5 hypervelocity reflected shock tunnel; see Hornung<sup>19</sup> and Hornung and Belanger.<sup>20</sup> The model is a smooth 5-degree half-angle aluminum cone similar to that used in a number of previous experimental studies in T5, 1 m in length, and is composed of three sections: a sharp tip (radius  $\sim 0.2$  mm) fabricated of molybdenum, an interchangeable mid-section which may contain a porous gas-injector section (in the present experiments this section is a smooth, solid piece of plastic), and the main body, which is instrumented with a total of 80 thermocouples evenly spaced at 20 lengthwise locations beginning at 221 mm from the tip of the cone, with each row located 38 mm from the last. These thermocouples have a response time on the order of a few microseconds<sup>21</sup> and have been successfully used for boundary layer transition determination in Adam and Hornung<sup>4</sup> and Rasheed et al.<sup>8</sup> The conical model geometry was chosen because of the wealth of experimental and numerical data available with which to compare the results from this program. Two photographs of the cone model are shown in Figure 1. The model is mounted such that the tip of the cone protrudes about 380 mm into the T5 nozzle at run time, in order to maximize the linear extent of the cone within the test rhombus defined by the expansion fan radiating from the nozzle's edge.

### IV. Computational Model

In order to obtain the flow properties over the test cone, we start with the flow properties in the tunnel reservoir, which serves as the inflow for the nozzle flow simulations. The reservoir conditions are obtained by solving for chemical and thermal equilibrium at the specified reservoir pressure and enthalpy using the

Chemical Equilibrium with Applications (CEA) code. These conditions are allowed to expand through the nozzle using the CFD solver described below. For the current computational analysis, it is assumed that the boundary layer on the nozzle walls becomes turbulent in the reservoir and remains in this state for the remainder of the nozzle. A second CFD solver is used to simulate the flow over the test cone, also described below. The freestream properties over the cone are approximated by sampling the nozzle flow at the centerline of the nozzle exit and are held constant over the length of the cone. In the experiment, the freestream properties vary over the length of the cone due to the location of the cone in the nozzle. In all cases the wall temperature for the nozzle and cone walls is 297 K. Also for the computations, the cone nose has been approximated as sharp.

We simulate the flow through the nozzle by solving the reacting, axisymmetric, two-dimensional Navier-Stokes equations with a structured-grid CFD solver as described in Candler<sup>22</sup> and Wagnild.<sup>11</sup> The solver uses an excluded-volume equation of state in order to properly capture the variation in gas properties at high pressure. The inviscid fluxes are calculated using the modified Steger-Warming flux vector splitting method and are second-order accurate with a MUSCL limiter as the TVD scheme. The viscous fluxes are second-order accurate. The time advancement method is the implicit, first-order DPLR method. The turbulent boundary layer flow is modeled using the one-equation, Spalart-Allmaras<sup>23</sup> model with the Catris-Aupoix<sup>24</sup> compressibility correction. The nozzle flow is calculated on a single-block, structured grid with dimensions 492 cells by 219 cells in the streamwise and wall-normal directions, respectively. The grid is clustered near the nozzle wall in order to sufficiently resolve the boundary layer.

The mean flow for the stability analysis is calculated using a structured-grid, axisymmetric CFD solver, which solves the reacting Navier-Stokes equations and is part of the STABL software suite.<sup>25</sup> This flow solver is also based on the finite-volume formulation and is similar to the one used to simulate the nozzle flow with the exception of the excluded volume equation of state. This specialized equation of state is not necessary for this solver because the static pressure over the cone is not sufficiently high to require an altered equation of state. The mean flow is computed on a single-block, structured grid with dimensions of 1001 cells by 301 cells in the streamwise and wall-normal directions, respectively. The wall-normal span of the grid increases down the length of the cone, from 4.1 mm at the tip to 23.5 cm at the base, allowing for the shock to be fully contained within the grid for all cases tested. The grid is clustered at the wall as well as at the nose in order to capture the gradients in these locations.

The stability analyses are performed using the PSE-Chem solver, which is also part of the STABL software suite. PSE-Chem<sup>26</sup> solves the reacting, two-dimensional, axisymmetric, linear parabolized stability equations to predict the amplification of disturbances as they interact with the boundary layer. The PSE-Chem solver includes finite-rate chemistry and translational-vibrational energy exchange. The parabolized stability equations predict the amplification of disturbances as they interact with the boundary layer. The transition location is then predicted using the semi-empirical  $e^N$  approach, in which transition is assumed to occur when a disturbance has grown by a factor of  $e^N$  from its initial amplitude. The critical value of  $N$  is empirical and depends, among other factors, on the disturbance environment; therefore,  $N$  must be calibrated for a particular wind tunnel facility. Conventional, non-quiet, supersonic wind tunnels have been generally understood to have a transition  $N$  factor in the range of 5–6.<sup>27</sup> Both the mean flow and stability analysis solvers in STABL are capable of selectively freezing both chemical reactions and molecular vibration, allowing for the determination of internal molecular effects on boundary layer disturbances.

A seven-species chemistry model including  $\text{CO}_2$ ,  $\text{CO}$ ,  $\text{N}_2$ ,  $\text{O}_2$ ,  $\text{NO}$ ,  $\text{N}$ ,  $\text{O}$  is used to approximate the flow through the nozzle as well as over the cone for all conditions tested. In all computations, a finite-rate chemical reaction model is used, with reaction rates based on Park<sup>28</sup> and Bose and Candler.<sup>29,30</sup> The



**Figure 1. Top: Aluminum cone, 1m in length, instrumented with 80 thermocouples in 20 rows. Bottom, from right to left: molybdenum tip, plastic holder with 316L stainless steel 10 micron porous section, aluminum cone body.**

equilibrium coefficients are calculated from fits based on Park<sup>31</sup> and McBride et al.<sup>32</sup> It is assumed that the vibrational-vibrational energy exchanges occur on a relatively short time scale, allowing for a single temperature governing all vibrational modes. It is also assumed that rotation and translation are coupled and governed by the translational temperature. The translational-vibrational energy exchanges are governed by the Landau-Teller model for the simple harmonic oscillator. The vibrational relaxation times are governed by the Millikan and White model with several empirical corrections given in Camac<sup>18</sup> and Park.<sup>28</sup> The viscosity for each species is calculated using Blottner fits and the mixture quantities are calculated using Wilke's semi-empirical mixing law.

## V. Computational Predictions

Using the methods described above, seven test gas mixtures are simulated, each at four different freestream conditions. The gas mixtures are given based on the mass fraction of carbon dioxide in the mixture and are 0.0, 0.1, 0.2, 0.3, 0.5, 0.75, 1.0. The freestream conditions are chosen based on the reservoir pressure and the reservoir enthalpy and are 10 MJ/kg and 50 MPa, 8.5 MJ/kg and 45 MPa, 7 MJ/kg and 40 MPa, and 5 MJ/kg and 30 MPa. For each gas mixture, the formation enthalpy of the mixture is omitted from the reservoir enthalpy in order to make a proper comparison between test cases. To determine the predicted transition location on the test cone, a transition N factor of 5 is chosen.

The transition locations along the cone surface are extracted from the results of the stability analyses of each case and are compiled in Figure 2. One objective of the current computations is to determine the regime in which a transition delay can be obtained. The data in Figure 2 show that an increase of the mass fraction of carbon dioxide in the 5 MJ/kg case has only a small effect on the transition location. At 7 MJ/kg, the transition location moves toward the rear of the cone by about 5 cm at 100% CO<sub>2</sub>. The 8.5 MJ/kg case shows a shift in transition of approximately 61 cm. The 10 MJ/kg case results in the largest shift in the transition location, approximately 66 cm at 100% CO<sub>2</sub>, indicating that carbon dioxide has a large potential for transition delay in this enthalpy range.

In order to damp acoustic vibrations within the boundary layer, energy must be transferred into the gas molecules' internal modes, the energy content of which depends upon vibrational specific heat. Vincenti and Kruger<sup>33</sup> present Equation (3) for vibrational specific heat, where  $\Theta_i$  is the characteristic vibrational temperature of each mode of the gas molecule, and  $R$  is the gas molecule's gas constant. The exponential factors dominate the vibrational contribution from each mode, and indicate that an increase in temperature causes an increase in both total specific heat and the contribution to specific heat from each vibrational mode.

Specifically, as  $\Theta_i/T$  becomes large (for small  $T$ ), the summand tends to zero, which means there is no contribution to the vibrational specific heat from that vibrational mode. As  $\Theta_i/T$  becomes small (for large  $T$ ), the summand

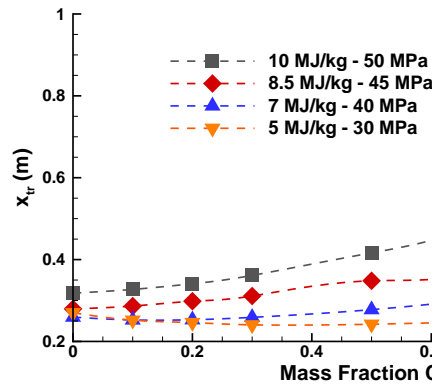


Figure 2. Comparison of the transition location based on a critical N factor of 5 versus mass fraction of CO<sub>2</sub> for each of the four freestream conditions.

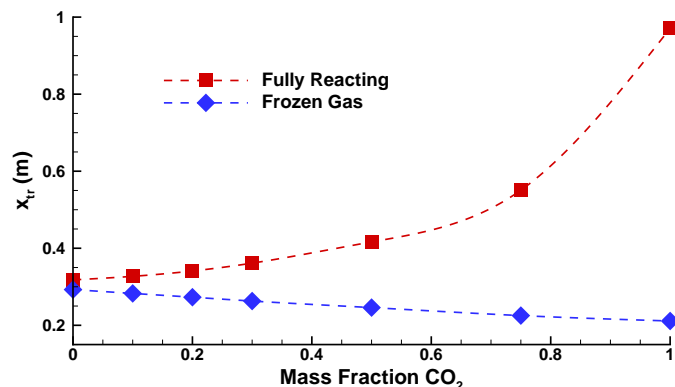


Figure 3. A comparison of the transition location versus mass fraction of CO<sub>2</sub> based on a N factor of 5 between a fully reacting and a frozen gas stability analysis at 10 MJ/kg and 50 MPa.

tends to unity, and the maximum contribution from a given vibrational mode is therefore  $R$ . As temperature increases within the boundary layer, each mode becomes more fully excited and capable of exchanging more energy from acoustic vibrations. Temperature tends to increase with enthalpy. Table 1 on page 8 records reservoir enthalpy and  $T^*$ , a characteristic boundary layer reference temperature, for each experiment.

$$C_{v,vib} = R \sum_i \left\{ \left( \frac{\Theta_i}{T} \right)^2 \frac{e^{\Theta_i/T}}{(e^{\Theta_i/T} - 1)^2} \right\} \quad (3)$$

Using the ability of the stability analysis in STABL to freeze the chemical and vibrational rate processes, we can determine the effect of these rate processes on the damping of second mode disturbances. An example of this type of calculation is demonstrated by comparing the transition location for a fully reacting stability analysis and a frozen gas stability analysis for the 10 MJ/kg case, as shown in Figure 3. Using a reacting mean flow and a frozen gas stability analysis, the data show that adding carbon dioxide promotes transition. When the chemical and vibrational rate processes are included in the stability analysis, the transition location moves further down the cone due to carbon dioxide's ability to damp boundary layer disturbances. By calculating the change in transition location, we can compare the effectiveness of disturbance damping in each of the four freestream conditions, shown in Figure 4. For all cases tested, the addition of chemical and vibrational rate processes results in a shift in the transition location towards the rear of the cone that increases with an increasing mass fraction of carbon dioxide in the test gas. From these data, it becomes clear that the damping ability of carbon dioxide is most effective for the 10 MJ/kg case, for the reasons described above. Interestingly, the addition of carbon dioxide in the 5 MJ/kg case has little or no effect as indicated in Figure 2, despite the disturbance damping ability of molecular vibration demonstrated in Figure 4. In this case, the optimum disturbance damping frequency of carbon dioxide is no longer similar to the boundary layer disturbance frequencies.

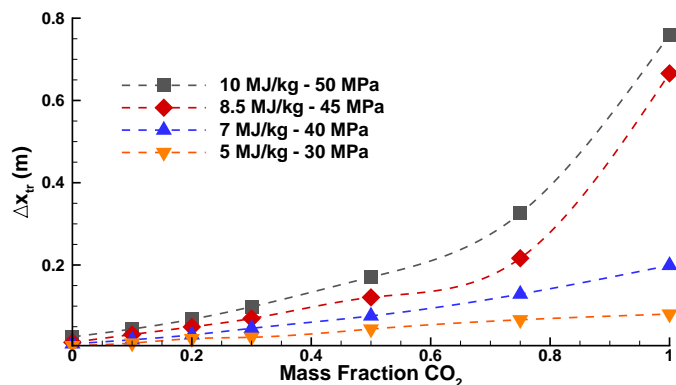


Figure 4. Comparison of the change in transition location due to vibrational relaxation versus mass fraction of CO<sub>2</sub> based on a transition N factor of 5 for each of the three freestream conditions tested.

It is also noted that the relatively small effect of vibrational damping shown in Wagnild et al.<sup>34</sup> is due to the total enthalpy of the flow considered in their study, approximately 4.5 MJ/kg. As demonstrated in Figure 4, the vibrational damping of carbon dioxide causes a smaller change in transition location with a decreasing flow enthalpy. Thus, a small change in amplification at 4.5 MJ/kg is expected.

## VI. Experimental Results

Although there have been several previous experimental campaigns on transition in T5 (Germain,<sup>3</sup> Adam and Hornung,<sup>4</sup> Leyva et al.,<sup>9</sup> Jewell et al.<sup>12</sup>), based on recent experience with T5 operations, it is desirable to conduct new experiments with special attention paid to repeatability and cleanliness of the tunnel. Based on the computations described above, we choose three carbon dioxide/air gas mixtures which were tested in T5 on the 5-degree half-angle cone, with reservoir enthalpies varying from 7.68–9.65 MJ/kg and reservoir pressures held as consistently as possible near 58 MPa, but varying from 53.4–60.7 MPa, to attempt to reproduce the largest shift in transition location implied by the computations. The gas mixtures, by mass fraction of carbon dioxide in the mixture, are 0.0 (e.g. all air), 0.5, 1.0. A summary of run conditions and results is presented in Table 1 on page 8. For the 0.5 mass fraction case, the CO<sub>2</sub> and air are not premixed.

The shock tube is filled sequentially and the gases allowed to diffuse into each other for approximately 15 minutes before each experiment.

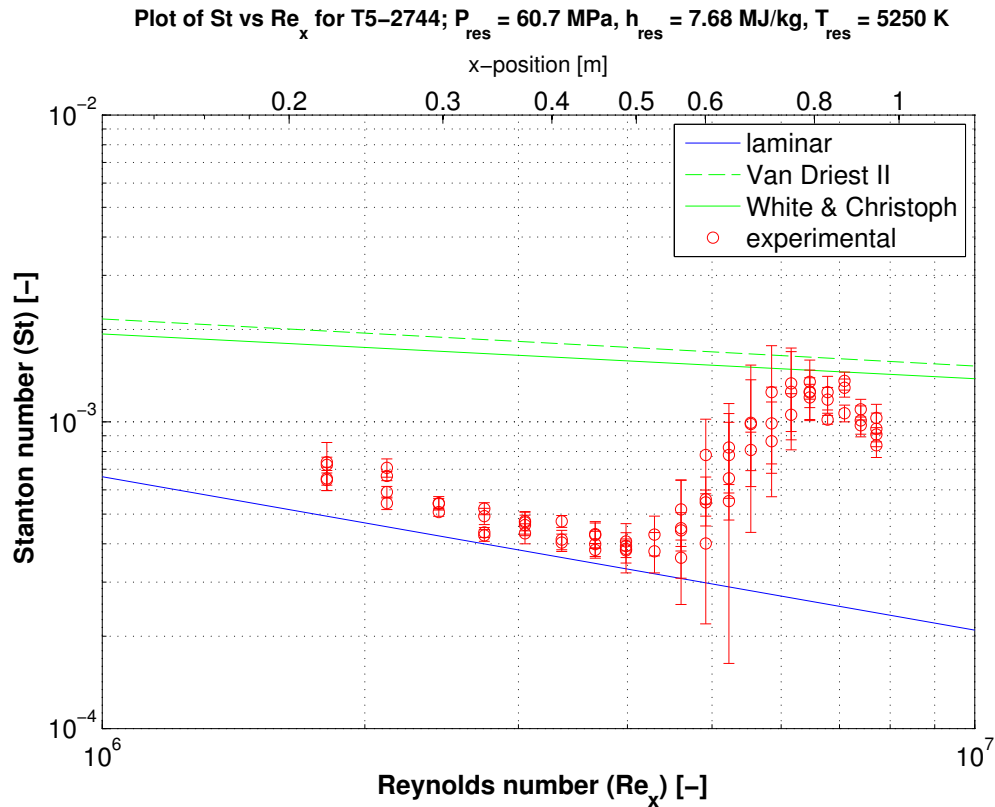


Figure 5. Time-averaged non-dimensional plot of heat transfer results in terms of Stanton number vs. Reynolds number for T5 shot 2744 in 100% air, with the laminar similarity correlation indicated in blue and two common turbulent correlations in green. The bars on each point represent the RMS values of each thermocouple's signal, and transition onset occurs at  $Re = 4.14 \times 10^6$ , which is 0.505 m from the tip of the cone.

One example of results from the present tests, shot 2744 in air, is shown in Figure 5. Normalized heat-transfer results at 7.68 MJ/kg and 60.7 MPa are presented. The circles are time-averaged measurements from each of 80 thermocouples for the  $\sim 1$ ms steady flow time, and the bars represent the root mean squared values from each sensor. The RMS bars are initially small in the laminar zone as the heat transfer levels are consistently at the laminar value, increase in size in the transitional zone as the flow becomes intermittent, and may then decrease in size again as the flow approaches the fully turbulent zone and heat transfer levels are consistently near the turbulent value. A slight drop-off from the fully turbulent value is observed in the last two rows of thermocouples, as they are positioned near the maximum extent of the T5 test rhombus and may intersect with the expansion fan emanating from the lip of the nozzle. For this experiment, transition is observed at 0.505 m from the tip of the cone.

Flow conditions in T5 are calculated from three tunnel measurements: the shock speed, initial shock tube fill pressure and composition, and reservoir pressure at the end of the shock tube during the run time. Shock speed is measured by two time of arrival pressure transducers positioned 2.402m apart, with an approximate measurement uncertainty of  $8 \times 10^{-6}$  s. The uncertainty in the shock speed measurement thus increases as the measured time of arrival difference decreases. At a shock speed of 3000 m/s, typical for the present study, the uncertainty is 30 m/s. The shock tube fill pressure uncertainty is 0.25 kPa, and the measured reservoir pressure uncertainty is typically 4 MPa. Uncertainties on the calculated quantities, including those represented by the error bars in Figures 6-8, are estimated by perturbing Cantera<sup>35</sup> condition computations<sup>36</sup> within the range of the uncertainties on the measured shock speed, reservoir pressure, and initial shock tube pressure. Only experiments with measured shock speeds that reasonably matched the adjusted shock speed curve predicted by the shock jump conditions from the burst pressure and initial conditions were included in the present data set.

Transition  $x$ -locations over the range of enthalpies for each gas mixture are summarized in Figure 6. A

**Table 1. Run conditions and results included in the present study. In the last three columns, the > symbol indicates that the flow was laminar to the last measurable thermocouple location, which is recorded.**

Experiment	$w_{\text{CO}_2}$ (-)	$h_{\text{res}}$ (MJ/kg)	$P_{\text{res}}$ (MPa)	$T^*$ (K)	$x_{\text{tr}}$ (m)	$\text{Re}_{\text{tr}}$ (-)	$N_{\text{tr}}$ † (-)
2720	1	9.65	59.3	1845	> 0.824	> $5.31 \times 10^6$	> 4.63
2729	0.5	8.45	57.7	1688	0.721	$5.01 \times 10^6$	9.24
2730	0.5	7.80	58.1	1593	0.639	$4.90 \times 10^6$	9.48
2732	0.5	7.84	57.0	1592	0.714	$5.25 \times 10^6$	
2739	0	8.03	57.5	1618	0.547	$3.98 \times 10^6$	
2740	0	7.97	57.3	1608	0.544	$3.96 \times 10^6$	
2741	0	8.34	56.9	1665	0.567	$3.89 \times 10^6$	10.57
2742	0	8.64	55.7	1719	0.581	$3.80 \times 10^6$	
2743	0	9.09	56.3	1789	0.639	$3.94 \times 10^6$	10.58
2744	0	7.68	60.7	1565	0.505	$4.14 \times 10^6$	10.99
2745	1	9.67	58.5	1837	> 0.797	> $5.00 \times 10^6$	
2747	1	9.36	60.3	1803	> 0.855	> $5.75 \times 10^6$	> 5.02
2749	0.5	9.59	60.4	1860	> 0.829	> $5.19 \times 10^6$	> 8.93
2750	0.5	9.00	60.0	1776	> 0.829	> $5.58 \times 10^6$	> 9.57
2751	1	9.04	60.2	1756	> 0.835	> $5.75 \times 10^6$	
2754	1	9.41	53.4	1799	> 0.805	> $4.90 \times 10^6$	
2756	1	8.72	57.5	1710	> 0.821	> $5.62 \times 10^6$	> 5.57

† N factor was not calculated for every experiment.

strong correlation between reservoir enthalpy and transition location is apparent for all gas mixtures, and delays of up to 30% (at 9.2 MJ/kg) are observed for flows containing CO<sub>2</sub> compared to experiments in pure air.

Figure 7 presents the same data in terms of the Reynolds number evaluated at boundary layer edge conditions, defined in Equation (4). Edge conditions are calculated from the conditions at the nozzle exit by iteratively solving the Taylor-Maccoll equation for a conical shock.

$$\text{Re}_{\text{tr}} = \frac{\rho_e u_e x_{\text{tr}}}{\mu_e} \quad (4)$$

While experiments with CO<sub>2</sub> in the freestream remain distinct from air tests, this approach results in similar transition Reynolds numbers within each gas mixture condition, weakening the trend with reservoir enthalpy seen in the  $x$ -location data in Figure 6. In terms of Re, delays up to 38% (at ~9.2 MJ/kg) are observed for the measured transition location in flows containing CO<sub>2</sub> compared to experiments in pure air.

Within a hypervelocity boundary layer, strong temperature gradients between the wall and the freestream result in strong gradients in fluid properties. To define a single representative Reynolds number, it is convenient to choose a single so-called reference temperature at which to evaluate density and viscosity. Experiments by Adam<sup>4</sup> showed that computing the transition Reynolds number at reference conditions strongly separated pure CO<sub>2</sub> results from pure air and N<sub>2</sub> data. The Dorrance<sup>37</sup> reference temperature, defined in Equation (5) has the same form as the Eckert reference temperature but may be used for other gases as well as air.

$$\frac{T^*}{T_e} = \frac{1}{2} + \frac{\gamma - 1}{2} \frac{\sqrt{\text{Pr}}}{6} M_e^2 + \frac{1}{2} \frac{T_w}{T_e} \quad (5)$$

The Dorrance temperature is used to calculate the quantities in Equation (6), the Reynolds number with density and viscosity evaluated at reference conditions.

$$\text{Re}_{\text{tr}}^* = \frac{\rho^* u_e x_{\text{tr}}}{\mu^*} \quad (6)$$

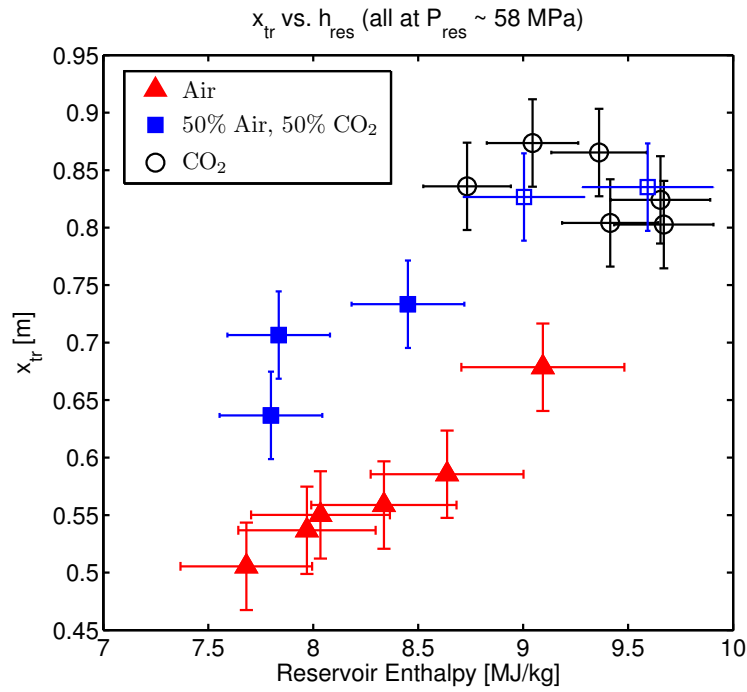


Figure 6. Location of transition on the cone surface vs. reservoir enthalpy, with reservoir pressure held near 58 MPa for all experiments. Solid symbols represent experiments which showed transition at the location indicated; hollow symbols represent experiments where no transition was observed, and are placed at the location of the last measurable thermocouple for that test.

The results of the present study calculated in terms of  $Re^*$  are given in Figure 8. This approach effectively correlates observed transition locations for each gas mixture across the entire range of enthalpies examined, clearly separating air, CO<sub>2</sub> and mixture cases. In terms of  $Re^*$ , delays up to 140% (at  $\sim 9.2$  MJ/kg) are observed for the measured transition location in flows containing CO<sub>2</sub> compared to experiments in pure air. Using a similar cone in T5, and over a similar enthalpy range, Adam<sup>38</sup> reported values of  $Re^*_{tr}$  between  $1.00 \times 10^6$  and  $1.66 \times 10^6$  in pure air and between  $5.40 \times 10^6$  and  $8.06 \times 10^6$  in pure CO<sub>2</sub>. The present air  $Re^*_{tr}$  values are significantly higher than Adam's air results, but the present CO<sub>2</sub> and air/CO<sub>2</sub> mixture results overlap with Adam's CO<sub>2</sub> results.

## VII. Computational Analysis of Experiments

Using the computational method described above, several of the experimental cases are analyzed to determine the transition N factor. The results of several cases in this analysis are shown in Figure 9, which plots the maximum N factor reached along the length of the cone. The air shots are indicated with solid lines, the 50% CO<sub>2</sub> shots are indicated with dashed lines, and the 100% CO<sub>2</sub> shots are indicated with dot-dashed lines. For the conditions presented, it is apparent that the second mode amplification is decreasing with an increasing mass fraction of CO<sub>2</sub> as indicated by the magnitude of the N factor along the cone. The experimental transition locations of each shot are marked with hollow black diamonds on their corresponding maximum N factor curve.

The transition N factors for the 50% CO<sub>2</sub> cases lie below the air shots. However, both freestream compositions show transition near  $N \sim 10$ . The calculated maximum disturbance amplification in the 100% CO<sub>2</sub> shots results in  $N < 6$ , apparently insufficient to cause transition, although other factors may be important. The transition N factors of each shot where transition was observed are compiled in Figure 10 versus the reservoir enthalpy. The error bars on each datum indicate change in transition N factor due to a 4 cm uncertainty in the measurement of the transition location. It appears that in both the air and 50% CO<sub>2</sub> cases, an N factor of  $\sim 10$  is appropriate for the prediction of transition location. However, as this is a purely empirical observation, we have no reason to expect that this should be the case for all mixtures and enthalpies. One potential reason for the slightly lower transition N factors in the 50% CO<sub>2</sub> shots may be that the stability analysis is overpredicting the damping ability of carbon dioxide. This could result from a

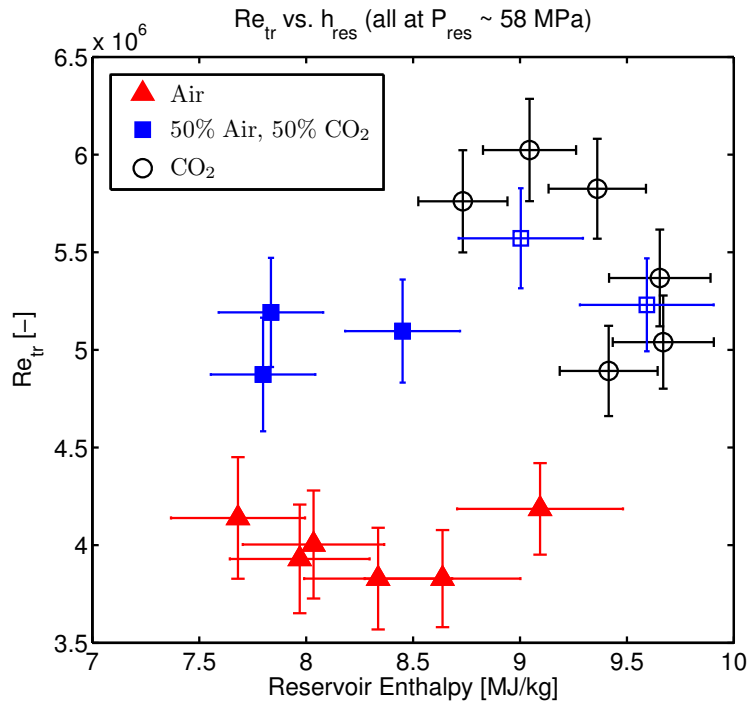


Figure 7. Reynolds number at transition (evaluated at edge conditions) vs. reservoir enthalpy, with reservoir pressure held near 58 MPa for all experiments. Solid symbols represent experiments which showed transition at the location indicated; hollow symbols represent experiments where no transition was observed, and are placed at the location of the last measurable thermocouple for that test.

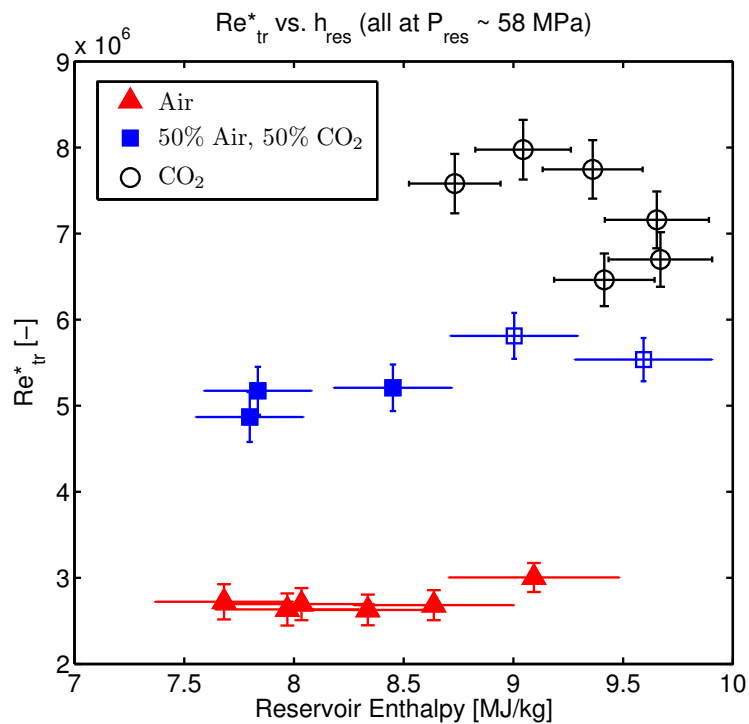


Figure 8. Reynolds number at transition (evaluated at Dorrance reference conditions) vs. reservoir enthalpy, with reservoir pressure held near 58 MPa for all experiments. Solid symbols represent experiments which showed transition at the location indicated; hollow symbols represent experiments where no transition was observed, and are placed at the location of the last measurable thermocouple for that test.

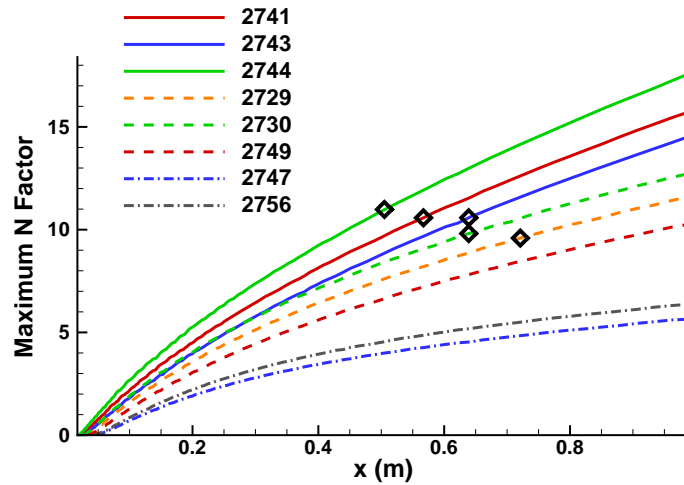


Figure 9. Maximum N factor vs. distance along the surface of the cone as computed by STABL for the conditions of the T5 shot indicated in the legend. The experimentally measured transition locations are indicated by hollow black diamonds where applicable. The solid lines (2741, 2743, 2744) are air cases, the dashed lines (2729, 2730, 2749) are 50% air, 50% CO<sub>2</sub> cases, and the dot-dashed lines (2747, 2756) are CO<sub>2</sub> cases.

different vibrational relaxation rate than that predicted by Camac's rates, or perhaps the simple harmonic oscillator model assumption is too idealistic for this experiment.

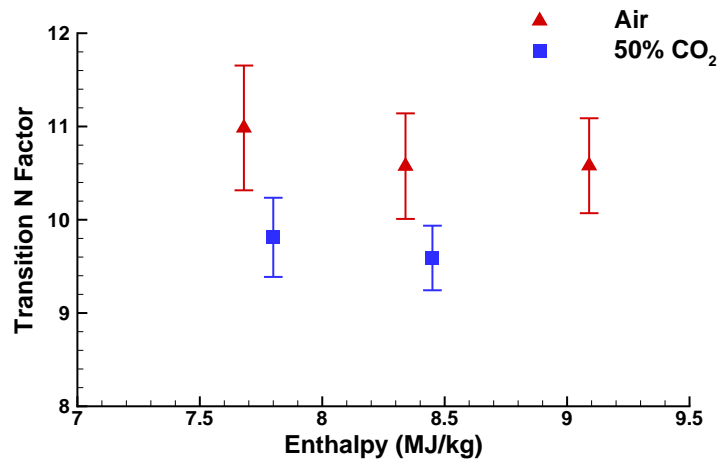


Figure 10. Transition N factor vs. reservoir enthalpy as computed by STABL for the experimental conditions at which transition was measured. The error bars represent the maximum change in N factor when varying the transition location by  $\pm 4$  cm.

The present experimental results are a closer match to the present computations than an earlier study,<sup>5</sup> which used a similar methodology with the assumption that transition occurred at an N factor of  $\sim 10$ , and found that transition Reynolds numbers were overpredicted by a factor of 2 when compared experimentally with T5 experiments performed by Adam.<sup>4</sup> These experimental and computational data also show more consistent behavior with varying conditions than an analysis performed by Wagnild.<sup>11</sup> Additionally, a computational analysis by Gronvall et al.<sup>39</sup> found a consistent transition N factor of approximately 8 for transition on a sharp 5-degree half-angle cone in the free-piston shock tunnel HIEST. Both Gronvall et al. and the current study indicate transition at higher levels of amplification than previous estimates for non-quiet tunnels. The current estimate of  $N \sim 10$  for T5 may be at least partially due to the suppression of particulate-induced transition through much more thorough cleaning of the compression tube, shock tube, nozzle, and other wetted components of T5 than has been standard practice in the past.

## VIII. Conclusions and Future Work

Consistent transition N factors greater than 10 have been found over a 5-degree half-angle in the T5 hypervelocity shock tunnel for air flows with reservoir enthalpies above 7.68 MJ/kg and reservoir pressures near 58 MPa. N factors greater than 9 have been calculated for 50% air/CO<sub>2</sub> mixtures at equivalent enthalpy and pressure conditions. Transition location is an increasing function of both the reservoir enthalpy and CO<sub>2</sub> concentration. Addition of 50% CO<sub>2</sub> by mass results in an increase in transition distance of Re\* by a factor of two, but the N factor is comparable in all cases, N~9–11. This suggests that the suppression of the second mode through the absorption of energy from acoustic disturbances through vibrational relaxation is a mechanism for delaying transition both in high-enthalpy carbon dioxide flows and, more usefully, high-enthalpy flows consisting of a mixture of CO<sub>2</sub> and air.

These results are quite promising. Future work will include the installation of a premixing tank for studies using fully mixed CO<sub>2</sub> and air in the shock tube, to address concerns about completeness of the gaseous mixing process prior to each experiment; additional mass fraction cases; studies in gases other than CO<sub>2</sub>; and ultimately continuation of the boundary-layer injection work begun in Jewell et al.<sup>12</sup>

## Acknowledgments

The authors thank Mr. Nick Parziale for his assistance in running T5, Mr. Bahram Valiferdowski for his work with design, fabrication, and maintenance, and Prof. Hans Hornung for his advice and support. The experimental portion of this project was sponsored by the Air Force Office of Scientific Research under award number FA9550-10-1-0491 and the NASA/AFOSR National Center for Hypersonic Research. The computational work was sponsored by the Air Force Office of Scientific Research grant FA9550-10-1-0352. Sandia National Laboratories is a multi-program laboratory managed and operated by Sandia Corporation, a wholly owned subsidiary of Lockheed Martin Corporation, for the U.S. Department of Energy's National Nuclear Security Administration under contract DE-AC04-94AL85000. The views expressed herein are those of the authors and should not be interpreted as necessarily representing the official policies or endorsements, either expressed or implied, of AFOSR, Sandia, or the U.S. Government.

## References

- <sup>1</sup>Mack, L. M., "Boundary-layer linear stability theory. special course on stability and transition of laminar flow advisory group for aerospace research and development," Tech. rep., 1984, AGARD Report No. 709.
- <sup>2</sup>Malik, M. R., "Hypersonic flight transition data analysis using parabolized stability equations with chemistry effects," *Journal of Spacecraft and Rockets*, Vol. 40, No. 3, 2003, pp. 332–344.
- <sup>3</sup>Germain, P., *The Boundary Layer on a Sharp Cone in High-Enthalpy Flow*, Ph.D. thesis, California Institute of Technology, Pasadena, CA, 1993.
- <sup>4</sup>Adam, P. H. and Hornung, H. G., "Enthalpy effects on hypervelocity boundary-layer transition: Ground test and flight data," *Journal of Spacecrafts and Rockets*, Vol. 34, No. 5, 1997.
- <sup>5</sup>Johnson, H. B., Seipp, T. G., and Candler, G. V., "Numerical study of hypersonic reacting boundary layer transition on cones," *Physics of Fluids*, Vol. 10, 1998, pp. 2676–2685.
- <sup>6</sup>Fujii, K. and Hornung, H. G., "A Procedure to Estimate Absorption Rate of Sound Propagating Through High Temperature Gas," Tech. rep., California Institute of Technology, Pasadena, CA, Aug. 2001, GALCIT Report FM2001.004.
- <sup>7</sup>Fedorov, A. V., Malmuth, N. D., and Hornung, H. G., "Stabilization of hypersonic boundary layers by porous coatings," *AIAA journal*, Vol. 39, No. 4, 2001, pp. 605–610.
- <sup>8</sup>Rasheed, A., Hornung, H. G., Fedorov, A. V., and Malmuth, N. D., "Experiments on passive hypervelocity boundary-layer control using an ultrasonically absorptive surface," *AIAA Journal*, Vol. 40, No. 3, 2002, pp. 481–489.
- <sup>9</sup>Leyva, I. A., Laurence, S., Beierholm, A. W., Hornung, H. G., Wagnild, R., and Candler, G., "Transition delay in hypervelocity boundary layers by means of CO<sub>2</sub>/acoustic instability interactions," *47th Aerospace Sciences Meeting*, AIAA, Orlando, FL, 2009, AIAA 2009-1287.
- <sup>10</sup>Wagnild, R. M., Candler, G. V., Leyva, I. A., Jewell, J. S., and Hornung, H. G., "Carbon Dioxide Injection for Hypervelocity Boundary Layer Stability," *48th Aerospace Sciences Meeting*, AIAA, Orlando, FL, 2010, AIAA 2010-1244.
- <sup>11</sup>Wagnild, R. M., *High Enthalpy Effects on Two Boundary Layer Disturbances in Supersonic and Hypersonic Flow*, Ph.D. thesis, University of Minnesota, Minneapolis, MN, 2012.
- <sup>12</sup>Jewell, J. S., Leyva, I. A., Parziale, N. J., and Shepherd, J. E., "Effect of Gas Injection on Transition in Hypervelocity Boundary Layers," *Proceedings of the 28th International Symposium on Shockwaves*, Manchester, UK, 2011.
- <sup>13</sup>Fedorov, A., "Transition and stability of high-speed boundary layers," *Annual Review of Fluid Mechanics*, Vol. 43, 2011, pp. 79–95.
- <sup>14</sup>Stetson, K. F., "Hypersonic boundary-layer transition," *Advances in Hypersonics*, edited by J. Bertin, J. Periauz, and J. Ballman, Birkhauser, Boston, MA, 1992, pp. 324–417.
- <sup>15</sup>Kinsler, L. E., Frey, A. R., Coppens, A. B., and Sanders, J. V., *Fundamentals of acoustics (Third Edition)*, John Wiley & Sons, Inc., New York, 1982.

- <sup>16</sup>Clarke, J. F. and McChesney, M., *The dynamics of real gases*, Vol. 175, Butterworths, 1964.
- <sup>17</sup>Zeldovich, Y. B. and Raizer, Y. P., *Physics of shock waves and high-temperature hydrodynamic phenomena*, Academic Press, New York, NY, 1967.
- <sup>18</sup>Camac, M., "CO<sub>2</sub> relaxation processes in shock waves," *Fundamental Phenomena in Hypersonic Flow*, edited by J. Hall, Cornell University Press, 1966, pp. 195–215.
- <sup>19</sup>Hornung, H., "Performance data of the new free-piston shock tunnel at GALCIT," *17th Aerospace Ground Testing Conference*, AIAA, Nashville, TN, 1992, AIAA 92-3943.
- <sup>20</sup>Hornung, H. and Belanger, J., "Role and techniques of ground testing for simulation of flows up to orbital speed," *16th Aerodynamic Ground Testing Conference*, AIAA, Seattle, WA, 1990, AIAA 90-1377.
- <sup>21</sup>Marineau, E. C. and Hornung, H. G., "Modeling and calibration of fast-response coaxial heat flux gages," *47th Aerospace Sciences Meeting*, AIAA, Orlando, FL, 2009, AIAA 2009-0737.
- <sup>22</sup>Candler, G. ., "Hypersonic nozzle analysis using an excluded volume equation of state," AIAA 2005-5202.
- <sup>23</sup>Spalart, P. R. and Allmaras, S. R., "A one-equation turbulence model for aerodynamic flows," *30th Aerospace Sciences Meeting and Exhibit*, AIAA, Reno, NV, 1992, AIAA 92-0439.
- <sup>24</sup>Catris, S. and Aupoix, B., "Density corrections for turbulence models," *Aerospace Science and Technology*, Vol. 4, No. 1, 2000, pp. 1–11.
- <sup>25</sup>Johnson, H. B., *Thermochemical Interactions in Hypersonic Boundary Layer Stability*, Ph.D. thesis, University of Minnesota, Minneapolis, MN, 2000.
- <sup>26</sup>Johnson, H. B. and Candler, G. V., "Hypersonic boundary layer stability analysis using PSE-Chem," *35th Fluid Dynamics Conference and Exhibit*, AIAA, 2005, AIAA 2005-5023.
- <sup>27</sup>Schneider, S. P., "Effects of high-speed tunnel noise on laminar-turbulent transition," *Journal of Spacecraft and Rockets*, Vol. 38, No. 3, 2001, pp. 323–333.
- <sup>28</sup>Park, C., Howe, J. T., Jaffe, R. L., and Candler, G. V., "Review of Chemical-Kinetic Problems of Future NASA Missions, II: Mars Entries," *Journal of Thermophysics and Heat Transfer*, Vol. 8, No. 1, 1994, pp. 9–23.
- <sup>29</sup>Bose, D. and Candler, G. V., "Thermal Rate Constants of the N<sub>2</sub> + O → NO + N Reaction Using Ab Initio 3A'' and 3A' Potential Energy Surfaces," *Journal of Chemical Physics*, Vol. 104, No. 8, 1996, pp. 2825–2833.
- <sup>30</sup>Bose, D. and Candler, G. V., "Thermal Rate Constants of the O + N → NO + O Reaction Based on the 2A' and 4A' Potential-Energy Surfaces," *Journal of Chemical Physics*, Vol. 107, No. 16, 1997, pp. 6136–6145.
- <sup>31</sup>Park, C., *Nonequilibrium Hypersonic Aerothermodynamics*, Wiley, New York, 1990.
- <sup>32</sup>McBride, B. J., Zehe, M. J., and Gordon, S., "NASA Glenn coefficients for calculating thermodynamic properties of individual species," Tech. rep., 2002, Report TP-2002-21155.
- <sup>33</sup>Vincenti, W. G. and Kruger, C. H., *Introduction to Physical Gas Dynamics*, Wiley, New York, 1965.
- <sup>34</sup>Wagnild, R. M., Candler, G. V., Subbareddy, P., and Johnson, H., "Vibrational Relaxation Effects on Acoustic Disturbances in a Hypersonic Boundary Layer over a Cone," *50th Aerospace Sciences Meeting*, AIAA, Nashville, TN, 2012, AIAA 2012-0922.
- <sup>35</sup>Goodwin, D., "Cantera: An object-oriented software toolkit for chemical kinetics, thermodynamics, and transport processes," Available: <http://code.google.com/p/cantera>, 2009, Accessed: 12/12/2012.
- <sup>36</sup>Browne, S., Ziegler, J., and Shepherd, J., "Numerical solution methods for shock and detonation jump conditions," Tech. rep., California Institute of Technology, Pasadena, CA, July 2008, GALCIT Report FM2006.006.
- <sup>37</sup>Dorrance, W. H., *Viscous hypersonic flow: theory of reacting and hypersonic boundary layers*, McGraw-Hill, 1962.
- <sup>38</sup>Adam, P. H., *Enthalpy Effects on Hypervelocity Boundary Layers*, Ph.D. thesis, California Institute of Technology, Pasadena, CA, 1997.
- <sup>39</sup>Gronvall, J. E., Johnson, H. B., and Candler, G. V., "Boundary Layer Stability Analysis of the Free-Piston Shock Tunnel HIEST Transition Experiments," *48th Aerospace Sciences Meeting*, AIAA, Orlando, FL, 2010, AIAA 2010-0896.

# Shock tunnel operation and correlation of boundary layer transition on a cone in hypervelocity flow

J.S. Jewell<sup>1</sup>, J.E. Shepherd<sup>1</sup>, and I.A. Leyva<sup>2</sup>

## 1 Introduction

The Caltech T5 reflected shock tunnel is used to produce hypervelocity flow over a range of velocities and pressures by varying the test gas and operating parameters of reservoir enthalpy ( $h_{res}$ ) and reservoir pressure ( $P_{res}$ ). One area of research in T5 is the measurement of boundary layer behavior and transition from laminar to turbulent flow on a smooth 5-degree half-angle cone [3, 1, 11]. To design experiments that involve the measurement or manipulation of instability and transition processes (for example, Jewell et al. [7]), it is important to choose tunnel conditions for which the expected transition location is at least approximately known. In the present paper, we discuss the selection of tunnel operating parameters, the correlation of those parameters with measurements of boundary layer transition, and some observations on the analysis of transition location in terms of local boundary layer properties.

## 2 Tunnel Operation

Flow conditions in T5 are calculated from three tunnel measurements: the shock speed, initial shock tube fill pressure and composition, and reservoir pressure at the end of the shock tube during the run time [4]. Only experiments with measured shock speeds that fall within the uncertainty for the adjusted shock speed curve predicted by the shock jump conditions from the primary diaphragm burst pressure, driver gas composition, and initial shock tube conditions are included in the present data set.

There are a number of other potential sources of measurement error, bias, or uncertainty. These include: nonideal gas behavior in the reservoir due to the high

---

<sup>1</sup>California Institute of Technology, 1200 E. California Blvd., Pasadena, CA 91125, USA

<sup>2</sup>Air Force Research Laboratory, 4 Draco Dr., Edwards AFB, CA 93524, USA

pressure; the extrapolation of the shock speed (which decays as it propagates down the shock tube) to the end wall; nonuniformity of reservoir conditions due to non-ideal shock reflection; and the method of correcting flow conditions from the ideal reflected-shock pressure to measured reservoir pressure using an isentropic expansion. Furthermore, the 1-D nozzle computation does not account for boundary layer growth within the nozzle, off-design operation conditions that lead to flow nonuniformity, or vibration-translation nonequilibrium and freezing within the nozzle, which is significant for the  $N_2$  cases. For the uncertainties that can be quantified, we have combined these to obtain the error bounds on measured properties that are shown in this paper. The tunnel parameters for the present studies in air and nitrogen

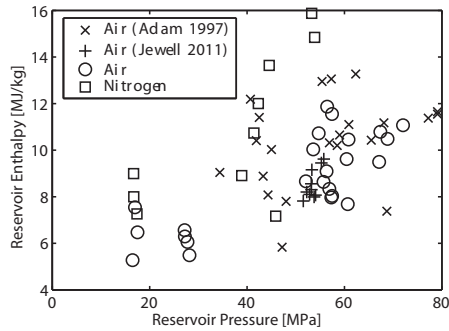


**Fig. 1** Tunnel operating parameters  $h_{res}$  and  $P_{res}$  for the present studies in air and  $N_2$ , compared with past results from Adam [1] and Jewell et al. [5].

are compared with those of two past data sets in air in Figure 1. The present work both overlaps and extends the parameters of the past studies, especially for low pressure and enthalpy. The  $R^2$  values for the correlation between the two parameters are respectively 0.52 and 0.65 for the present  $N_2$  and Air data sets, and respectively 0.10 and 0.59 for the Adam [1] and Jewell et al. [5] data sets.

Freestream conditions are taken as the conditions at the nozzle exit. The 100:1 area ratio contoured nozzle is designed to operate at Mach 6. Because the shape is optimized for a single condition, there is significant variation of the exit Mach number over the range of tunnel operating parameters, presented in Figure 2 for air over the conditions of the present study.

### 3 Experiments

The experimental model is a 1-m long, smooth, 5-degree half-angle cone with a nominally sharp tip of radius 0.18 mm and oriented at a zero angle of attack. The range of Reynolds numbers evaluated at the boundary layer edge and Dorrance [2] reference temperature, which is used as representative of conditions within the

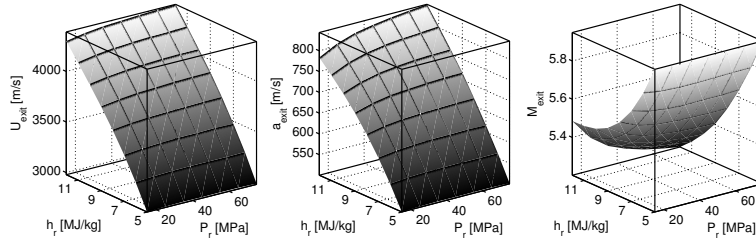


**Fig. 2** Calculated nozzle exit velocity, sound speed, and Mach number in air over a range of tunnel operating parameters  $h_{res}$  and  $P_{res}$ .

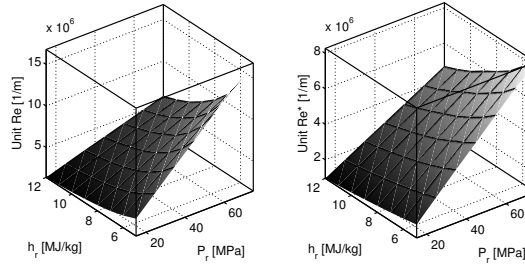


**Fig. 3** Reynolds number evaluated at the boundary layer edge in air (left) and at Dorrance reference conditions in air (right) over a range of tunnel operating parameters  $h_{res}$  and  $P_{res}$ .

boundary layer, is presented for air in Figure 3. The cone is instrumented with 80 thermocouples, providing heat transfer measurements from which transition location may be determined. Heat transfer results are normalized by Stanton number and Reynolds number, and the location of transition onset determined as described in Jewell et al. [7].

Parameters for experiments that bracket the range of conditions studied in both air and  $N_2$  are presented in Table 1. A supplemental report [6] is available online, which includes the full tables and plots for all 34 experiments included in the present study.

## 4 Results and Analysis

Results for the location  $X_{tr}$  of transition onset on the cone are presented in terms of  $h_{res}$  and  $P_{res}$  in Figure 4 for both  $N_2$  and air. Multivariable linear regression analysis is performed on these data sets (for details, see [6]). Both the present  $N_2$  and air results have a positive dependence on  $h_{res}$  (linear model coefficient of 0.56 for  $N_2$ , 0.55 for air) and a negative dependence on  $P_{res}$  (linear model coefficient of  $-0.45$  for  $N_2$ ,  $-0.15$  for air). The historical air data of Adam and Hornung[1], are analyzed in the same way, and likewise show a significant positive dependence of  $X_{tr}$  on  $h_{res}$

**Table 1** Parameters for selected experiments spanning the present range of conditions for air and N<sub>2</sub>.

	Gas	$h_{res}$ [MJ/kg]	$P_{res}$ [MPa]	$Re/m$ [1/m]	$Re^*/m$ [1/m]	$X_{tr}$ [m]	$\delta_{99tr}$ [mm]	$f_{tr}$ [kHz]
2744	Air	7.68	60.7	$8.19 \times 10^6$	$5.39 \times 10^6$	0.51	0.98	1094
2758	Air	11.07	72.0	$6.11 \times 10^6$	$4.79 \times 10^6$	0.74	1.26	1002
2764	Air	5.27	16.5	$3.62 \times 10^6$	$1.83 \times 10^6$	0.52	1.65	551
2773	N <sub>2</sub>	8.99	16.7	$2.02 \times 10^6$	$1.25 \times 10^6$	0.67	2.26	522
2776	N <sub>2</sub>	7.17	45.9	$7.09 \times 10^6$	$3.94 \times 10^6$	0.39	0.97	1102
2783	N <sub>2</sub>	15.88	53.3	$3.20 \times 10^6$	$2.62 \times 10^6$	0.63	1.56	966

(linear model coefficient of 0.72) and negative dependence on  $P_{res}$  (linear model coefficient of  $-0.28$ ).

Both the present N<sub>2</sub> and air results have a positive dependence on  $P_{res}$  (linear model coefficients of 0.31 for N<sub>2</sub>, 0.59 for air) for the transition Reynolds number evaluated at Dorrance reference conditions,  $Re_{tr}^*$ , but neither have a dependence on  $h_{res}$  that is statistically significant. The historical air data of Adam and Hornung[1] likewise show a significant positive dependence of  $Re_{tr}^*$  on  $P_{res}$  (linear model coefficient of 0.34), but no statistically significant dependence on  $h_{res}$ .

The usual approach [12] for representing boundary layer transition onset is in terms of a transition location Reynolds number  $Re_{tr}$  or  $Re_{tr}^*$  and previous analysis [1] of T5 data has utilized this approach. However, in hypervelocity flow with a cold wall, the principal boundary layer instability mechanism is the predominantly inviscid acoustic or Mack mode [9]. Unlike the viscous instability of low-speed boundary layers, at high speeds the role of viscosity is primarily in determining the mean flow. The properties of the acoustic instability are determined by the local boundary layer thickness and profiles of velocity and thermodynamic properties. This suggests the approach of correlating transition distance with  $X_{tr}/\delta_{99}$  and the acoustic properties of the boundary layer rather than a Reynolds number.

As shown in Figure 5(l),  $X_{tr}/\delta_{99}$  is relatively independent of edge Mach number but shows a systematic dependence on the gas type and pressure. The scaled distance ranges from about 300 for low pressure tests up to 600 for high pressure. The radiation of acoustic disturbances from the turbulent boundary layer on the nozzle wall and the jet shear layer is an important source of disturbances in ground-testing facilities [12], and varying receptivity of the boundary layer to these radiated disturbances is a likely explanation for the trends observed in Figure 5.

Lowering the pressure creates a thicker boundary layer, and therefore lowers the most amplified second mode frequency  $f \approx 0.6U_e/2\delta_{99}$ . This may account for the striking correlation of  $X_{tr}/\delta_{99}$  with the frequency  $f_{tr}$  that is shown in Figure 5(r). The influence on transition location can be explained by the measurements of Parziale et al. [10], who showed that in T5, most of the noise in the free stream is at relatively low frequencies ( $< 500$  kHz), and observed a decrease in rms density fluctuations with increasing frequency. This is consistent with the present observa-

tions of earlier transition, at lower most-amplified frequencies, for lower values of  $P_{res}$  in both air and  $N_2$ .

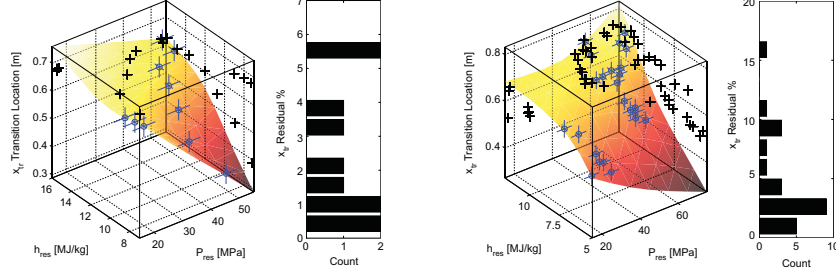


**Fig. 4** (l) Transition onset location  $X_{tr}$  for  $N_2$ , and (r) air in terms of reservoir enthalpy  $h_{res}$  and pressure  $P_{res}$ .

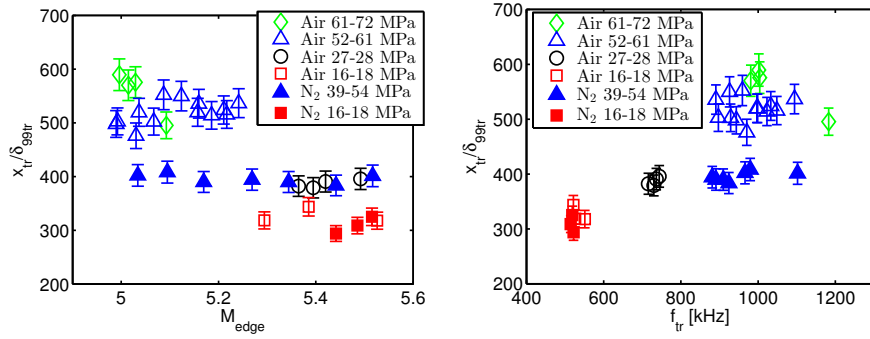


**Fig. 5** (l) Scaled transition distance  $X_{tr}/\delta_{99tr}$  vs.  $M_{edge}$ , the boundary layer edge Mach number. (r) Scaled transition distance  $X_{tr}/\delta_{99tr}$  vs.  $f_{tr}$ , the approximate most-amplified second mode frequency at transition.

## 5 Conclusion

We have re-examined the correlation of transition onset data with tunnel operating conditions by modeling transition onset location with two-dimensional response surfaces in terms of  $h_{res}$  and  $P_{res}$  variables. We observe a positive correlation of  $X_{tr}$  with  $h_{res}$  in both air and  $N_2$  and a negative correlation of  $X_{tr}$  with  $P_{res}$ . The parameter  $Re_{tr}^*$  exhibits a positive correlation with reservoir pressure in both gases. Controlling for variations in  $P_{res}$ , no statistically significant dependence of  $Re_{tr}^*$  on  $h_{res}$  was found for either the present air or  $N_2$  data or the historical air data in Adam

and Hornung[1]. We explore an alternative normalization of the transition onset location by the local laminar boundary layer thickness  $X_{tr}/\delta_{99}$  and find that this is essentially independent of the edge Mach number for a given gas type and pressure range (Figure 5). We examine the correlation of transition onset with the most amplified acoustic frequency in the boundary layer and find that lower frequencies correlate with smaller values of normalized transition distance  $X_{tr}/\delta_{99}$ , suggesting that the frequency-dependent amplification of the tunnel noise may be responsible for the observed systematic variations in transition onset distance.

**Acknowledgements:** The authors thank the T5 group members: Prof. Hans Hornung, Mr. Nick Parziale, and Mr. Bahram Valiferdowsi; Dr. Ross Wagnild for substantial assistance with the flow and boundary layer analysis; and Miss Elizabeth Jewell for her statistical advice. This project was sponsored by the Air Force Office of Scientific Research under award number FA9550-10-1-0491 (J. Schmisser, program manager). The views expressed herein are those of the authors and should not be interpreted as necessarily representing the official policies or endorsements, either expressed or implied, of AFOSR or the U.S. Government.

## References

1. Adam P.H. and Hornung H.G. (1997) Enthalpy Effects on Hypervelocity Boundary-Layer Transition: Ground Test and Flight Data. *Journal of Spacecraft and Rockets*, Vol. 34, No. 5, pp. 614–619.
2. Dorrance W.H. (1962) *Viscous Hypersonic Flow: Theory of Reacting and Hypersonic Boundary Layers*. McGraw-Hill.
3. Germain P. and Hornung H.G. (1997) Transition on a Slender Cone in Hypervelocity Flow. *Experiments in Fluids*, Vol. 22, pp. 183–190.
4. Hornung H.G. (1992) Performance data of the new free-piston shock tunnel at GALCIT. AIAA 92-3943.
5. Jewell J.S., Leyva I.A., Parziale N.J. and Shepherd J.E. (2011) Effect of gas injection on transition in hypervelocity boundary layers. *Proceedings of the 28th International Symposium on Shock Waves*, Vol. 1, pp. 735–740.
6. Jewell J.S., Shepherd J.E., and Leyva I.A. (2013) Supplemental data for “Shock tunnel operation and correlation of boundary layer transition” Available at <http://www2.galcit.caltech.edu/T5/publications/publications.html>
7. Jewell J.S., Wagnild R.M., Leyva I.A., Candler G.V. and Shepherd J.E. (2013) Transition within a hypervelocity boundary layer on a 5-degree half-angle cone in air/CO<sub>2</sub> mixtures. AIAA 2013-0523.
8. Leyva I.A., Jewell J.S., Laurence S., Hornung H.G. and Shepherd J.E. (2009) On the impact of injection schemes on transition in hypersonic boundary layers. AIAA 2009-7204.
9. Mack L.M. (1984) Boundary-layer stability theory. *Special Course on Stability and Transition of Laminar Flow*. AGARD Report 709.
10. Parziale N.J., Shepherd J.E. and Hornung H.G. (2012) Reflected shock tunnel noise measurement by focused differential interferometry. AIAA 2012-3261.
11. Rasheed A., Hornung H.G., Fedorov A.V. and Malmuth N.D. (2002) Experiments on Passive Hypervelocity Boundary-Layer Control Using an Ultrasonically Absorptive Surface. *AIAA Journal*, Vol. 40, No. 3.
12. Schneider S.P (2001) Effects of High-Speed Tunnel Noise on Laminar-Turbulent Transition. *Journal of Spacecraft and Rockets*, Vol. 38, No. 3, pp. 323–333.

**AFRL-RQ-ED-TR-2013-0054**  
**Primary Distribution of this Report:**

AFRL/RQRE (1 CD)  
Dr. Ivett Leyva  
4 Draco Drive  
Edwards AFB CA 93524-7048

AFRL/RQRE (1 HC)  
Record Custodian  
4 Draco Drive  
Edwards AFB CA 93524-7048

AFRL/RQ Technical Library (2 CD + 1 HC)  
6 Draco Drive  
Edwards AFB CA 93524-7130

Chemical Propulsion Information Analysis Center  
Attn: Tech Lib (Mary Gannaway) (1 CD)  
10630 Little Patuxent Parkway, Suite 202  
Columbia MD 21044-3200

Defense Technical Information Center  
(1 Electronic Submission via STINT)  
Attn: DTIC-ACQS  
8725 John J. Kingman Road, Suite 94  
Ft. Belvoir VA 22060-6218